Simulating Distributed Energy Resource Responses to Transmission System-Level Faults Considering IEEE 1547 Performance Categories on Three Major WECC Transmission Paths

Richard Wallace Kenyon and Barry Mather

National Renewable Energy Laboratory

NREL is a national laboratory of the U.S. Department of Energy
Office of Energy Efficiency & Renewable Energy
Operated by the Alliance for Sustainable Energy, LLC

This report is available at no cost from the National Renewable Energy Laboratory (NREL) at www.nrel.gov/publications.

Contract No. DE-AC36-08GO28308

Technical Report
NREL/TP-5D00-73071
February 2020

Simulating Distributed Energy Resource Responses to Transmission System-Level Faults Considering IEEE 1547 Performance Categories on Three Major WECC Transmission Paths

Richard Wallace Kenyon and Barry Mather

National Renewable Energy Laboratory

Suggested Citation
Kenyon, Richard Wallace, and Barry Mather. 2020. *Simulating Distributed Energy Resource Responses to Transmission System-Level Faults Considering IEEE 1547 Performance Categories on Three Major WECC Transmission Paths*. Golden, CO: National Renewable Energy Laboratory. NREL/TP-5D00-73071. https://www.nrel.gov/docs/fy20osti/73071.pdf.

NREL is a national laboratory of the U.S. Department of Energy
Office of Energy Efficiency & Renewable Energy
Operated by the Alliance for Sustainable Energy, LLC

This report is available at no cost from the National Renewable Energy Laboratory (NREL) at www.nrel.gov/publications.

Contract No. DE-AC36-08GO28308

Technical Report
NREL/TP-5D00-73071
February 2020

National Renewable Energy Laboratory
15013 Denver West Parkway
Golden, CO 80401
303-275-3000 • www.nrel.gov

NOTICE

This work was authored by the National Renewable Energy Laboratory, operated by Alliance for Sustainable Energy, LLC, for the U.S. Department of Energy (DOE) under Contract No. DE-AC36-08GO28308. Funding provided by the U.S. Department of Energy Office of Energy Efficiency and Renewable Energy Solar Energy Technologies Office. The views expressed herein do not necessarily represent the views of the DOE or the U.S. Government.

Acknowledgments

This work was supported by the U.S. Department of Energy (DOE) Office of Energy Efficiency and Renewable Energy (EERE) Solar Energy Technologies Office (SETO) Agreement Number DE-EE0007673.

The authors specifically thank Michele Boyd (DOE) for supporting this and other Solar Energy Evolution and Diffusion Studies 2 - State Energy Strategies projects; and Maury Galbraith, David Manning, and Richard McAllister of the Western Interstate Energy Board (WIEB) for partnering with us on the "Enhanced Distributed Solar Photovoltaic Deployment via Barrier Mitigation or Removal in the Western Interconnection" project. We also thank Lori Bird, David Hurlbut and Elaine Hale of the National Renewable Energy Laboratory (NREL) for their leadership of the project and project management support. Additionally, special thanks to Billy Roberts with the National Renewable Energy Laboratory's Geographic Information System team for developing the informative spatial voltage influence figures 1, 4, 13, 17, and 21.

The idea for this report and others completed by this project was developed with input from several of our colleagues at NREL and the project's technical advisory committee (TAC). Lori Bird, Kara Clark, Michael Coddington, Paul Denholm, Barry Mather, Michael Milligan, Bryan Palmintier, and Mark Ruth (NREL) provided input to an initial screening analysis of photovoltaic reliability barriers. The barriers screening analysis was then reviewed by the TAC, as was a research plan developed in response to the screening results. We thank the TAC for their participation in those processes as well as for the review and guidance they provided throughout the execution of the research. The results and findings in this report and the broader project do not necessarily reflect their opinions or the opinions of their institutions. The TAC comprises the following individuals:

Jim Baak	Stem, Inc.
Carl Linvill	Regulatory Assistance Project
Guru Belavadi	Arizona Corporation Commission
Toby Little	Arizona Corporation Commission
Kent Bolton	Western Electricity Coordinating Council
Clyde Loutan	California Independent System Operator
Tom Flynn	California Energy Commission
Louise Nutter	Federal Energy Regulatory Commission
Enoch Davies	Western Electricity Coordinating Council
Vijay Satyal	Navigant Inc.
Jennifer Gardner	Western Resource Advocates
Courtney Smith	California Energy Commission
Daniel Haughton	Arizona Public Service

The authors thank the contributors to the other reports developed under the auspices of this project. Specifically, thanks to Elaine Hale for her coordination of use cases, to the extent possible, between some reports in the series. We also acknowledge the helpful review comments received from David Hurlbut.

List of Acronyms

APS	Arizona Public Service
CAISO	California Independent System Operator
CMPLDWG	composite load model with generation
DER	distributed energy resource
DG	distributed generation
DITS	distribution informed transmission simulation
FIDVR	fault-induced delayed voltage recovery
GIS	geographic information system
IEEE	Institute of Electrical and Electronics Engineers
p.u.	per unit
PSLF	Positive Sequence Load Flow
PV	photovoltaic
RAS	remedial action scheme
SCE	Southern California Edison
TAC	technical advisory committee
WECC	Western Electricity Coordinating Council
WWSIS	Western Wind and Solar Integration Study

Executive Summary

The quantity of distributed energy resources (DERs) has increased substantially during the past two decades, and as a result, how these resources respond to power system disturbances has changed from minimally consequential to potentially critical. Transmission-level disturbances such as line and bus faults can negatively affect the voltage profile across vast regions of the Western Interconnection, with these voltages propagating downward to the distribution system and thus to DERs. Figure A shows an example plot of a modeled voltage sag on the Western Interconnection caused by a single transmission-level fault. As shown, the voltage sag is greatest near the fault, but the area of potential impact is considerably larger, thus leading to an interest in the reaction of DERs to these faults. These transmission-level faults might generate adverse voltages on the terminals of many DERs, which might or might not trip offline depending on implemented ride-through criteria. With DERs having a current aggregate penetration level of approximately 9 GW on the Western Interconnection, unless appropriate power system planning is undertaken, power system faults—which in the past would have resulted in only the loss of a minor amount of DERs—might now, or soon, have a larger impact on system stability because of the potential widespread tripping of DERs.

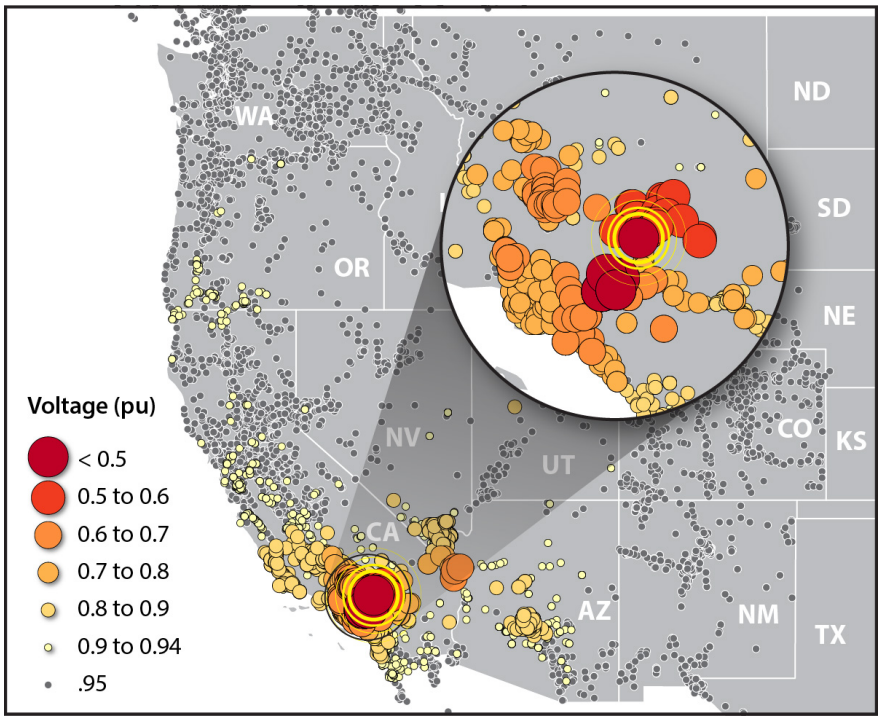

Figure A. Path 61 low-voltage bus GIS mapping

Most interconnections of DERs in the United States adhere to the Institute of Electrical and Electronics Engineers (IEEE) 1547 standard. The first version of IEEE 1547 was released in 2003. Following this release, it was found that commanded inverter operation during power system disturbances varied widely because of the range of allowable responses outlined in the standard as well as various manufacturer interpretations. With the realization of larger penetrations of DERs than originally envisioned in the original standard, the impacts of these various responses became problematic from a power system reliability perspective. The updated version of the standard, IEEE 1547-2018, was released in April 2018 in part to more precisely define a DER's appropriate response during power system disturbances. IEEE 1547-2018 has defined performance categories that are effectively a menu of ride-through characteristics that can be applied to various DER technologies or for various overall DER penetration scenarios. Highlighting the various responses, Figure B shows the aggregate output of 6,150 inverters for three different categories of ride-through criteria compliant with a category of IEEE 1547-2018 and a worst-case scenario (lowest ride-through

performance likely) for IEEE 1547-2003. The results shown were generated from 123 individual distribution circuit simulations loosely cosimulated with a transmission simulation investigating the power system response to a specific event. The aggregated response of all connected DERs on the power system is shown for each of the four ride-through categories. As can be observed, the results show significant differences in the modeled amount of DER generation lost immediately following and up to 30 seconds after the transmission-level fault occurs, demonstrating the potential widespread impact of transmission-level faults on DERs as well as the capability of new IEEE 1547-2018 ride-through performance categories to largely mitigate widespread DER generation loss.

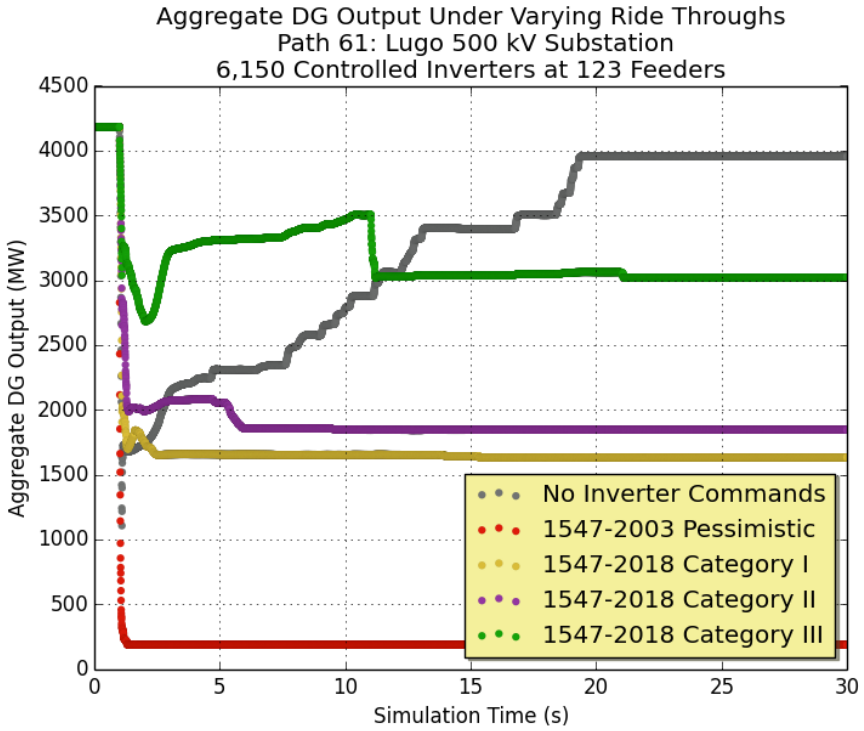

Figure B. Path 61 aggregate distributed generation output for various IEEE 1547 criteria ("No Inverter Commands" indicates no distribution modeling; output recovery coincident with voltage recovery)

This work also presents the results of a Western Interconnection transfer path contingency study using General Electric's Positive Sequence Load Flow (PSLF) dynamic transmission system modeling tool. Metrics developed from this study combine the magnitude of the voltage variation with the amount of DER located at every node within the model to generate location-relevant scores indicative of how system faults anywhere in the Western Interconnection might cause unintended DER losses (see Figure C). This study indicated a number of faults on transfer paths within the Western Interconnection where faults could have a significant impact on DERs. From this initial study, we selected three regions within the Western Interconnection for further investigation: the Front Range of Colorado; the Greater Phoenix, Arizona area; and Southern California. Within each region we selected the transfer path that generated the largest effect on system-wide voltage profiles to examine the sensitivity of the DER ride-through response for various IEEE 1547 performance categories. The transfer paths analyzed include Path 36 within Xcel Energy's territory, Path 54 within the Arizona Public Service (APS) territory, and Path 61 within the Southern California Edison (SCE) territory. We also modeled the impact of the considerable voltage diversity present in the distribution system and thus at the terminals of the various DERs present in a system. These distribution-level models were analyzed using quasi-static time-series (QSTS) simulations in OpenDSS augmented with controlled inverter responses adherent to the pertinent ride-though performance category being evaluated. Finally, to assess the impact of these various performance categories on the overall power system stability, we used the OpenDSS results for the amount of

DER that would trip offline or resume operation as a function of time to control the modeled DER-based generation in PSLF during a resimulation of the transmission system subjected to the same fault scenario.

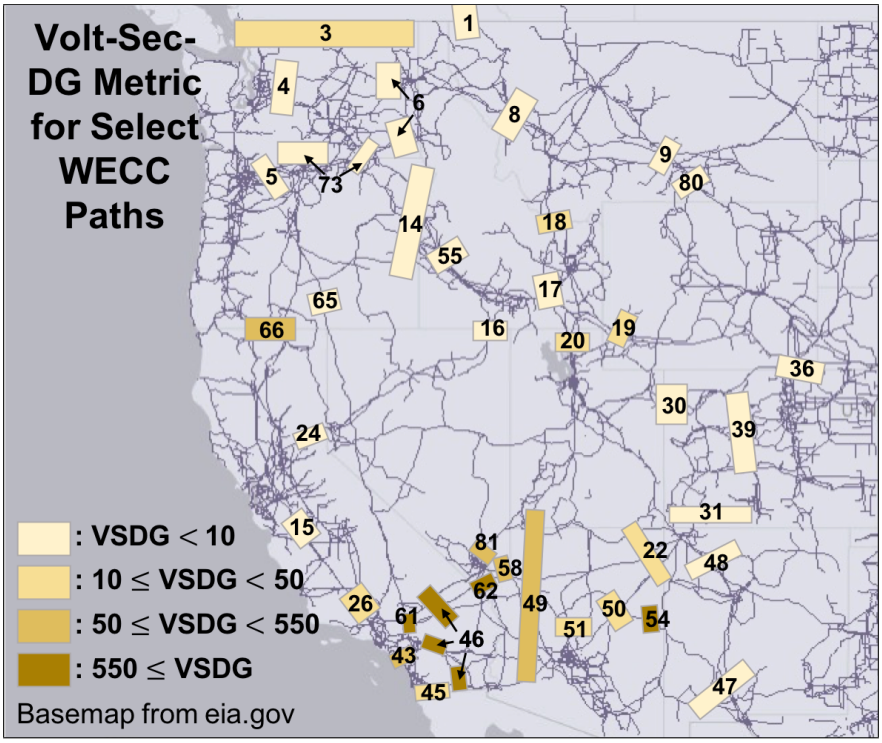

Figure C. Averaged volt-sec-DG scores for select paths of the Western Interconnection

Table A provides the peak reduction in DERs as a function of performance category adherence obtained from modeling. Note that these provide only the magnitude of reduction, whereas the timed loss/recovery is a primary factor to system stability. For instance, the APS result shows equal magnitude reductions for Category I, Category II, and Category III. Not captured by these results is that for Category III, nearly half of the output reduction occurs 10 seconds into the simulation, as opposed to nearly coincident reduction with the fault for categories I and II (see Figure 38). The equal magnitudes are the result of an extreme fault-induced delayed voltage recovery (FIDVR) event that depresses the voltages for much longer than all evaluated ride-through criteria. The simulations for SCE show a more typical FIDVR-type response to the fault, where the time for the near-full recovery of the power system was about 30 seconds. The magnitude of changes in the amount of DER generation for the given fault showed that the applied IEEE 1547 ride-through performance category plays a significant role in potentially limiting the amount of DER generation ultimately tripping offline.

Table A. Peak Distributed Energy Resource Real Power Reduction by Performance Criteria

Location: Faulted Path	2003	2018 Category I	2018 Category II	2018 Category III
Xcel: Path 36	130 MW	100 MW	100 MW	80 MW
APS: Path 54	1,390 MW	1,330 MW	1,330 MW	1,330 MW
SCE: Path 61	4,000 MW	2,550 MW	2,340 MW	1,500 MW

Key Findings

The key findings of this research effort are summarized in the following six bullet items:

- Under heavy loading conditions representative of summer peak load in the Western Interconnection, the potential for widespread influence on voltage profiles following a transmission-level fault is significant. This highlights the potential for large losses of DERs depending on the implemented low-voltage ride-through criteria. Even with this large influence, however, the colocation of the fault with high DER penetrations is the primary factor when considering potential generation losses caused by faults (see the magnitude differences between the Colorado Front Range and Southern California cases in Table 16).
- The newly introduced volt-sec and volt-sec-DG metrics provide suitable analysis tools for making relative comparisons of the influence of a variety of transmission-level faults on the overall power system voltage profiles. In particular, the volt-sec-DG metric effectively highlights the relative impact of these faults on potential DER loss.
- The specific performance of DERs during fault conditions can have a large impact on the recovery of the power system. This highlights the importance of understanding the true operation of inverter-based generation during power system transient events and the need for improved models.
- FIDVR events generate persistent low-voltage profiles at distribution voltage levels, which can in some instances persist beyond the trip times specified in the IEEE-2018 ride-through criteria, leading to the loss of DER generation.
- The IEEE 1547-2003 standard allows for a nearly immediate momentary reduction in the power output of DERs for relatively small voltage deviations from nominal, which can potentially result in a large loss of generation. For instance, the large penetrations of DERs in California lead to a nearly 4 GW loss of generation for specific faults in Southern California. Other interpretations or implementations of IEEE 1547-2003 could allow significant voltage ride-through capability, greatly reducing this potential generation loss.
- Performance categories I and II from IEEE 1547-2018 yield similar aggregate DER real power responses and similar overall system recovery characteristics. Implementation of the Category III ride-through criteria of IEEE 1547-2018 yields respectively smaller total real power output reductions.

Table of Contents

List of Figures

List of Tables

1 Introduction

1.1 Background

As the penetration level of distributed energy resources (DERs) increases, it has become apparent to power system operators that the traditional assessments of dynamics and stability must be revisited (Distributed Energy Resources Task Force 2017). Although the current DER penetration level in the United States is 2% of installed generating capacity (19 GW of approximately 1 TW), in 2016 13% of new capacity additions came from DERs, at 3.4 GW (Federal Energy Regulatory Commission 2018). These growth rates vary substantially depending on the region, with some regions experiencing little growth, and other regions—such as the California Independent System Operator (CAISO), which had more than 7,500 MW online (15% of historic peak demand) as of 2016—experiencing significant growth. In addition to the load-balancing challenges associated with DERs operating under limited visibility (Bravo et al. 2015), anticipating the response of DERs to system disturbances has become problematic, particularly with regard to the time-dependent ride-through performance as defined in the Institute of Electrical and Electronics Engineers (IEEE) 1547 standards, both the 2003 and 2018 versions.

DER growth is creating a generation shift from fewer large synchronous sources to a set of smaller asynchronous, power electronics-interfaced generators (Federal Energy Regulatory Commission 2018). The former affords a simpler analysis of system disturbances, particularly during faults, when synchronous generator dynamics are primarily dictated by the physics of rotating machinery and electromagnetic coupling. Inverter-interfaced generation responses, however, are a mix of power electronics physics, control system characteristics, measurement fidelity, and manufacturer programming (North American Electric Reliability Corporation 2017; Bravo et al. 2015; North American Electric Reliability Corporation, 2018a; Plet and Green 2014). The sheer quantity of inverter-interfaced generation, combined with manufacturer diversity and varying interpretations of interconnection standards, has instilled a gap in understanding the aggregate response of DERs to power system disturbances (Bravo et al. 2015). Herein lies the primary impetus for this study.

Within the Western Interconnection, there have been multiple transmission faults resulting in the loss of transmission-connected photovoltaic (PV) generation because of power electronics-based grid interface characteristics (North American Electric Reliability Corporation 2017, 2018a). The 2016 Blue Cut Fire caused multiple system faults with resultant PV loss, the largest at nearly 1,200 MW (North American Electric Reliability Corporation 2017). In 2017, the Canyon 2 Fire in Southern California caused transmission-level faults, with one causing a 900-MW loss of PV (North American Electric Reliability Corporation, 2018a). Recognizing this causal relation, Southern California Edison (SCE) and CAISO then positively identified 11 instances when a transmission fault caused significant PV generation loss within the SCE territory during a seven-month period between August 2016 and February 2017 (North American Electric Reliability Corporation 2017). Although these example events involve predominantly transmission-connected PV, they are demonstrative of the need to better understand, plan, and coordinate the responses of power electronics-interfaced generation systems. Distribution-connected PV generation (i.e., the majority of DERs) deserves similar treatment because it is also a considerable and growing generation source, as previously stated. The current credible generation contingency on the Western Electricity Coordinating Council (WECC) system is the loss of two Palo Verde units at 2,740 MW (North American Electric Reliability Corporation 2002; Distributed Energy Resources Task Force 2017). Considering current DER current penetration levels and growth rates, it is possible that a worst-case WECC contingency could soon come in the form of a transmission-level fault causing DERs to trip offline. Thus, this study seeks to improve the modeling and understanding of DER response to regional voltage events to properly identify DER requirements and avoid DERs becoming a large contingency.

Figure 1 is a voltage mapping of all buses contained within the WECC model. The data set represents the per-unit (p.u.) voltages 100 ms (six cycles) after initiation of a three-phase fault on the Shultz 500-kV substation of WECC Path 4 (faulted bus identified by yellow rings in the figure). The set is normalized to show only buses with voltages that dipped to less than 0.95 after the fault—i.e., any bus less than 0.95 in the simulation before the fault initiation is not displayed. With this figure, we recognize that transmission-level faults can significantly alter the terminal voltage of DER units over large areas (Mohammadi, Moradi, and Leborgne 2017; Electric Power Research Institute

2016; Heine and Lehtonen 2003), which can potentially lead to a large loss of generation (North American Electric Reliability Corporation, 2018b). For this reason, we developed metrics that quantify the overall voltage influence of a fault on a transmission system to better grasp the potential DER loss as a result of a transmission-level fault.

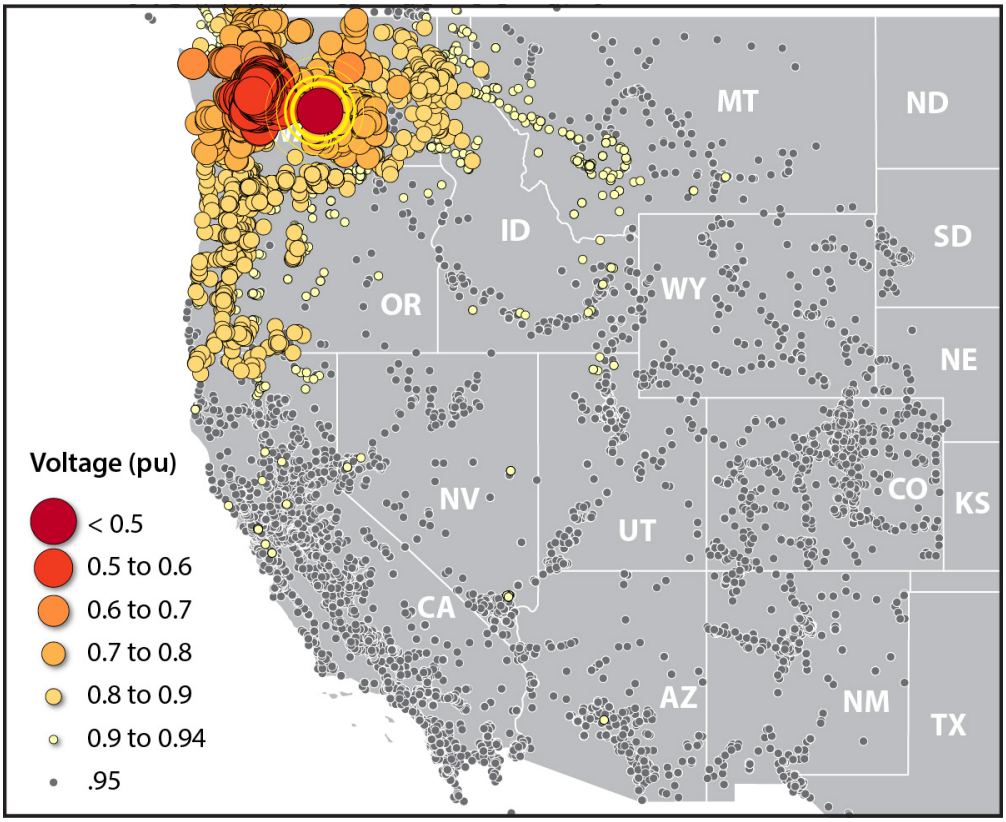

Figure 1. Path 4 voltage GIS mapping

This study departs from the traditional paradigm of in-depth frequency analysis of transmission-level contingencies and instead focuses on the overall system voltage response. Because the intention is to derive an anticipated DER response based on IEEE 1547 compliance, a focus on the system voltage is necessary because even slight deviations (dips less than 0.95 p.u.) can cause DER tripping and result in a significant generation loss. The *Western Wind and Solar Integration Study Phase 3* (WWSIS-3) found more than 800 MW of DER trips after a fault on the Midway-Vincent segment of Path 26 (Miller et al. 2014). Additionally, it is observed that the cost to the system is nearly 4 Mvar for every megawatt of lost DER, indicating a significant stress on the voltage stability of the system following a coincident fault and significant DER blocking (Miller et al. 2014). This aspect becomes particularly problematic when considering that these low voltages caused by the fault are the root of DER tripping in the first place, essentially yielding a positive feedback loop. As a result, although frequency is a more common metric of analysis for system-wide response to faults, the WWSIS study and our subsequent analysis indicate that a focus on voltage levels is of similar importance.

Although significant effort has been made to make the simulation results as realistic as possible, note that the scenarios investigated are likely not entirely representative of the actual response of the Western Interconnection. For instance, the WECC model used for this study is relatively old and does not include recent transmission upgrades that might mitigate some of the voltage stress seen in the scenarios investigated. The model of WECC does, to our best efforts, represent a realistic dispatch of generators for high wind and solar scenarios, which is why it was chosen. Also, no remedial action schemes were modeled, which could assist in faster frequency and voltage recovery

following a transmission-level fault. This study is not intended to identify an existing reliability concern within WECC, and the studies findings do not support such a conclusion. Rather, this study shows that modeling methods to better understand the impact of DERs on the bulk system are available, and comparisons between DER voltage ride-through performance requirements can be made in relative terms. These comparisons are intended to better inform decisions regarding the implementation of these requirements. Finally, it is the authors' hope that this report is not considered the definitive treatment of the impacts of DERs on the bulk system but instead is a useful document for informing current DER voltage ride-through requirement decisions and a good reference for future work in this research area.

1.2 IEEE 1547: A Brief History

To facilitate and ease the interconnection of DERs of all types requesting interconnection to utilities' distribution systems in the United States, a large working group was formed in the late 1990s within the IEEE Standard Association to develop what became IEEE 1547-2003 (IEEE 1547-2003 2003). This standard has been widely accepted by state commissions and has become the de facto standard for DER interconnection across the United States. Further, language and settings (often with slight adjustments) within this standard have been used to inform or serve as a template for other DER interconnection technical standards in other countries. IEEE 1547-2003 has been very successful in that it has allowed the interconnection of multiple gigawatts of DERs, dominated by PV systems, across the country in a safe and relatively efficient manner. Further, the standard allowed for the development of equipment that meets the requirements of the standard, via (UL 1741 2010), ensuring desired functionality for DER operation in coordination with the interconnected distribution system.

Starting around 2010, the growth in the amount of DER connected to distribution systems and the aggregate of DERs interconnected within a single synchronous interconnection began to increase concerns regarding the limitations of IEEE 1547-2003. The original version of the standard was developed when the total penetration of DERs was quite small and largely dominated by emergency backup systems (e.g., diesel backup systems at hospitals, data centers) and combined heat and power systems. PV systems, in 2003 and earlier, were expensive and not in wide use. Thus, the 2003 standard focused almost wholly on distribution-level concerns caused by DER interconnection such as distribution system protection. This led to an overall philosophy that DERs, under IEEE 1547-2003, would disconnect from the distribution system whenever the system was determined to be under stress (also called abnormal conditions in the standard). For instance, if the voltage or frequency was off nominal, the DER would trip off-line to allow the utility equipment on the distribution system to operate under "normal" conditions as if the DER did not exist. Additionally, voltage regulation of the distribution system using DERs was not allowed.

As the DER market became more economically attractive, DER penetration levels increased on some distribution circuits, and voltage regulation by the interconnected DERs was identified as a potential low-cost option for mitigating the impacts of variable DERs, such as PV systems. Additionally, utilities and system operators began to increase awareness and concern that DERs, in aggregate, could start to have a significant impact on the bulk system if they were to cease operation when the grid was stressed. Studies such as (Miller et al. 2014; Kaestle and Varna 2011) demonstrated the impacts of DERs ceasing operation should the system frequency deviate from nominal because of other contingencies at the bulk system level. These studies and the experience of utilities with relatively high levels of interconnected DERs helped inform initial amendments to the standards. IEEE 1547-2014a (IEEE 1547-2014a 2014) was an amendment to IEEE 1547-2003 but with a few important changes addressing these concerns in a timely manner and largely to allow time for the full revision of the original standard. IEEE 1547-2014a specifically allows voltage regulation by the interconnected DER and greatly increased the flexibility for voltage and frequency ride-through for DERs to enable DERs to support—or at least not disrupt—the bulk system. "Ride-through" denotes the time that a DER continues to operate even when the grid voltage or frequency is off-nominal.

Relatively recently, a full revision of IEEE 1547 was completed (IEEE 1547-2018 2018). IEEE 1547-2018 expands significantly on the 2003 and 2014a version in many ways, but for the purposes of this study the most salient changes relate to two items: (1) the full definition of required voltage and frequency ride-through capabilities and (2) the creation of various performance categories within the standard. These performance categories were created within

the standard because of a desire to maintain the technology-agnostic scope of IEEE 1547 while still acknowledging the various capabilities of the different DER types. For instance, IEEE 1547-2018 has three voltage ride-though performance categories: Category I (Cat I) was developed with consideration of the minimum capabilities of reciprocating synchronous generators, whereas Category II (Cat II) takes advantage of the ride-though capabilities of inverter-based generation. Category III (Cat III) extends the Category II functionality and was developed considering high-penetration DER deployments. Although IEEE 1547-2018 fully defines these performance categories, it is not yet known how these performance categories will be applied to various DERs as governing bodies adopt the new standard and utilities begin to specify required settings. State commissions might not specify different performance categories for different types of DERs and might rather choose a single performance category to apply to their state—resulting in the performance categories not being related to DER technology but instead to the current or future penetration of DERs. Regardless, the new standard presents new options for higher levels of bulk system coordination and support, but it also requires many more technical decisions to be made. IEEE 1547-2003 is a 16-page document, whereas IEEE 1547-2018 is more than 130 pages, which reflects the increased complexity.

For this study, the voltage response characteristics of both IEEE 1547-2003 and the three performance categories of IEEE 1547-2018 are considered. Although the voltage ride-through characteristics from IEEE 1547-2018 are well defined, the specific voltage and timing settings are adjustable. The default settings given in the standard are used in this study, but note that other settings could be required, although it is not clear who would determine the alternative settings. Also, for IEEE 1547-2003, there are no technical requirements for voltage ride-through; rather, there is a requirement that a DER must disconnect from the system no later than a specified time if the voltage is out of range. This is often referred to as a "must trip" requirement. Within this study, the IEEE 1547-2003 voltage ride-though responses are typically divided into pessimistic, meaning that DERs trip off quickly (this might be the case if DER manufacturers want to easily meet IEEE 1547-2003 requirements); and optimistic, where the DERs trip at the limit of the "must trip" limit, effectively providing the maximum amount of equivalent voltage ride-through.

1.3 Simulation Methodology

This study makes use of two distinct simulation programs: the GE Positive Sequence Load Flow (PSLF), which performs balanced transmission-level power flow and dynamic simulations; and OpenDSS, which performs three-phase distribution simulations on distribution feeders. Typically, these two simulators are used in isolation, but in this study post-simulation data hand offs are managed to generate a "manually operated" form of cosimulation. Rather than explicit cosimulation, in which multiple simulations advance together in time with active information hand offs, this study uses an iterative procedure in which the results from one simulation are used to inform a subsequent simulation during the same time frame/contingency. An enumerated approach is given as follows:

1. A complete PSLF Western Interconnection study is performed with shorter simulations to locate transmission-level faults of interest that pertain to the location/utility territory of interest: (Arizona Public Service (APS), SCE, and Xcel.
2. The faults selected are resimulated with PSLF to the chosen full length (30 seconds), from which voltage profiles of all DERs containing composite load models with generation (CMPLDWG) are extracted in a quarter-cycle time series.
3. These voltage time series are used an input to distribution simulations using OpenDSS. These simulations determine a feeder's expected time-varying voltage profile given a feeder head voltage profile as determined by the initial PSLF simulation. These feeders are populated with inverters (50 single-phase inverters randomly placed) compliant to a select type of IEEE 1547 criteria. The aggregate output of these inverters, which varies because of the feeder head voltage profile, is used to generate output commands for the DERs in the PSLF simulations.
4. The PSLF fault simulations are reperformed, but the output of the DER is now commanded by the OpenDSS results. *In this way, a granularity and timing aspect not managed in PSLF is provided to the PSLF simulation*.

Instead of aggregate models, the response of thousands of individually modeled DERs to their specific observed voltage is modeled. Additionally, the time-dependent ride-through capabilities of each DER is modeled at dynamic solution time scales but with distribution modeling tools that then pass the results to PSLF.

5. If the system response is substantially different, particularly with respect to voltage levels, then steps 3 and 4 are rerun with the new voltage time series. This serves as an iterative approach to determine a better tuned system response to the type of 1547 criteria under investigation.

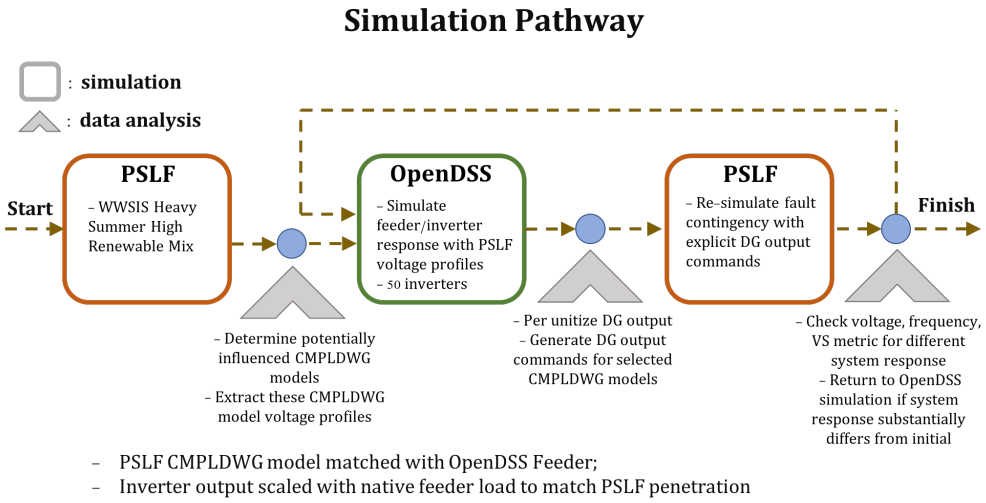

Figure 2. Simulation flowchart

An overall simulation methodology is depicted in Figure 2. The simulations are represented and briefly described by the rounded-edge boxes, and the data analysis/extraction are indicated by the chevrons. When applicable, the recursive approach between the OpenDSS and distribution-informed PSLF simulations is represented by the feedback loop. The figure shows the chronological order of simulations as previously enumerated.

1.3.1 Tips for Reading This Report

A large amount of information is presented graphically in this report, and keeping track of what is presented can become challenging. With this in mind, the authors have taken steps to streamline and standardize the charts to make the report as easy to read as possible. In particular, two coloring schemes are implemented to convey the material being presented. First, all data curves presented for the five different IEEE 1547 criteria as well as the initial PSLF simulation results are given a specific color for all plots in the report. The color convention is as follows:

Data Curve Coloring

- **Black:** data from the initial PSLF simulations with no distributed generation commands
- **Red:** IEEE 1547-2003 pessimistic interpretation simulation results; either OpenDSS- or OpenDSS-informed PSLF simulations
- **Blue:** IEEE 1547-2003 optimistic interpretation simulation results; either OpenDSS- or OpenDSS-informed PSLF simulations
- **Yellow:** IEEE 1547-2018 Category I simulation results; either OpenDSS- or OpenDSS-informed PSLF simulations

- **Purple:** IEEE 1547-2018 Category II simulation results; either OpenDSS- or OpenDSS-informed PSLF simulations
- **Green:** IEEE 1547-2018 Category III simulation results; either OpenDSS- or OpenDSS-informed PSLF simulations. Iteration results are presented in shades of green.

For the second scheme, because the same types of data are presented but for different responses (system frequency, faulted bus voltage, etc), the background of the legend is colored according to the type of plot presented. For instance, all frequency plots have a lime green legend background. The legend coloring convention is as follows:

Legend Background Coloring

- **Royal Yellow:** aggregate distributed generation output plot of affected CMPLDWGs pertinent to simulation
- **Lime Green:** overall system frequency plot, calculated per Appendix 6.2
- **Jade:** running volt-sec metric plot
- **Beige:** faulted substation voltage profile in per unit.

These conventions are upheld throughout the report, and they become especially helpful in chapters 3 and 4 when a variety of system results for different IEEE 1547 scenarios are presented. Although the reader can identify the charts from these two color schemes alone, the charts are also labeled with the requisite information for identification presented in each title.

2 Transmission System Simulations

The bulk power system transmission simulations were performed with the GE PSLF software (Version 21 GE Energy Consulting, n.d.). PSLF models AC power flow for steady-state analysis and dynamic simulations. The dynamic model templates used for PSLF are highly detailed, and individual models used for existing generation in the Western Interconnection are generated directly by the generator owners; these parameters must be certified before integration with the working Western Interconnection model (Zhu et al. 2018). PSLF operates under the symmetrical component theory, which transforms three-phase circuits into positive-, negative-, and zero-sequence components. Under the assumption of a balanced system, the negative- and zero-sequence components can be assumed to be negligible and thus are not modeled, significantly reducing the computational complexity. Because of a near-balanced state in most transmission systems, the error in this assumption is minimal. This study makes use of the Western Interconnection model, which is kept up to date and used by WECC for stability studies.

2.1 Simulation Specifics

The specifics of the power flow case and transmission simulation methodology are provided in the following subsections.

2.1.1 Western Wind and Solar Integration Study

For the WWSIS study, WECC planning cases were modified to reflect high-renewable penetrations for system loading at particular times of the year (Miller et al. 2014). For this study, we used the Heavy Summer High Mix 2023 power flow case from the WWSIS study, which has a high penetration of renewables (see Table 1 for the specific renewable penetration levels). For the WWSIS study, the load on the system was determined via scaling the actual system load with accepted load growth values. The specific original WECC planning case used a base load from August 25, 2012, at 13:20 PT. Because distributed generation, which is colocated with load and acts as a negative load, was added to the system for the High Mix case, the net load on the transmission system is reduced with respect to the Low Mix case. The specific loading on the system at the time of this load flow is suitable for this study because at near high noon, a peak in the distributed generation is anticipated, making this an appropriate time to assess the impacts of DER ride-through capabilities. Note that although we use this power flow for our study, it is not necessarily the full dispatch of distributed generation on the system. This dispatch was acquired through PLEXOS modeling paired with historical weather data, which indicates that distributed generation output in some areas is reduced because of weather. We did not look further into this aspect, and we simply proceeded with the distributed generation outputs as found in the WWSIS study.

2.1.2 Composite Load Modeling

For the WWSIS study, 70% of the system load was represented with the CMPLDWG dynamic model. This changed the loading from static (i.e., a ZIP model consisting of constant impedance, constant current, and constant power load fractions) to one that contains four motor models, a substation transformer, an equivalent feeder circuit impedance, and an electronic load in addition to a static load. See Figure 3 for the CMPLDWG topology. The fractional representation and associated parameters were developed for the WWSIS study based on WECC information; these parameters were not adjusted for this study. In addition to the loading, a PV distributed generation component is included, which was represented within the CMPLDWG by the PVD1 model. In this study, the distributed generation contributed only real power, acting as a negative load on the far end of the feeder in the CMPLDWG model. The operation of this aggregated distributed generation is dictated by the PVD1 model, which is presented in detail in Appendix 6.1. The low-voltage ride-through of the distributed generation in the CMPLDWG is dictated by two parameters, Vt0 & Vt1, set to 0.7 and 0.8 p.u., respectively, for all models. Vt1 is the voltage at which the distributed generation output began to be fractionally reduced, and Vt0 is the voltage at which all distributed generation was

Table 1. WWSIS WECC Heavy Summer High Mix Case

Devices	Quantity
Buses	21,184
Generation sources	4,578
Composite loads	4,398
Composite loads w/nonzero distributed generation	3,549
Generation Source	Real Power (MW)
Wind	14,339
Utility-scale solar	11,194
Concentrating solar power	6,642
Distributed solar (CMPLDWG)	8,951
Conventional sources	162,700
Renewable penetration	20%
Load Type	Real Power (GW)
Composite	143.9
Non-composite/static	48.2
Synchronous motor	1.8

offline. The fraction of distributed generation reduction was determined by the slope between 100% at Vt1 and 0% at V0. The recovery of the distributed generation was immediate, meaning for any voltage between Vt0 and Vt1, the corresponding fraction of distributed generation was immediately back online, and once the voltage was above Vt1, full output was restored. This model of operation glosses over likely important characteristics and nuances of distributed generation operation, and hence it is one of the impetuses of this study. For the initial transmission studies, these parameters were maintained in accordance with the WWSIS-3 study of Vt0 = 0.7 and Vt1 = 0.8.

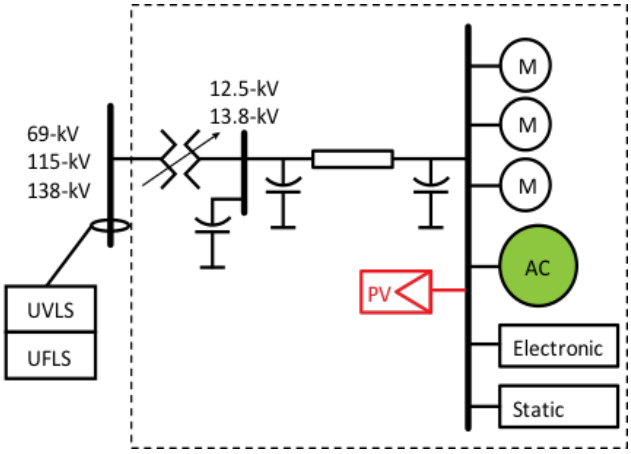

Figure 3. CMPLDWG

An important aspect of the CMPLDWG model is the fourth motor model, which is intended to represent the operation of residential air conditioners (e.g., single-phase AC units with motor-stalling characteristics). During low-voltage conditions, residential air-conditioner compressors will stall within a few cycles, which generates a reactive power demand 5–8 times greater than steady state (Bravo et al. 2015; Bravo and Chassin 2016). This spike in reactive power demand leads to the traditional fault-induced delayed voltage recovery (FIDVR) response in parts of the WECC model. Before the CMPLDWG was adopted, FIDVR responses—although recorded many times by phasor

measurement units on the Western Interconnection (Abed and Salazar 2014)—were not reproduced by PSLF simulations. With the integration of the CMPLDWG model, FIDVRs are now modeled with PSLF for faults in certain locations, as shown in the Path 61 and Path 54 studies (see Sections 2.3.2 and 2.3.3). These FIDVR events are of particular interest because the prolonged low voltages could lead to more extensive distributed generation tripping.

Figure 4 is a mapping of all distributed generation located at the CMPLDWG models throughout the WECC system, with output and penetration representing the current states in the Heavy Summer power flow case. The size of the circle indicates the megawatt quantity of distributed generation located at that bus, and the color captures the penetration level with respect to the native load at this particular moment in the load flow. The aggregate of all distributed generation represented in this figure is 8,951 MW, as stated in Table 1. This photo is included to provide the reader with an understanding of both the granularity of load/distributed generation modeling in the simulation as well as the location-specific output and penetration of the distributed generation in the system. Note that the penetration numbers given in the figure are calculated using the existing loading of the WECC case and are not calculated using the annual peak load value for each node of the system. The stated penetration values can be thought of as instantaneous penetration of DER. For instance, the penetration in Phoenix is less than Salt Lake City, but there is a large amount of residential air-conditioner load in Phoenix, which decreases the instantaneous penetration because of a higher native load. Clearly, the majority of distributed generation is located in California, Nevada, Arizona, and New Mexico, although a nontrivial amount is found in almost all load locations.

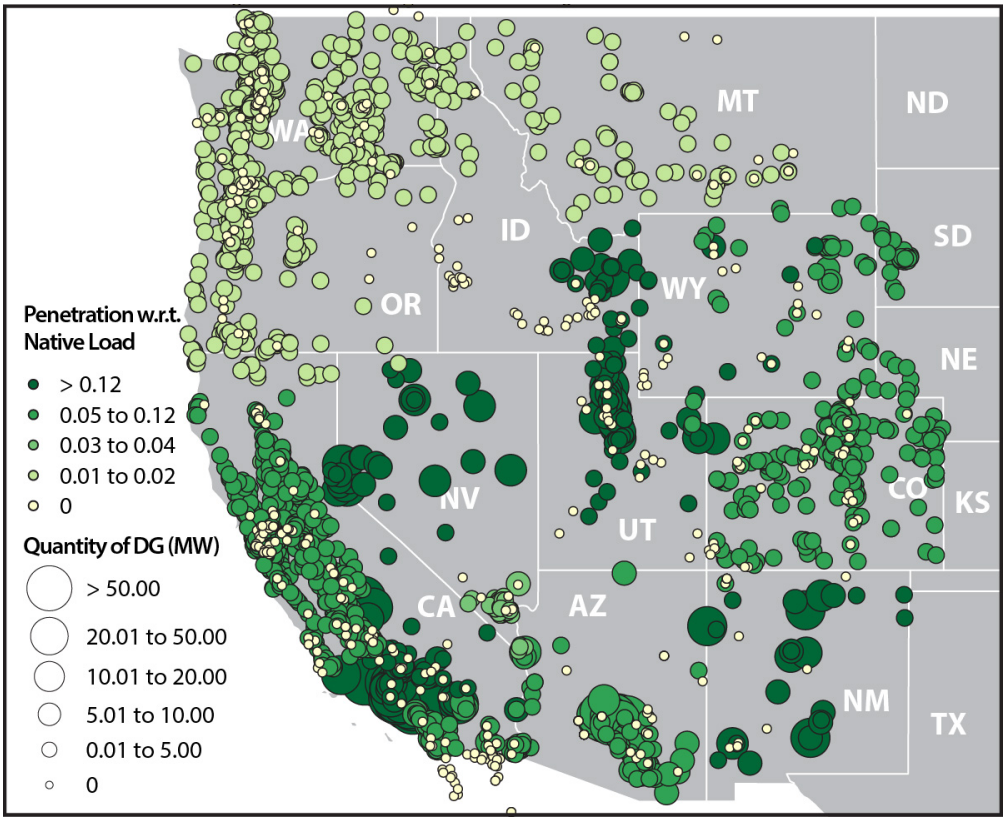

Figure 4. GIS map of CMPLDWG models and distributed generation output

2.1.3 Fault Characteristics and Implementation

The methodology regarding fault implementation was adopted directly from the WWSIS-3 study and, in particular, from the section of the study focused on Path 26. For this analysis, a three-phase bolted fault (Z = 0 + j0) is implemented close to the Vincent 500-kV substation, which is cleared six cycles (0.1 second) later with both 500-kV lines between Midway and Vincent switched out of service (Miller et al. 2014). For a sensitivity analysis, the fault reactance is increased incrementally until a traditional FIDVR event is observed (see the initial dispatch curve in Figure 5). This occurs at a fault impedance of Z = 0 + j0.0375, which is stated as a proxy for a single-phase fault in the WWSIS study (Miller et al. 2014). For this study, the same fault implementation procedure is followed, with subsequent line tripping occurring at the time of fault clearing. For the case of double circuits, as in WWSIS, both circuits are tripped.

To validate the model and approach, the authors re-created the scenarios found in the WWSIS study and compared results. All comparisons were found to be satisfactory, indicating that the model and simulations were operating correctly using the results from the WWSIS as a baseline. One change that occurred between this study and WWSIS was an upgrade in the PSLF version. WWSIS used Version 18 of PSLF, but at the time of this study, Version 21 was available and the upgrade was made. Upon adopting the most recent version (with no changes to the power flow or dynamic models), it was found that a reduction in fault reactance was necessary to generate the same WWSIS FIDVR response for a fault at the Vincent substation (i.e., the reference fault evaluated). With a slight reduction in reactance, the impedance used for this study is:

$$Z = 0 + j0.034 \tag{2.1}$$

For all simulations, the system response is evaluated for 1 second following initialization with no disturbances at a quarter-cycle time step. One second into the simulation, the fault is implemented, which is then cleared at 1.1 seconds (six cycles) with associated line tripping emulating the clearing of the fault. The simulation is then continued for an additional 28.9 seconds, rounding out a 30-second total duration simulation. This is the PSLF process for the bulk of this study, except when initial exploratory simulations were performed to identify faults of interest based on the metrics explained in sections 2.2.2 and 2.2.3. For these investigations, the simulations were terminated after 6 seconds for two reasons: the majority of the simulations had returned to steady-state conditions after 6 seconds, and the computation time of the large number of fault scenarios investigated (400 in total) with full 30-second simulations was cumbersome.

2.1.4 Once-Through Cooling Redispatch

Within CAISO, some generators have been shuttered because of once-through cooling compliance since the WWSIS study was completed (California Independent System Operator, n.d.). In an effort to adjust the initial model to better reflect the current system, once-through cooling adjustments were made to the WWSIS Heavy Summer case. Essentially, generators that were closed were physically decoupled from the Western Interconnection system by removing the relevant tie line. The lost generation was recovered by increasing the dispatch of nearby generators with available headroom. A summary of the generators removed from the simulation is provided in Table 2. This list is not comprehensive of all once-through cooling closures because many occurred prior to the development of the WWSIS models and were already reflected in them. Additionally, the San Onofre Nuclear Generating—a generator that is no longer in operation—is present in the model, but it was not dispatched in the power flow case selected.

Figure 5 shows voltage magnitude profiles at the Vincent 500-kV substation of Path 26 for two separate simulations. The first shows a FIDVR response matching the WWSIS-3 results, which is a corroboration of an appropriate simulation implementation for this study. The second shows the voltage response for the same fault simulation but after the once-through cooling redispatch measures. Although no specific analysis was performed to determine the change in responses, it is speculated that the increase in generation electrically closer to the loads fed by Path 26 reduces the real power flow on this interface. A decreased real power flow serves to reduce the reactive power consumption of the interface, allowing for a larger reactive power reserve, which mitigates the FIDVR event.

Table 2. Once-Through Cooling Adjustments

Station	Unit	Output Reduction (MW)
Moss Landing	6	750
-	7	750
Pittsburgh	7	640
Humboldt Bay	1	66
	2	66
Morro Bay	4	330
Total redispatch	N/A	2602

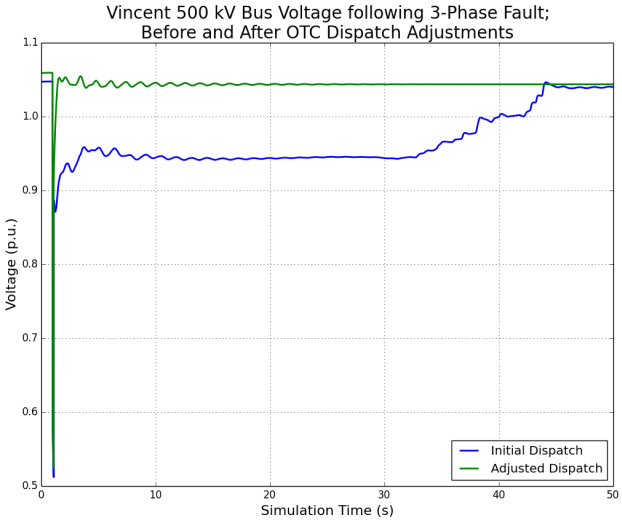

Figure 5. Faulted voltage profiles on the Vincent 500-kV substation

2.2 Finding Faults of Interest

The Western Interconnection is one of four synchronous AC power system interconnections covering North America; the others are the Eastern Interconnection, Quebec Interconnection, and the Electric Reliability Council of Texas. The Western Interconnection covers 14 states of the United States, and it is partitioned roughly where the Great Plains and the Rocky Mountains meet. It includes the Canadian provinces of Alberta and British Columbia as well as a small portion of Mexico on the Baja California Peninsula. A population close to 80 million is served by the Western Interconnection bulk power system, which consists of approximately 120,000 miles of transmission lines and reaches a peak demand in the vicinity of 150 GW in the summer, as of 2016 data (Western Electricity Coordinating Council 2016).

The spatial diversity of load and generation on the Western Interconnection bulk power system yields simple partitions into 38 balancing authority areas, between some of which are interties conducting bulk interarea power flow (Western Electricity Coordinating Council 2016). These interties are known as paths and range from 0.5 mile (Path 62) to nearly 2,000 miles in length (Path 65, the Pacific DC Intertie). Of the 66 Paths in the Western Interconnection, most are single/double circuits between two, three, or four substations operating at 230/345/500 kV. Paths are critical components of the Western Interconnection, and remedial action schemes are often implemented to ensure stability following path contingencies (Xu and Vittal 2010). Because these paths typically include high-voltage lines, the faults on these paths are expected to yield a large influence on overall system voltages (Romero-L and Gallego 2017). This fact, combined with the criticality of paths, is the impetus for selecting the WECC paths as the set of

operational contingencies of interest for fault simulation analyses.

2.2.1 Volt-Sec/Distributed Generation Metrics

In an effort to evaluate the entire voltage deviation from the normal operating regime (i.e., 0.95–1.05 p.u.) across the entire Western Interconnection, a basic metric was devised to accrue overall voltage deviations for each time step throughout a dynamic simulation. This metric was first introduced in the work by Kenyon and Mather, (Kenyon and Mather 2018). The deviation from a chosen voltage at each bus weights the time interval during which the bus is less than the selected voltage. The aptly titled "volt-sec" metric is defined as follows:

$$VS_t^n = \Delta t \left(max \left\{ 0, v_L - b_n^t \right\} \right) \tag{2.2}$$

$$Volt - Sec = \sum_{t \in S^{sim}} \sum_{n=1}^{N} VS_t^n \tag{2.3}$$

Where:

v_L : voltage capture point (0.95 p.u.)
b_n^t : voltage of bus n at time t
Δt : sample time
N : set of buses in model
S^{sim} : set of time samples.

If applied to simulations with voltage deviations less than v_L, a metric score is generated. If the simulations are of equal time length, these scores are comparable as a relative measure of system voltage response. This metric does not capture the magnitude of individual voltage deviations, e.g., 5 buses 0.1 p.u. less than v_L score the same as one bus 0.5 p.u. less than v_L. By tracking the size of the low-voltage bus set, however, an average voltage response of susceptive buses can be calculated.

Because one interest of this study is to identify high-risk contingencies with respect to distributed generation, a second metric quantifies the risk to aggregate distributed generation on a system during a contingency. This second metric simply weights the contribution of each bus to the volt-sec metric with the quantity of distributed generation (MW) located at each bus. The metric is defined as follows:

$$VSDG_t^n = \Delta t \left(max \left\{ 0, v_L - b_n^t \right\} \right) DG_n \tag{2.4}$$

$$Volt - Sec - DG = \sum_{t \in S^{sim}} \sum_{n=1}^{N} VSDG_t^n \tag{2.5}$$

Where the previous notation holds, and:

DG_n : generation (MW) of distributed generation at bus n.

This metric provides a measure of the overall system voltage deviation at buses where distributed generation is located. Because the distributed generation response in part depends on voltage, high scores for volt-sec-DG might indicate system disturbances affecting a large amount of distributed generation. The volt-sec-DG metric requires a realistic dispatch of distributed generation in the dynamic model for a realistic contingency analysis.

A visualization of these metrics is provided in Figure 6, which shows the voltage profile of the Chevmain 66-kV substation following a fault at the Lugo 500-kV substation on Path 61. In Figure 6(a), the portion of the voltage

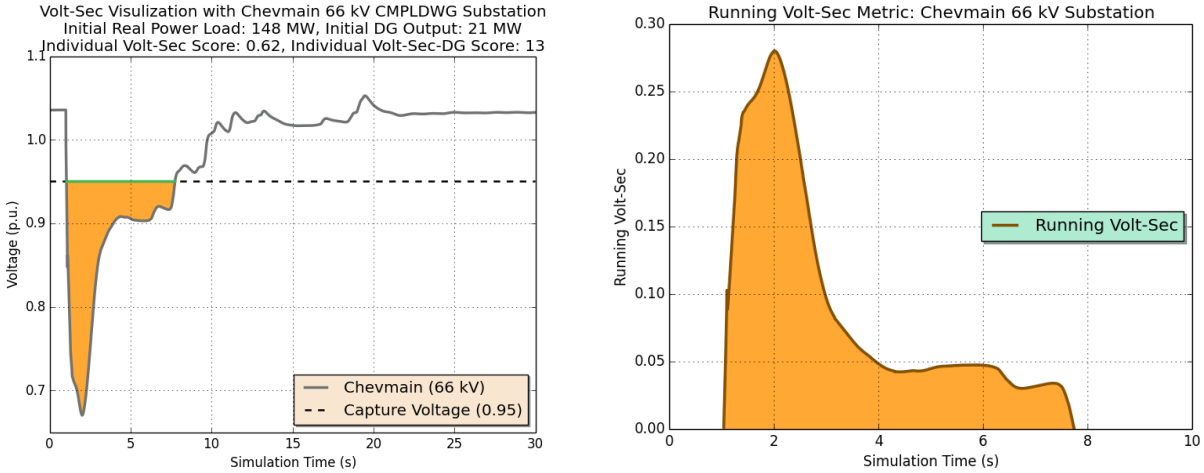

(a) Chevmain 66-kV voltage profile

(b) Chevmain running volt-sec metric

Figure 6. Volt-sec visualization

profile contributing to the volt-sec metric is the part of the green curve less than 0.95 p.u. The overall contribution of this voltage to the volt-sec score is the area shaded orange. This individual volt-sec score is 0.62. A CMPLDWG is located at the Chevmain 66-kV substation with distributed generation output of 21 MW. As a result, this voltage profile individually contributes 12 (0.62 x 21) to the overall volt-sec-DG score. With no distributed generation present, this volt-sec-DG contribution would be zero. Figure 6(b) shows the running volt-sec metric, which is the magnitude of the difference between the bus voltage and the 0.95 cutoff point with respect to time. Essentially, this plots Eq. 2.2 for every time step of a simulation. This measure, when applied to the entire system, is used frequently in this report to compare system responses to various simulation criteria. Again, the area shaded in Figure 6(b) is the contribution to the volt-sec score, whereas the instantaneous value is the contribution to the running volt-sec metric.

Using these metrics, the fault simulation methodology was implemented on all lines of all defined paths of the WECC system. For each line, two simulations are performed: one for a fault at each bus with the same connecting line tripped in each simulation (e.g., a single-line path will introduce two simulations). As explained in Section 2.1.3, these simulations model 6 seconds of total power system operation, with the fault occurring 1 second into the simulation. By maintaining an equal length for each simulation, the scores of the volt-sec and volt-sec-DG metrics are comparable on a relative scale. Four hundred simulations were performed across the entire Western Interconnection, and the results are presented in the following two sections. From these results, specific fault scenarios are selected for further studies based on impact and location.

2.2.2 Volt-Sec Results

With volt-sec scores of the 400 fault simulations performed on the Western Interconnection, a sorted score distribution of the results was created. The associated percentage with each simulation score indicates the percentage of simulations that scored higher on the volt-sec metric. The scatter plot in Figure 7 shows this distribution with volt-sec scores displayed as green dots. More than 90% of the simulations (360 simulations) scored very low with respect to the most severe scoring fault scenarios. Approximately 5% of the simulations scored quite high with respect to the others, which indicates that the simulations either exhibited prolonged low voltages for a relatively small set of buses or a more spatially diverse voltage depression of lower magnitude. Because the Path 66 and Path 3 simulations diverged, these results were not included in Figure 7. Note that remedial action schemes were not included in the model, and failure of a simulation to converege is not necessarily indicative of an unstable power system condition. It is important to reiterate that these simulations last only for 6 seconds, a timescale too short to tease out traditional

FIDVR with recovery vs. extreme FIDVR with no recovery (i.e., the first 5 seconds post fault will be similar for both).

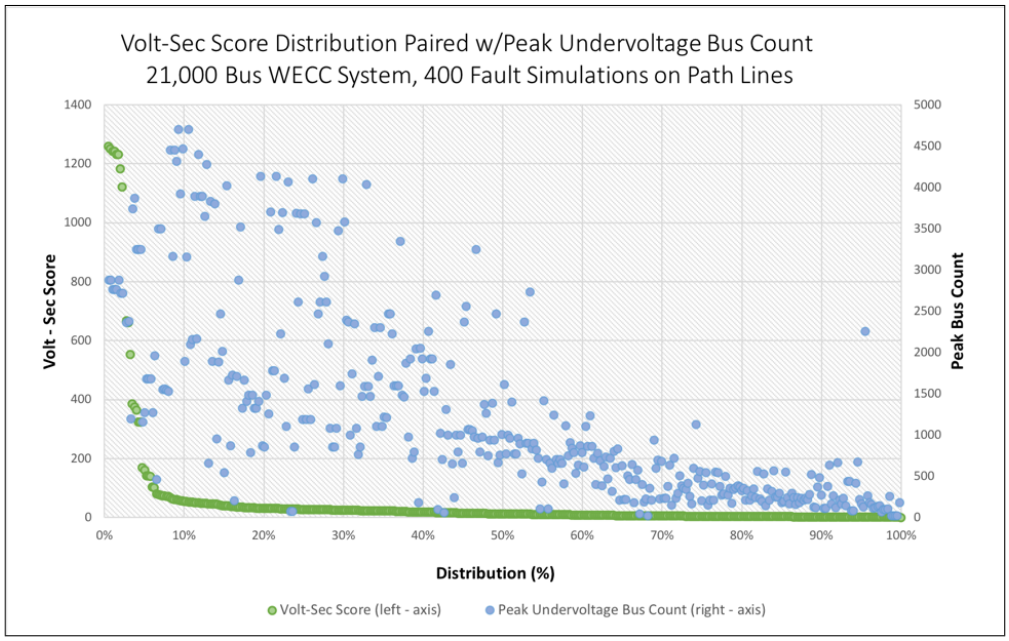

Figure 7. Volt-sec score results

Paired with each volt-sec score data point is the associated peak count of undervoltage buses throughout the simulation (i.e., the largest number of buses less than 0.95) from all time steps in the simulation. This moment occurs almost exclusively at the fault clearing time of 1.1 seconds, six cycles after the fault is initiated. This is also the moment in the simulation that corresponds with the voltage Geographic Information System (GIS) mapping in figures 1, 13, 17, and 21. In fact, the number of buses on the GIS maps without gray coloring is the peak bus count shown above. We can use this pair of data in Figure 7 as an indicator of the temporal extent of the low-voltage event. A smaller peak bus count paired with a larger volt-sec score indicates that the low-voltage event persists relatively longer to accrue such a high score. On the other hand, a small volt-sec score with a large peak bus count implies a shorter duration low-voltage event across a wider area.

Figure 8 shows a map of significant transmission lines within the Western Interconnection. This encompasses most lines of voltages at 115 kV, 230 kV, 345 kV, and 500 kV. Representing WECC path corridors are rectangular blocks that introduce a cut across the transmission lines constituting the path. Note that these blocks might cover non-path lines because of the resolution/size of the rectangular blocks necessary for clarity. As a final method of presenting the volt-sec scores, these representational blocks are shaded according to the average score for the related simulations. For instance, Path 61 is a single 500-kV line, which means that two simulations were performed, with each causing a fault on one of the buses. These volt-sec scores were 26 and 364 at the Victorville and Lugo substations, respectively. Therefore, the Path 61 average is 195, and the block is shaded according to the $50 \leq VS \leq 300$ category. Because many paths have more than one transmission line (more then 10, in a few cases), some of these blocks represent the average value of more than 20 simulations.

The results as plotted on the Western Interconnection system are not unexpected. Areas with large load centers and high residential air-conditioner penetrations score high (Southern California, southern Nevada, Arizona). The results from the Path 66 simulation are presented in this image, although the score is the largest because of system separation. It is initially surprising that the northwest paths incur higher scores, but Figure 1 indicates that the enormous spatial extent of the low voltage is likely the primary contributing factor (these are faults of short duration and large spatial extent). Although these results are interesting, they do not necessarily correlate with impact on distributed

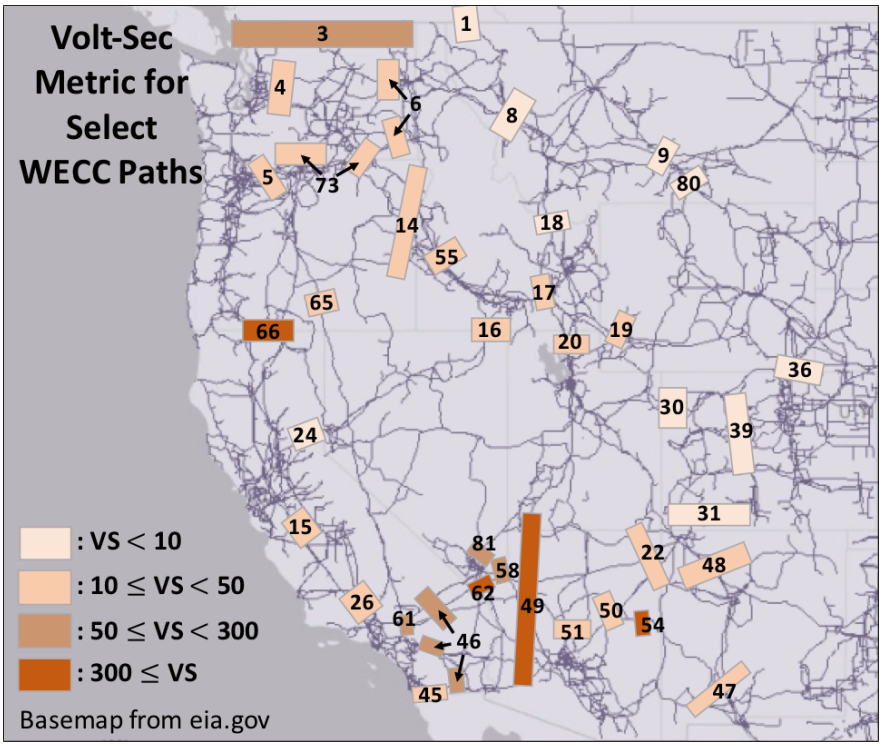

Figure 8. Averaged volt-sec scores for select paths of the Western Interconnection. Score shown by color and path number shown for reference.

generation resources, and therefore they do not specifically guide our selection process. The second metric, volt-sec-DG, will hone in on these faults with high impacts on distributed generation.

2.2.3 Volt-Sec-DG Results

The volt-sec-DG metric, as explained in Section 2.2.3, weights the voltage deviation of each by the megawatt quantity of distributed generation located at that substation. The 3,549 CMPLDWG models containing distributed generation out of 4,398 (and 21,184 substations total) serve to filter the impacts of the low voltages. Figures 9 and 10 are of the same presentation style as figures 7 and 8, with the exception that the peak quantity of the buses is replaced with the peak quantity of megawatts of distributed generation. This provides a snapshot of the peak quantity of distributed generation experiencing a voltage less than 0.95 p.u. during the simulation, which in a worst-case scenario might reflect lost generation if all connected distributed generation experienced a sympathetic, or commanded, trip. These values are on par with those discussed in (Zhu et al. 2018).

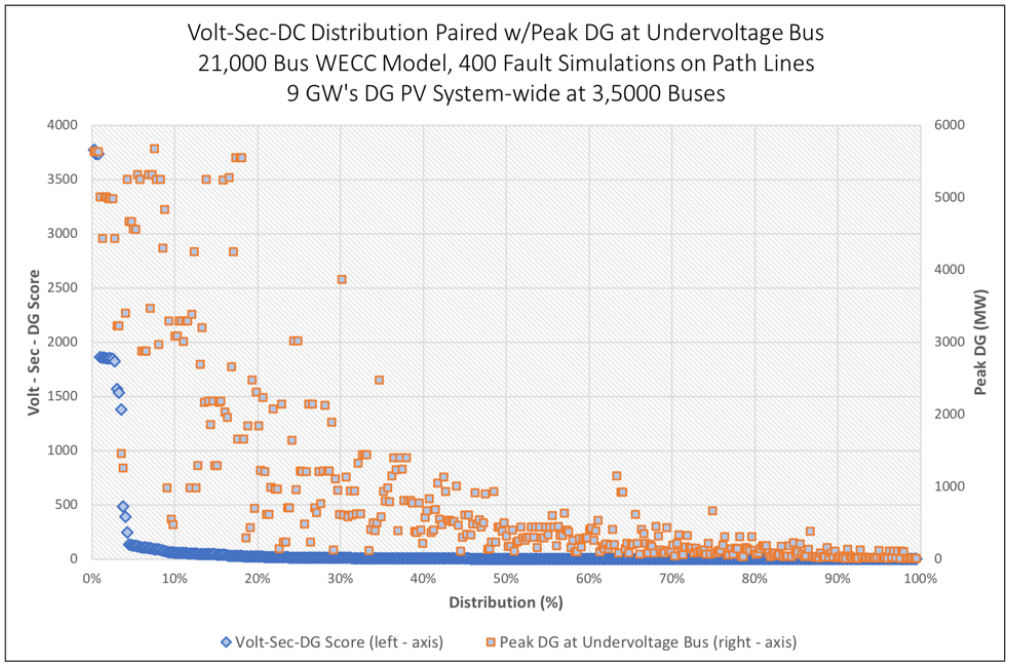

Figure 9. Volt-Sec-DG score distributions

With the attenuation of the distributed generation weighting in the volt-sec-DG metric, the mapping of the paths on which faults influence large quantities of distributed generation, presented in Figure 10, tells a more specific story. We see that the faults on paths in Southern California, southern Nevada, and Arizona influence large quantities of distributed generation, with prolonged low voltages. These results informed the selection of paths in California, Arizona, and Colorado, which have the greatest impact relative to other faults on other paths. Path 36, even though it has a relatively low volt-sec-DG metric, was chosen to inform potential regional impact even in areas without very large amounts of DER. Table 3 summarizes the scores of the fault scenarios selected for study in the remainder of this report. Note that the values in Table 3 for volt-sec distribution and volt-sec-DG distribution are the x-axis values from figures 7 & 9.

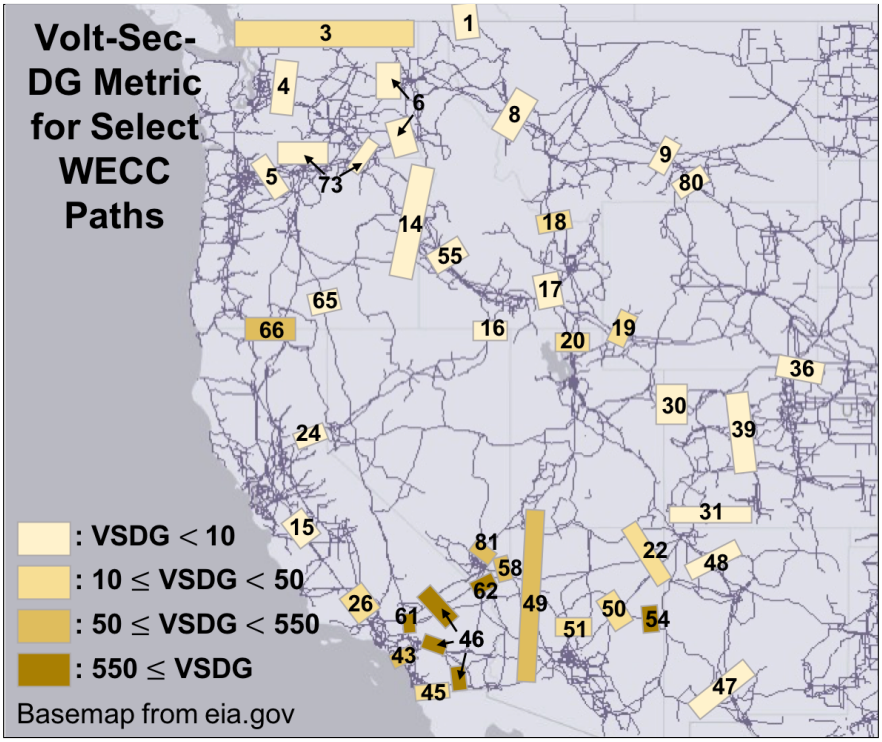

Figure 10. Averaged volt-sec-DG scores for select paths of the Western Interconnection

Table 3. Metric Scores for Selected Faults

Path	Faulted Bus	Volt-Sec Score	Volt-Sec Distribution (%)	VSDG Score	VSDG Distribution (%)
36	Ault 345 kV	11.2	52.8	8.2	31.9
54	Silver King 500 kV	552.0	3.3	1379.7	3.5
61	Lugo 500 kV	363.4	4.0	3769.8	0.0

2.3 Transmission System Simulation Takeaways

With the selected fault scenarios as presented in Table 3, we take a deeper look at the simulations of these three faults. The voltage profile at the faulted bus and the running volt-sec metric are presented along with a novel voltage distribution chart that provides percentile voltage levels pertinent to the quantity of buses with voltages less than 0.95 p.u. GIS bus voltage mappings in the same format as Figure 1 are provided to show the spatial extent of the initial low voltages across the entire system. The overall system frequency, calculated as described in Appendix 6.2, is also presented. Finally, the aggregate distributed generation output of the CMPLDWG models that experience output deviations is provided to show the overall fault simulation influence on distributed generation operation and provide a picture of the amount of distributed generation to be simulated on distribution feeders in the second phase of this study.

2.3.1 Xcel Territory: Path 36—Ault 345 kV

Along the border between northern Colorado and Wyoming are seven transmission lines, ranging from 115 kV to 345 kV, sourcing power to the greater Denver area. These lines constitute WECC Path 36. The path rating is 1,680 MW for north-to-south flows. During summer conditions, the path operates at more than 75% of the limit 43.0% of the time and at more than 90% for 4.2% of the time (Western Electricity Coordinating Council 2016).

The 345-kV line between the Ault (Colorado) and Laramie River (Wyoming) substations is part of Path 36, and this line is selected—because it has the highest metric scores of all lines in the path—for the analysis of the distributed generation response behavior in the Xcel Energy service territory. At the time of the fault implementation in the Heavy Summer High Mix power flow, the power flow on this line is 590 MW from Laramie River to Ault.

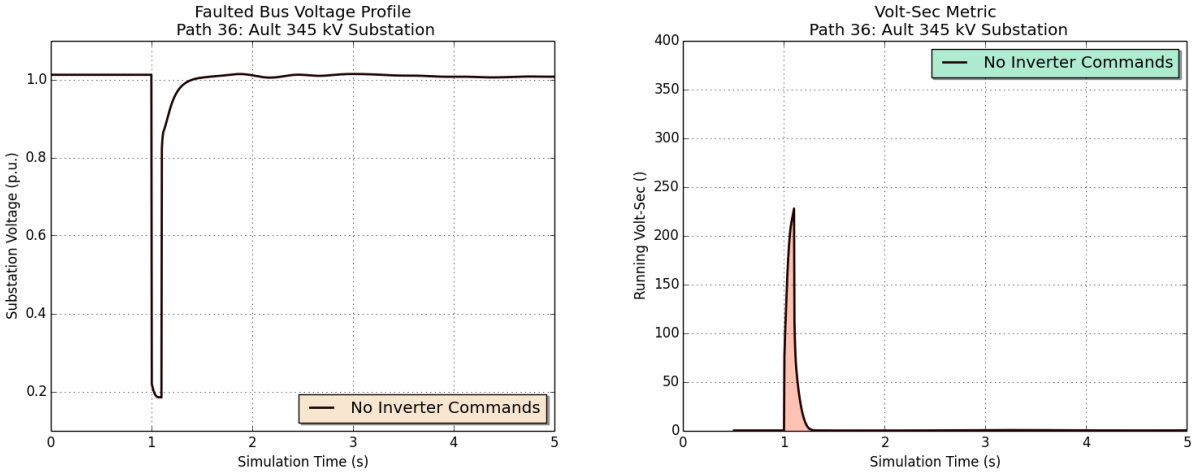

(a) Ault 345-kV voltage profile

(b) Running volt-sec metric

Figure 11. Path 36 bus voltage and volt-sec metric

The system response to the standard fault implementation is representative of a relatively weak grid response with rapid recovery. The faulted bus profile dips to a very low voltage during the fault, but recovery to within 5% of normal voltage levels occurs within 300 ms following the line clearing. The overall system voltage response can be understood from Figure 11, which is the running volt-sec for this fault scenario. Note the relatively high score of roughly 200 during the fault, which rapidly returns to zero following the fault clearing. The zero value indicates that all buses have returned to voltages greater than 0.95 p.u. The largest score a single bus can contribute to the running volt-sec is 0.95 (which indicates a voltage of zero and is unrealistic except for the faulted bus and a zero impedance fault, which means most buses will contribute much less), so we know that at least 400 substations have voltages less than 0.95. In fact, Figure 12 shows that slightly more than 900 buses have voltages less than 0.95 p.u. at the time of the fault clearing.

Figure 12 shows a percentile distribution of all buses with voltages less than 0.95. Although it is hard to decipher in this figure, there are percentile curves within the red envelope that match the 20%, 50%, and 80% of the buses less than 0.95. For such a rapid response, this chart does not provide much information because the recovery is so quick. For the Path 61 and Path 54 scenarios, however, this type of chart provides a significant amount of information regarding the overall voltage recovery of system. Regardless, we can ascertain from Figure 12 that all buses recover to near prefault voltage levels very quickly.

Figure 13 provides a GIS mapping of the system voltages for the moment the fault is cleared in the Path 36 scenario. Although no precise information is derived from this map, it provides a good picture regarding the extent of the low voltages with respect to geographic location/service territory. As expected, the low voltage is primarily in Colorado, with the severe voltage deviations occurring in the north-central part of the state. Because this moment in the simulation is when the peak number of buses are experiencing voltages less than 0.95 p.u., we can assume that the low-voltage geographic extent presented contains all buses that remain less than 0.95 p.u. throughout the simulation. Some exceptions to this assumption might occur, but for a general understanding of the fault scenario, it is suitable.

To complete the system response snapshot, Figure 14(a) provides the overall system frequency throughout the sim-

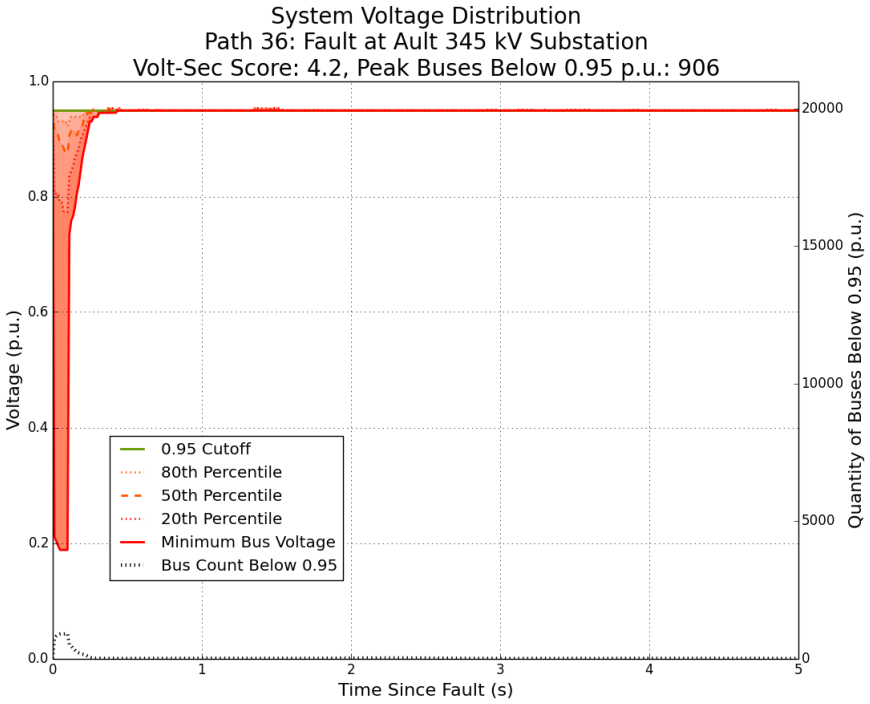

Figure 12. Path 36 low-voltage distribution

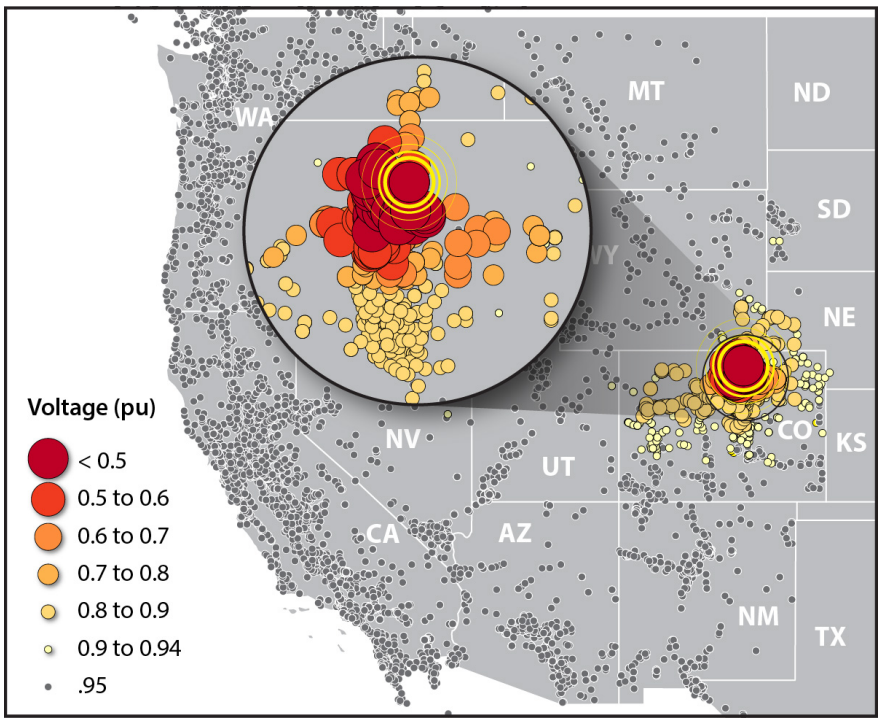

Figure 13. Path 36 low-voltage bus GIS mapping

ulation (see Appendix 6.2 for frequency calculation methodology). The system frequency shows a very minimal deviation from 60 Hz, with the rise in frequency attributable to voltage-dependent loads decreasing in real power demand on account of the brief low voltage. The load imbalance results in a frequency increase in accordance with the swing equation. Finally, Figure 14(b) shows the aggregate response of distributed generation in accordance with the CMPLDWG parameters: a brief decrease in output on account of the low voltage, with an immediate recovery following a return to normal voltage levels. This curve represents only the aggregate distributed generation at significantly affected substations. Thus, a peak of only 130 MW of aggregate affected generation is plotted instead of the approximately 9 GW of distributed generation on the entire system. Table 4 provides a compilation of pertinent statistics for this particular path, including the number of CMPLDWGs comprising 130 MW of distributed generation as well as the total native load at these CMPLDWGs.

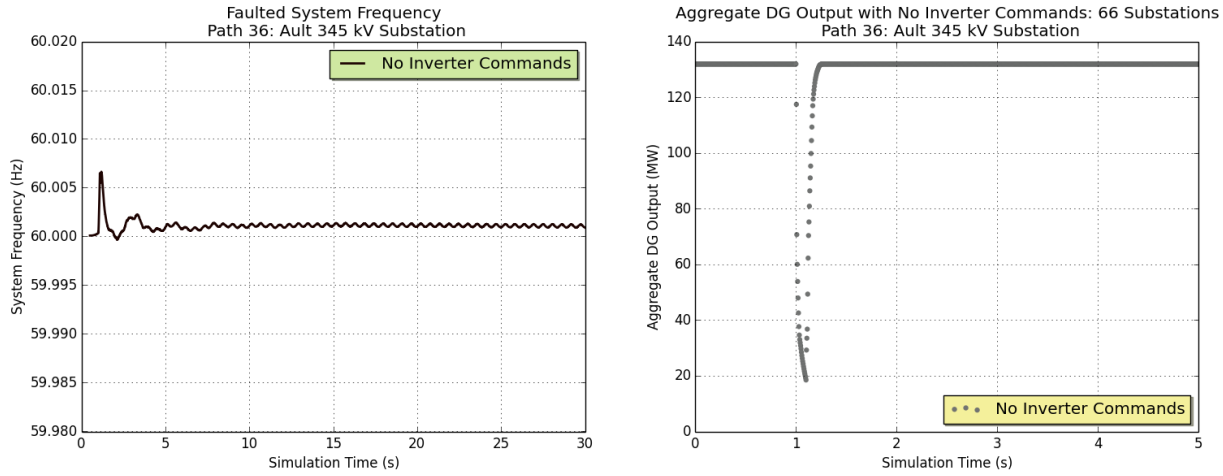

(a) Path 36 system frequency

(b) Path 36 distributed generation output

Figure 14. Path 36 system frequency and distributed generation output

Table 4. Summary of Path 36 Statistics

Item	Value
CMPLDWG models	66
Total distributed generation	135 MW
Total native load	2,050 MW
Peak buses less than 0.95 p.u.	906

2.3.2 Southern California Edison Territory: Path 61—Lugo 500 kV

A 500-kV single-circuit interfaces the SCE and Los Angeles Department of Water and Power service territories in Victorville, California. This transmission line is a 10-mile segment between the Lugo (SCE) and Victorville (Los Angeles Department of Water and Power) substations. The magnitude of power flow and location as an intertie between service territories distinguish it as a WECC path, denoted as Path 61. During the Heavy Summer High Mix case, real power flow on Path 61 is 1,700 MW from Victorville to Lugo, with a path limit rating of 2,400 MW for this direction of flow. This large flow from the Los Angeles Department of Water and Power to SCE is a result of net imports to the Los Angeles region, with a large sourcing of power through the Intermountain Power Plant DC link (Path 27) and high east/west Colorado River path flows (Path 49/Path 46). Throughout the summer months, this path operates at more than 75% of maximum loading 4.5% of the time. At 1,700 MW, or 70% of the maximum, this

indicates that the line is loaded significantly but not at a typical maximum for the season. As anticipated, a fault at the Lugo 500-kV substation followed by the removal of the Path 61 line results in a significant system response.

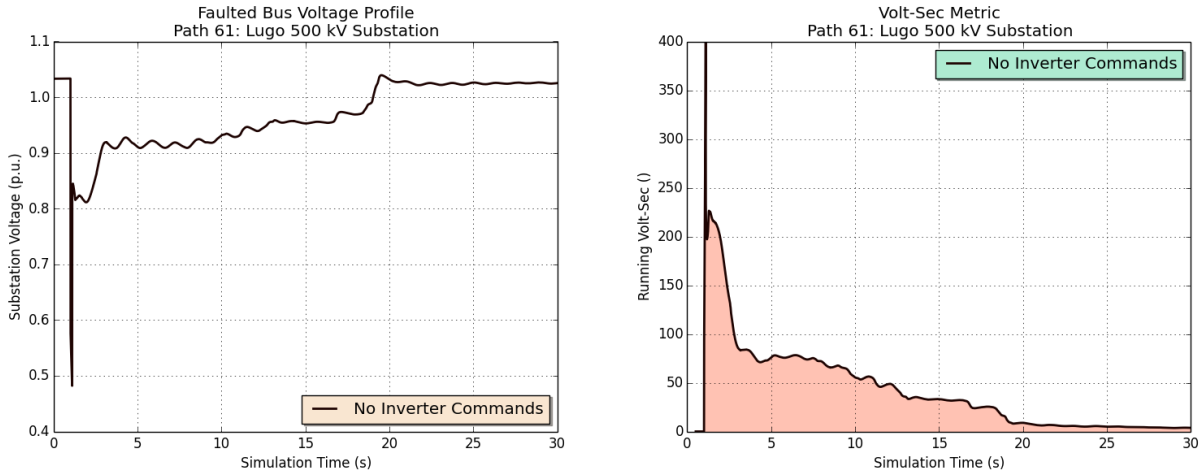

(a) Lugo 500-kV voltage profile

(b) Running volt-sec metric

Figure 15. Path 61 bus voltage and volt-sec metric

The Path 61 fault response is a quintessential FIDVR event. Figure 15(a) shows the voltage profile at the Lugo 500-kV substation for this event. The initial dip is extreme, as expected because of the fault location. Following the fault clearing, the voltage recovers substantially but remains less than the initial steady-state voltage level. This low voltage slowly recovers but persists for approximately 18 seconds before steady-state voltages are recovered. The utility of the volt-sec score is made apparent through Figure 15(b), the running volt-sec metric for this fault. Considering the magnitude alone and understanding that the profile is representative of approximately 3,000 buses at the fault, and 800 buses throughout the simulation (see the dotted curve in Figure 16), we view a system FIDVR event with subsequent recovery. Noting the similarity in the shape of the two charts in Figure 15, a voltage response similar to the Lugo 500-kV profile is anticipated at most substations. Indeed, rigorous voltage profile investigations have supported this expectation, with lower voltage substations experiencing a similar shape.

The utility of the voltage percentile distribution is demonstrated in Figure 16, which provides not only the running quantity of buses with voltages less than 0.95 p.u. throughout the first 5 seconds of the disturbance but also the distribution of voltages experienced by this quantity of buses. For instance, we can conclude that because the 50th percentile line hovers around 0.9 p.u. throughout the simulation, approximately 400 buses have voltages less than 0.9 p.u. during this time. Because this chart provides the distribution of all buses regardless of location or expected impact, we cannot make specific conclusions about distributed generation operation. Recognizing this as a FIDVR event, however, which is primarily load driven, we can anticipate the lower voltage buses to be load locations where distributed generation is located (i.e., areas with low voltage because FIDVR should also trip more distributed generation offline).

Figure 17 presents the spatial extent of low voltages. As with the other GIS images, the voltages of the substations for this mapping represent the system 100 ms after the fault is initiated, exactly when the fault is cleared. The moment shown in Figure 16 is at the pinnacle of the bus count spike (black dotted line). As evident from the inset, the severity of the voltage depression in the Los Angeles area is significant. The load centers of Phoenix and Las Vegas are also substantially affected. Referencing Figure 4, we see that a very large amount of distributed generation is located in the Southern California area. Considering the low voltages shown in Figure 17 and the persistence of these low voltages depicted in figures 16 & 15(b), a significant loss of distributed generation is expected.

Rounding out the Path 61 fault investigation are the frequency and aggregate distributed generation output plots

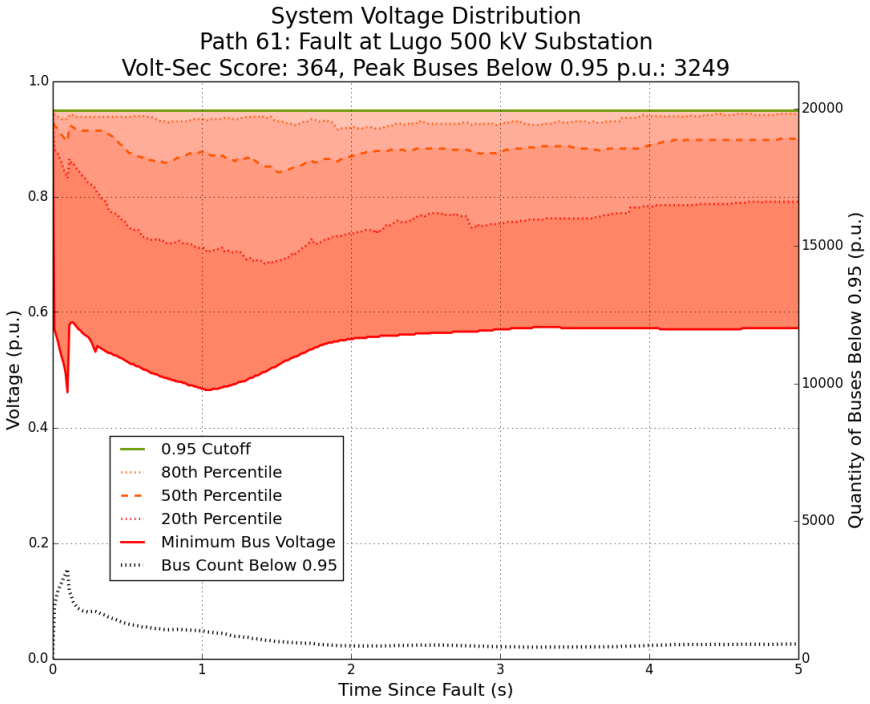

Figure 16. Path 61 low-voltage bus distribution

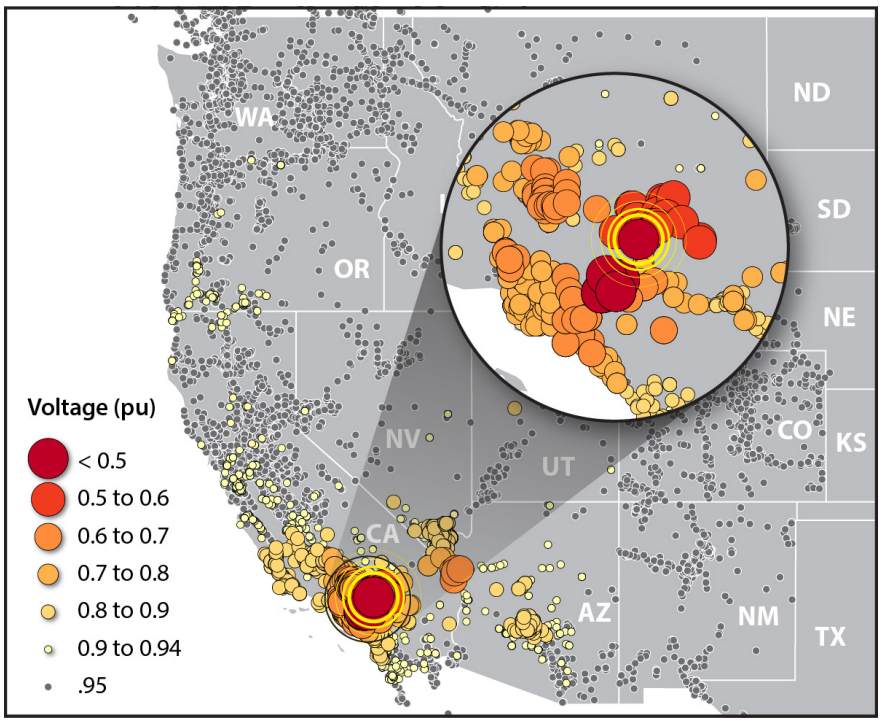

Figure 17. Path 61 low-voltage bus GIS mapping

found in Figure 18. The overall system frequency rises substantially (300 mHz) immediately following the fault, which is indicative of low voltages at the load causing voltage-dependent loads (either constant current or constant impedance) to drop in real power demand. This results in an excess of generation, causing the overall system frequency to rise in accordance with the swing equation governing the synchronous generator power balance. As the voltages recover, the frequency returns to 60 Hz, after a slight undershoot. The aggregate distributed generation output for all affected CMPLDWG models shows an enormous drop at the time of the fault of approximately 2.5 GW. This distributed generation output recovers with the voltage because the CMPLDWG model allows the distributed generation output to recover immediately with the voltage rise. Although the majority of this distributed generation is located in the SCE territory, at 2.9 GW total, 1.2 GW of the distributed generation in the Los Angeles Department of Water and Power and 100 MW of distributed generation in San Diego are also impacted. Table 5 provides a few Path 61 statistics that are used in subsequent simulations.

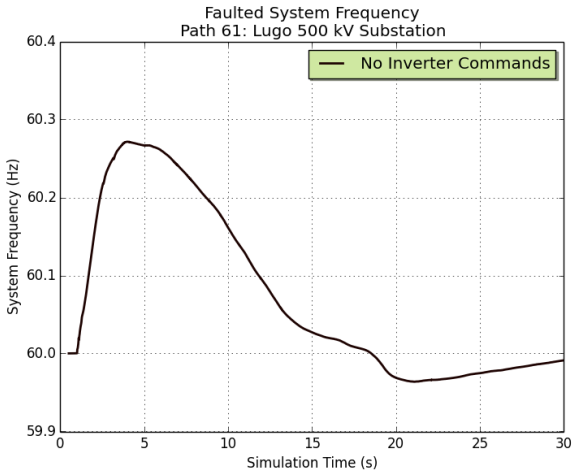

(a) Path 61 system frequency

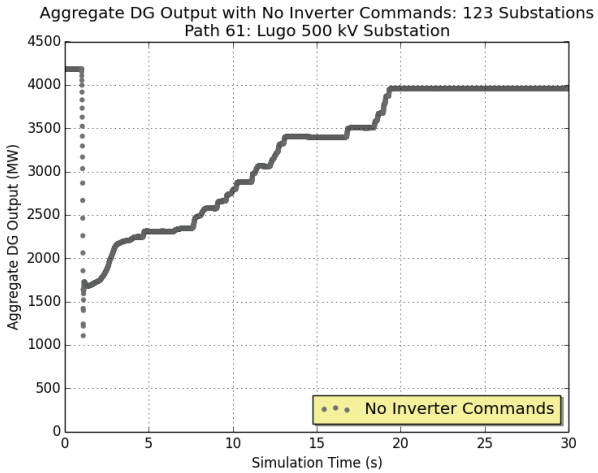

(b) Path 61 initial distributed generation output

Figure 18. Path 61 system frequency and distributed generation output

Table 5. Summary of Path 61 Statistics

Item	Value
CMPLDWG models	123
Total distributed generation	4,200 MW
Total native load	28,700 MW
Peak buses less than 0.95 p.u.	3249

2.3.3 Arizona Public Service Territory: Path 54—Silver King 500 kV

The third selected scenario is for a fault on Path 54, which not only primarily influences the third region of APS selected for investigation but also provides a very different system response. Whereas Path 36 provided a rapid recovery, and Path 61 provided a traditional FIDVR with recovery, the fault on Path 54 initiates a FIDVR event that persists for much longer than the 30 seconds of interest for these simulations. Note that a simulation for 90 seconds was performed for this fault scenario, and the system eventually recovers. As shown in the distribution simulations, this extended FIDVR event puts the full potential of the IEEE 1547-2018 Category III to test.

Path 54 consists of a single 500-kV circuit connecting the Coronado and Silver King substations. The line operates as a primary route for power flow between the Coronado generating station and the Phoenix metro area. Thus, the

power flow on this line is almost always from Coronado to Silver King, with a maximum rating of 1,500 MW in this direction. At the time of the fault, which occurs at the Silver King substation, the real power flow is 614 MW, or 41% of the path rating. The line never operates at more than 75% of maximum loading (Western Electricity Coordinating Council 2016), indicating that the loading at the time of the fault is likely not unusual.

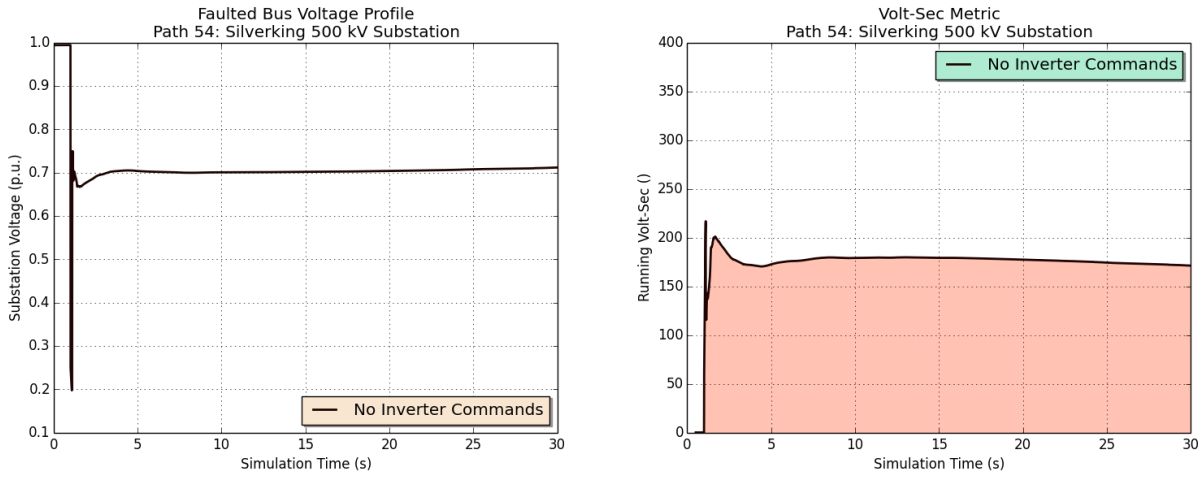

(a) Silver King 500-kV voltage profile

(b) Running volt-sec metric

Figure 19. Path 54 bus voltage and running volt-sec metric

Figure 19 provides the Silver King 500-kV substation and running volt-sec metrics for the Path 54 fault. The faulted substation voltage profile shows the anticipated during fault low voltage (1–1.1 seconds), followed by a persistent 0.7-p.u. voltage level for the remainder of the simulation. This indicates a FIDVR event with no or very slow recovery. Referencing the running volt-sec metric, indeed, a large number of buses remain at voltages less than 0.95 p.u. throughout the simulation, confirming that a FIDVR event is taking place. Note that the running volt-sec score is around 200, which is on par with the initial scores of both Path 36 and Path 61. Unlike the Path 61 FIDVR, there is very little movement in the running volt-sec metric, from which it is understood that the low-voltage levels persist for more than 30 seconds with little to no recovery. Figure 20 shows the distribution of voltage levels for this fault. Note that although the initial peak of less than 0.95 p.u. buses is only 1,199, compared to 3,249 for the Path 61 scenario, both simulations result in approximately 800 buses lower than 0.95 p.u. even 5 seconds after the fault. Again, nearly half of these buses are at voltages less than 0.9 p.u., and almost 20% of these buses are less than 0.7 p.u.

The GIS mapping of the low-voltage buses in Figure 21 shows that the range of influence is almost entirely restricted to the APS and immediately adjacent territories. The greater Phoenix area is particularly affected, with only a slight influence on the Las Vegas area. There is very little movement in bus voltages in Southern California.

Figure 22 rounds out the close look at the Path 54 scenario and for the transmission studies entirely. As with the Path 61 scenario, the overall system frequency increases after the fault because the voltage-dependent loads experience lower voltages and thus a lower real power demand. Unlike the Path 61 scenario, the system frequency shows only a slight recovery, which is expected considering the prolonged low voltages. The aggregate distributed generation output of the CMPLDWG models shows a near-complete falloff of output after the fault, with only a slight recovery, which indicates that the voltages at the CMPLDWG locations remain low. This output deficit persists throughout the simulation. Table 6 provides the final statistics relevant for the subsequent distribution simulations.

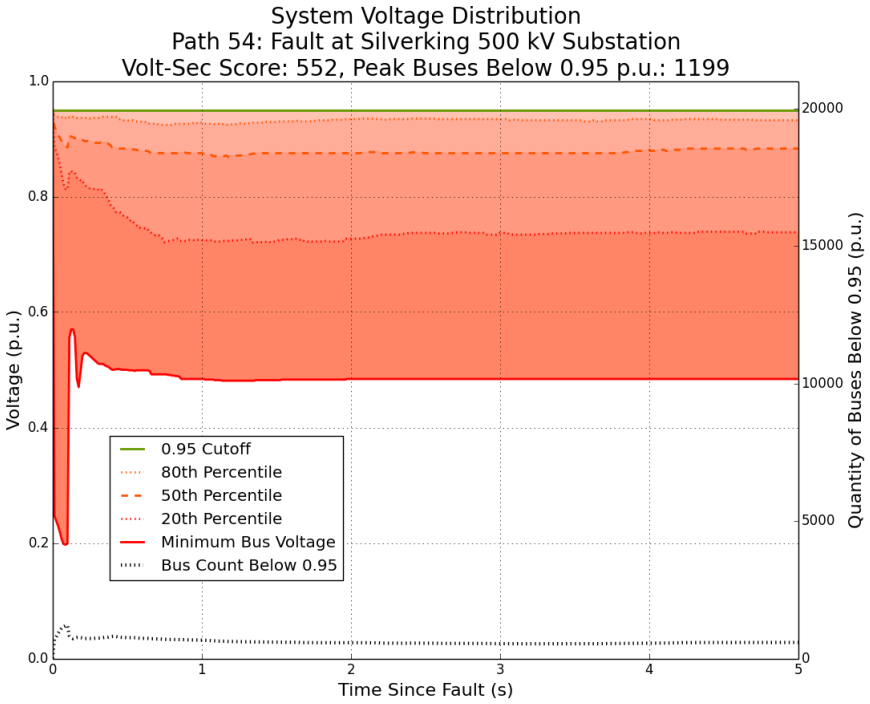

Figure 20. Path 54 low-voltage bus distribution

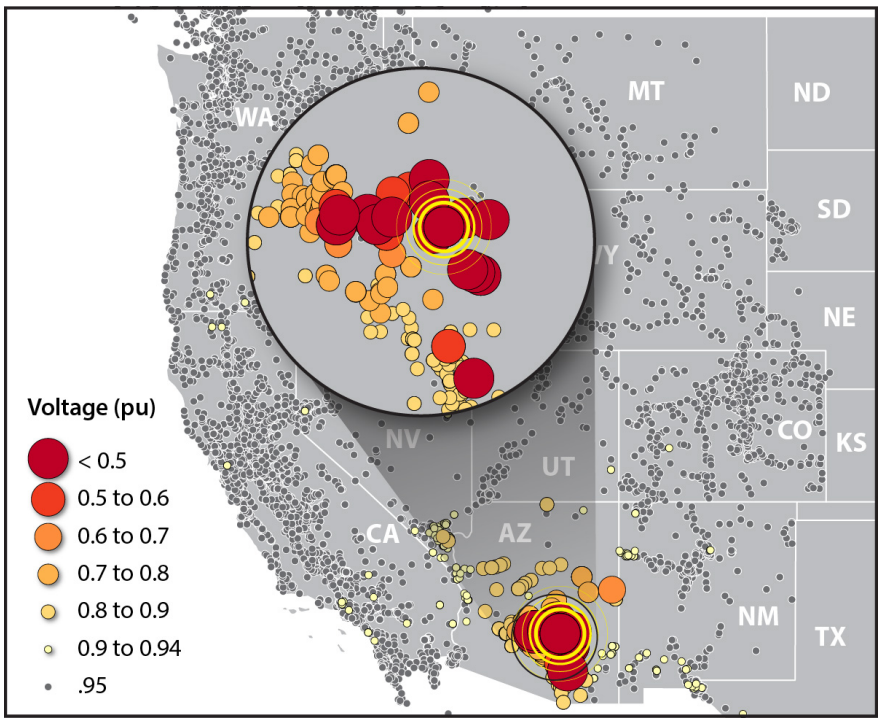

Figure 21. Path 54 low-voltage bus GIS mapping

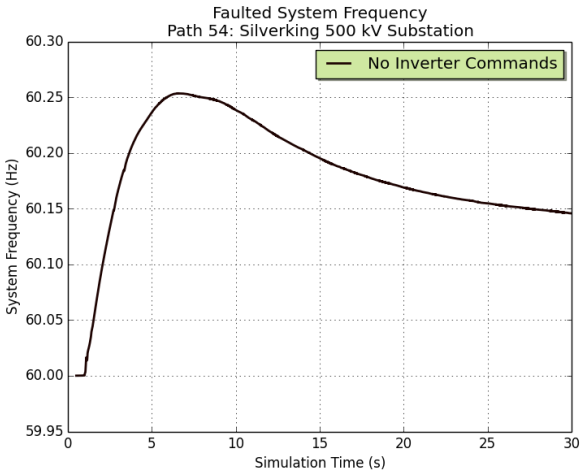

(a) Path 54 system frequency

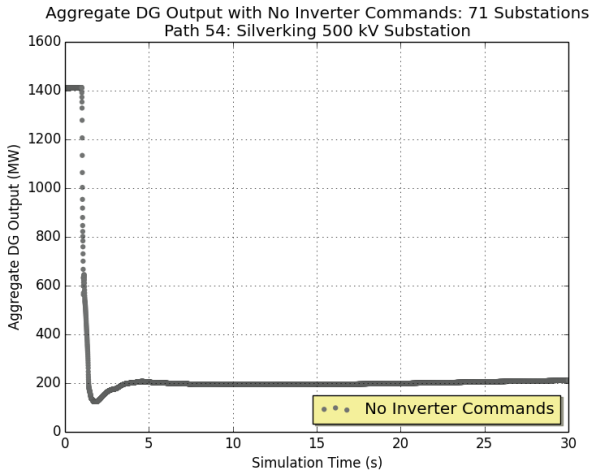

(b) Path 54 distributed generation output

Figure 22. Path 54 system frequency and distributed generation output

Table 6. Summary of Path 54 Statistics

Item	Value
CMPLDWG models	71
Total distributed generation	1,400 MW
Total native load	10,400 MW
Peak buses less than 0.95 p.u.	1199

3 Distribution System Simulations

The modeling software OpenDSS is used to perform the distribution system simulations with inverter-populated feeders. OpenDSS is interfaced with Python to manage timers for each inverter on the feeder, which track respective terminal voltages and model the various IEEE 1547 voltage ride-through performance categories. To bridge the simulation gap between PSLF and OpenDSS (a strict, balanced, transmission-level simulator versus a radial, unbalanced three-phase distribution simulator), each CMPLDWG model from PSLF is treated as an individual feeder simulation in OpenDSS. The particular distributed generation parameters of the CMPLDWG model are used to proportionally populate a feeder based on the initial feeder load. For instance, a CMPLDWG with a 5% distributed generation penetration level with respect to native load is represented by a feeder with 5% of native load compensated by inverter generation. Although the native loads are not always comparable (in fact, the loading on each feeder is not changed, and only the inverter output is scaled to achieve similar penetrations), this process allows for reasonable scaling and representation between the two simulations. Criteria that apply to all simulations are listed here:

- Fifty inverters were randomly located on each feeder. These are all single-phase and colocated with single-phase loads on secondaries.
- Distributed generation penetration is achieved by scaling equally the output of all 50 inverters. Penetration is determined as a fraction of feeder native load, with the penetration value as set in PSLF for the CMPLDWG.
- With all faults being balanced three-phase, the voltages of all three phases in OpenDSS are simply scaled to the positive-sequence voltage from PSLF; i.e., the per-unit output of PSLF directly scales the initial voltage of each phase at the feeder head.
- Thirty-second voltage curves from PSLF are simulated on the OpenDSS feeders, with a simulation time step matching the quarter-cycle (1/240-second) time step of PSLF.
- Each inverter tracks the terminal voltage and responds according to the IEEE 1547 criteria to which it is set.
- Only a single IEEE 1547 response is tested at a time; i.e., if IEEE 1547-2018 Category II is being simulated, all inverters respond with this criteria.
- To equate the total inverter feeder output with CMPLDWG output, the aggregate results of the OpenDSS simulation are per unitized, which is then used to scale the CMPLDWG output.
- Inverters are initially at full output and are current-limited at 1.1 p.u. current. This means that for voltages less than 0.91 p.u., the inverter operates as a constant current source.
- No automatic voltage regulation equipment (e.g., load tap changers, voltage regulators, and switched capacitor banks) is permitted to operate within the time frame of the OpenDSS simulations.

As a result of this approach, for each CMPLDWG model in the PSLF simulation with distributed generation that experiences a voltage less than 0.95, a feeder is simulated and populated with 50 inverters, the output of which is scaled to achieve the CMPLDWG distributed generation penetration. For instance, the Path 36 fault impacts 66 CMPLDWG models, and therefore 66 feeders are modeled using OpenDSS for this case. Additionally, because only one type of IEEE 1547 criteria is modeled at a time (of which there are five, as discussed in the following section), each feeder is simulated five times with the same paired voltage profile, once for each different IEEE 1547 criteria. The various IEEE 1547 response criteria are described in Section 3.1.

3.1 IEEE 1547 Abnormal Voltage Ride-Through Criteria

The primary objective of this study is to provide insight into the overall system response to low voltages under different IEEE 1547 response criteria. The two sources of this criteria, IEEE 1547-2003 and IEEE 1547-2018, are described in detail with an example simulation on a single feeder to provide the reader with intuition of the

anticipated response for each type of criteria. Because this study deals exclusively with low-voltage events, the high-voltage criteria are not discussed. These criteria apply to DERs comprehensively, of which distributed generation is a subset. Within the context of this report, these terms are equivalent because the only distributed resources modeled are the distributed generation components within the CMPLDWG models.

3.1.1 IEEE 1547-2003

The original IEEE 1547-2003 standard applies to only one set of voltage ride-through criteria (rather than the three categories in the 2018 standard), the compliance of which is dictated by the real power capacity of the generation unit. For generation with a peak output less than 30 kW, the clearing times represent a maximum; whereas for units that have a peak output larger than 30 kW, the clearing times have a default setting, but the specific setting could be set to an alternative value during the interconnection process. In practice, the majority of PV-based distributed energy resources have been installed with IEEE 1547 default values, and thus the default clearing times applicable to units less than 30 kW are used for this study. The clearing times represent the point at which the unit will cease to energize, which for this study is interpreted as a trip with no recovery. The adherence to this cease-to-energize criteria is a source of ride-through operation confusion, with the length of cessation and recovery varying widely in implemented equipment (North American Electric Reliability Corporation 2017, 2018a; Zhu et al. 2018). The voltages apply to the root mean square value of the fundamental.

Table 7. IEEE 1547-2003 Abnormal Voltage Ride-Through Criteria

Voltage (p.u.)	Clearing Time (s)
$V < 0.5$	0.16
$0.5 \leq V < 0.88$	2.0

In 2018, after a decade and a half of inverter development, installation, and standards implementation under IEEE 1547-2003, the results indicate that many forms of ride-through are possible while adhering to the criteria in Table 7 (Zhu et al. 2018) because the clearing times specified are the maximum clearing times. Tripping offline earlier than these maximum times is permissible, and unlike conventional generation, there is little penalty for inverter-based distributed generation to trip offline because they can easily resume generation. For small penetrations of distributed generation adherent to IEEE-1547, the exact response during a low-voltage event might be inconsequential; the penetrations are far exceeded by the margins of stability. With more than 9 GW on the Western Interconnection, however, a more precise understanding is necessary from a stability perspective because the generation output is now larger than the stability margin (e.g., considering a double Palo Verde contingency as the generation stability margin). To capture the array of possible responses, we adopted two different classifications of IEEE 1547-2003, dubbed "pessimistic" and "optimistic." In both cases, after the clearing time is exceeded, the distributed generation unit output goes to zero for the remainder of the simulation. The adapted clearing times for each class are given in Table 8.

Table 8. IEEE 1547-2003 Pessimistic and Optimistic Clearing Times

Voltage (p.u.)	Pessimistic Clearing Time (s)	Optimistic Clearing Time (s)
$V < 0.5$	0.0	0.0
$0.5 \leq V < 0.88$	0.0	2.0

For the case of voltages less than 0.5 p.u., both classes trip the DER immediately. The 10-cycle trip time given in the 2003 standard is meant as a compliance buffer; i.e., the unit will ostensibly initiate the cessation immediately, but the closed-loop response is allowed to max out at 10 cycles (0.16 s). Therefore, clearing immediately is sensible because the range of closed-loop responses will vary across manufacturers, and a pessimistic assumption provides a suitable baseline. The range of voltages between 0.5 and 0.88 p.u. sees the largest switch between cases. As shown in the 2018 standard, these voltages see a range of compliant operations. Therefore, in interpreting the 2003 standard, we

elected to have the pessimistic class clear immediately at any voltage less than 0.88 p.u., whereas the optimistic class will maintain distributed generation output for 2 seconds. Note that the optimistic operation is meant to show what the 2003 standard might have created if a specific operation were mandated and demonstrates the maximum level of voltage ride-through possible while still complying with the default IEEE 1547-2003 settings. In reality, there is little expectation of this type of distributed generation response, and in fact the likelihood to immediately trip has already been highlighted (North American Electric Reliability Corporation, 2018b; Zhu et al. 2018).

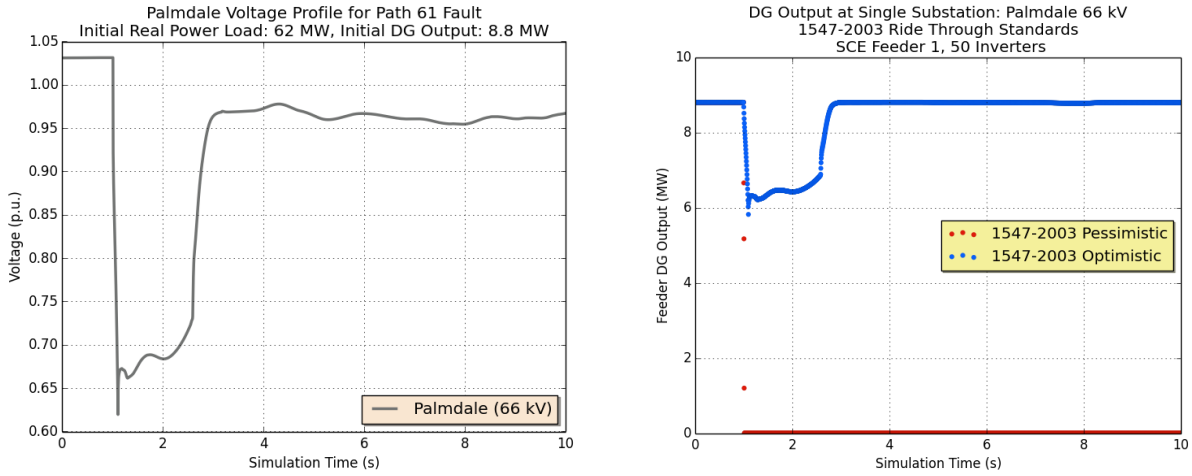

(a) Palmdale 66-kV substation voltage

(b) IEEE 1547-2003 distributed generation response

Figure 23. Palmdale voltage and IEEE 1547-2003 response

With these two classes, the resultant distributed generation output levels from an OpenDSS simulation are presented in Figure 23. The simulation implements the per-unit voltage profile of Figure 23(a) (the response of the Palmdale 66-kV CMPLDWG to the Path 61 fault) equally to all three phases at the feeder head. The feeder model is SCE Feeder 1. Two simulations are performed, one for each of the IEEE-1547 classes. The response of all 50 inverters on the feeder are aggregated and per unitized, which is then used to scale the initial distributed generation output of the Palmdale CMPLDWG throughout the 30-second simulation, instead of having the output dictated by the embedded PVD1 model in the CMPLDWG model. The results of only 10 seconds are shown here because no further change in distributed generation output was observed. The response for the pessimistic criteria is an immediate distributed generation loss, which is expected because the voltage at the feeder head (typically the highest voltage point on a feeder) goes to less than 0.88 p.u. The response of the optimistic case shows a decrease in output during the deep voltage dip (1–2.5 seconds), followed by a recovery to full output after 2.5 seconds. This output reduction is entirely because of the current limiting of all inverters at 1.1 p.u., which yields a constant current response for all voltages less than 0.91 p.u. Had the voltage dip to less than 0.88 p.u. lasted for more than 2 seconds, some amount of distributed generation would have tripped according to the IEEE-1547 compliance in this optimistic case. Note that the distributed generation loss—and recovery, where applicable—occurred following the substation dipping to less than roughly 0.95 p.u., reinforcing 0.95 as a suitable selection for the volt-sec(-distributed generation) metric cutoffs.

3.1.2 IEEE 1547-2018

The new IEEE 1547-2018 standard introduces language that precisely indicates the desired operation of DERs because there are now three different categories (I, II, and III) within the IEEE-1547 standard with different ride-through criteria for each. The following is a list of pertinent vocabulary and respective definitions:

- **Mandatory operation:** For conditions inside of the continuous operation regime, the DER shall maintain synchronism and current injection.

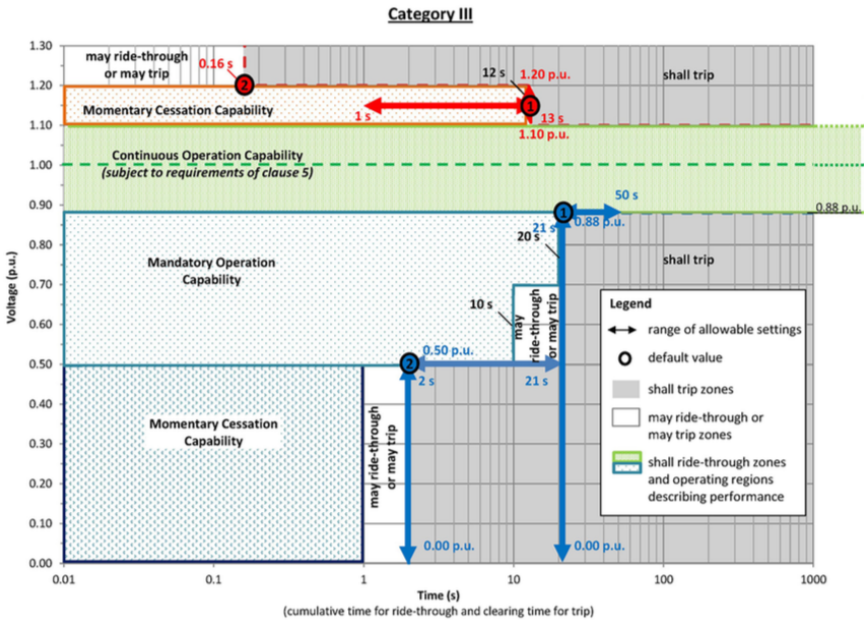

Figure 24. IEEE 1547-2018 Category III abnormal voltage ride-through capability (used with permission)

- **Permissive operation:** The DER is allowed to either enter momentary cessation or maintain continuous operation. The device is not allowed to trip and must maintain synchronism.
- **Momentary cessation:** The DER must not trip but shall cease to energize and follow a specific recovery envelope after voltage levels recover. The DER must return to 80% of predisturbance current levels within 0.4 second of voltage levels reaching the mandatory operating region.
- **May ride-through/trip**: The DER may either trip or enter momentary cessation.
- **Shall trip:** It is mandatory that the DER trip.

To asses the response of a DER, particularly under voltage conditions when the device might either continue injecting current or cease to energize, a pessimistic interpretation of the standard is followed. This contrasts with the IEEE 1547-2003 study, in which pessimistic and optimistic interpretations were both simulated to generate the response envelope, with the optimistic simulation accepted as an exemplary scenario only. This approach for IEEE 1547-2018 is legitimized because when assessing stability as it is critical to understand which generation elements remain online. The interpretation, as laid out in Table 9, is used for implementing the IEEE 1547-2018 criteria.

Table 9. IEEE 1547-2018 Operating Conditions Interpretation

IEEE 1547-2018 Standard	Implementation
Permissive operation	Momentary cessation
Momentary cessation	Momentary cessation
May ride-through/trip	Trip

Figures 24, 62, and 63 are graphical representations of the voltage ride-through capabilities of the three categories presented in the IEEE 1547-2018 standard. When implementing the pessimistic interpretations laid out in Table 9 to the ride-through criteria—in particular, the low-voltage regions—an easily derived implementation is derived for each category. The programmed operation for each of the three categories is provided in tables 10, 11, and 12. After the voltages recover (move from a lower to a higher voltage region), the criteria for the higher voltage level is appli-

cable, but there is an elapsed time from the beginning of the disturbance. For example, if the voltage of a Category III-compliant inverter goes to less than 0.5 p.u., the inverter enters momentary cessation. If the voltage rises to more than 0.5 p.u. within 1 second, the inverter begins recovery at a rate of 80% of initial current per 0.4 second. If the voltage remains at less than 0.7 p.u. for longer than 10 seconds minus the time in momentary cessation, however, the inverter will trip. If the voltage recovers to more than 0.7 p.u., then the 20-second trip time applies. In short, when the voltage profile is overlaid with the ride-through capability graphic of Figure 24, the inverter will trip if the voltage curve ever exits the momentary cessation or mandatory operation regions. Note that Figure 24 uses a logarithmic axis for time, whereas all voltages presented in this report use a linear time axis. Finally, for the case of Category II, there is a 0.16-second clearing time associated with voltages between 0.3 and 0.45 p.u. This class is rolled into the 0.32-second clearing time for voltages between 0.45 and 0.65 p.u., for simulation reasons, but also because of the observation that no CMPLDWG voltages rest between 0.3 and 0.45 p.u. in these simulations.

Table 10. IEEE 1547-2018 Category I OpenDSS Programmed Operation

Voltage (p.u.)	Operation
$V < 0.5$	Immediate trip
$0.5 \leq V < 0.7$	Momentary cessation until trip after 0.16 second
$0.7 \leq V < 0.88$	Trip after: $0.7s + (4s/pu) \times (V - 0.7pu)$
$0.88 < V$	Continuous operation

Table 11. IEEE 1547-2018 Category II OpenDSS Programmed Operation

Voltage (p.u.)	Operation
$V < 0.3$	Immediate trip
$0.3 \leq V < 0.65$	Momentary cessation until trip after 0.32 second
$0.65 \leq V < 0.88$	Trip after: $3s + (8.7s/pu) \times (V - 0.65pu)$
$0.88 < V$	Continuous operation

Table 12. IEEE 1547-2018 Category III OpenDSS Programmed operation

Voltage (p.u.)	Operation
$V < 0.5$	Momentary cessation until trip after 1 second
$0.5 \leq V < 0.7$	Continuous operation until trip after 10 seconds
$0.7 \leq V < 0.88$	Continuous operation until trip after 20 seconds
$0.88 < V$	Continuous operation

As defined by IEEE 1547-2018, the aggregate distributed generation responses for each category on a single feeder are shown in Figure 25. The responses for categories I and II show a near-instantaneous momentary cessation response of all distributed generation for voltages less than 0.7 and 0.65, respectively. As in the case for Palmdale, the voltage recovers just quickly enough that some of the Category II inverters respond to a somewhat recovered voltage and stay online, whereas all of the Category I inverters trip offline. The full response of Category II shows that roughly 75% of the inverters have tripped offline. The recovery of the remaining 25% include a voltage-recovery response (constant current response because of current limiting) and a recovery from momentary cessation. The Category III response is entirely dictated by the constant current operation of the current-limited inverters and is therefore quite similar to the optimistic IEEE 1547-2003 response.

Figure 26 shows the aggregate distributed generation response for the Chevmain 66-kV voltage profile from Figure 6(a). Because the lower voltages persist longer than for the Palmdale profile, we see the distinction between the optimistic and Category III response. Namely, approximately 2 seconds after the fault implementation, all the inverters trip for the optimistic response. For Category III, however, all inverters remain online. Category II shows a constant current response with a loss because of momentary cessation followed by tripping. The decrease around 6 seconds is

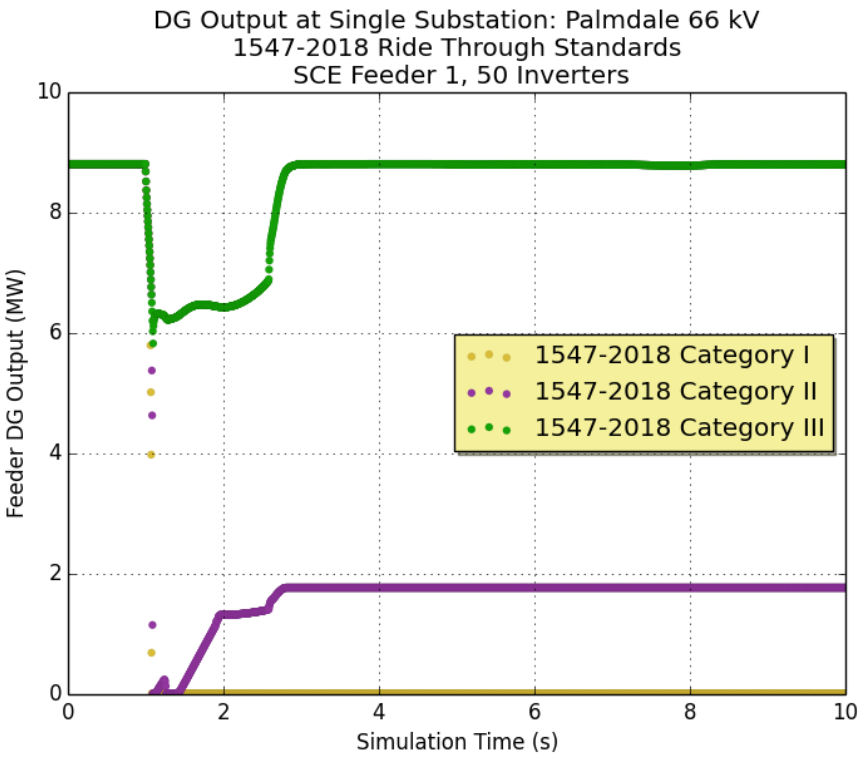

Figure 25. Palmdale IEEE 1547-2018 response

because of the sliding trip time for voltages between 0.65 and 0.88 p.u. The loss of distributed generation for Category I is rather quick because the voltage profile rapidly decreases to less than 0.7 p.u., after which the inverters enter momentary cessation for 10 cycles before tripping completely.

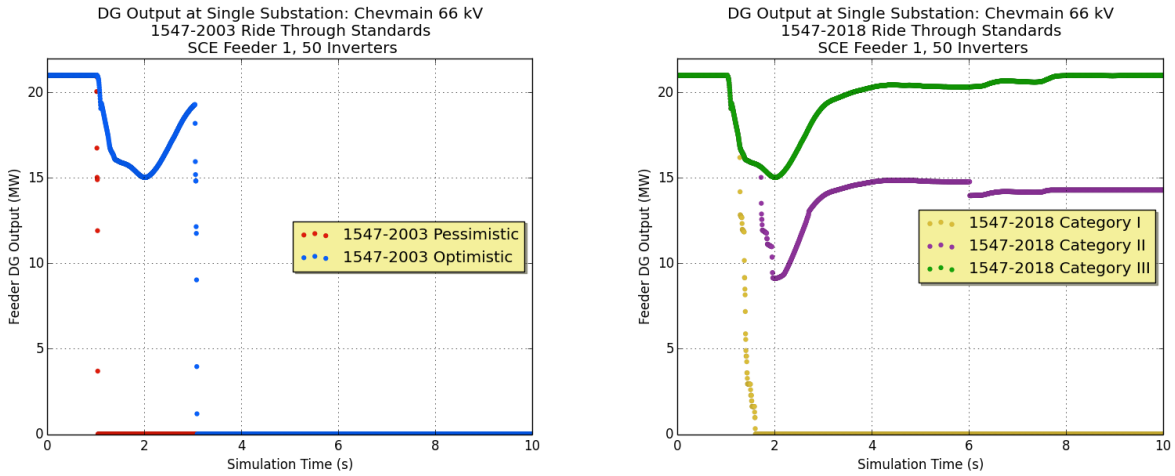

(a) Chevmain IEEE 1547-2003 response

(b) Chevmain IEEE 1547-2018 response

Figure 26. Chevmain IEEE 1547 response

Because of the numerous references to the various IEEE criteria throughout the rest of this report, the following shorthand is adopted:

- **pessimistic** $\Longrightarrow$ IEEE 1547-2003 pessimistic
- **optimistic** $\Longrightarrow$ IEEE 1547-2003 optimistic
- **CatI** $\Longrightarrow$ IEEE 1547-2018 Category I
- **CatII** $\Longrightarrow$ IEEE 1547-2018 Category II
- **CatIII** $\Longrightarrow$ IEEE 1547-2018 Category III

3.2 OpenDSS Simulations

With the OpenDSS simulation approach outlined and the five different types (pessimistic, optimistic, CatI, CatII, and CatIII) of IEEE 1547 ride-through thoroughly described and exampled on two voltage profiles, we now turn to the ensemble response for each of the three selected fault scenarios. For each fault scenario, a reported quantity of CMPLDWG models experiences shifts in distributed generation output because of the measured voltage profiles. The faulted voltage profiles from each model are used to perform OpenDSS simulations—one for each of the five types of ride-through—with distributed generation penetrations on the feeder of equal value to the distributed generation penetration of the CMPLDWG model. The feeder distributed generation output is then per unitized and used to scale the CMPLDWG distributed generation output. For each type of ride-through criteria, all inverters of all affected CMPLDWG models adhere to the same criteria; e.g., for simulating the pessimistic response, all inverters follow the pessimistic criteria.

3.3 Path 36: Xcel

For Path 36, which primarily impacts the Xcel service territory, three Xcel OpenDSS models were procured that are physical feeders within this territory. All three are residential feeder models. With no distinction between the feeders, they were randomly and equally assigned to represent PSLF CMPLDWG models based on the model load—that is, they do not necessarily equally represent distributed generation penetrations but instead are allocated based on the PSLF load, after which the distributed generation penetration is used to inform the appropriate output of the 50 inverters on the feeder to match the penetration. With 50 inverters on each feeder and 66 feeder simulations per ride-through criteria, the result is 3,300 inverters modeled for each criteria simulation.

Table 13. Xcel Feeder Summary

Feeder	Native Load (MW)	Type	Load Representation (%)	Allocated CMPLDWGs
1	12.30	Residential	33	28
2	6.06	Residential	37	25
3	12.00	Residential	30	22

A summary of allocation and the total number of CMPLDWG models represented by each feeder is provided in Table 13. Figures 27, 28, and 29 show the voltage and power flow profiles for each Xcel feeder used in this study. They are typical of residential feeders, extending between 6 and 8 km from feeder head to the most distant customer, with a 5–8% p.u. voltage drop across the entire feeder. Feeder 1 has an express portion, and hence no loads for the first 3 km.

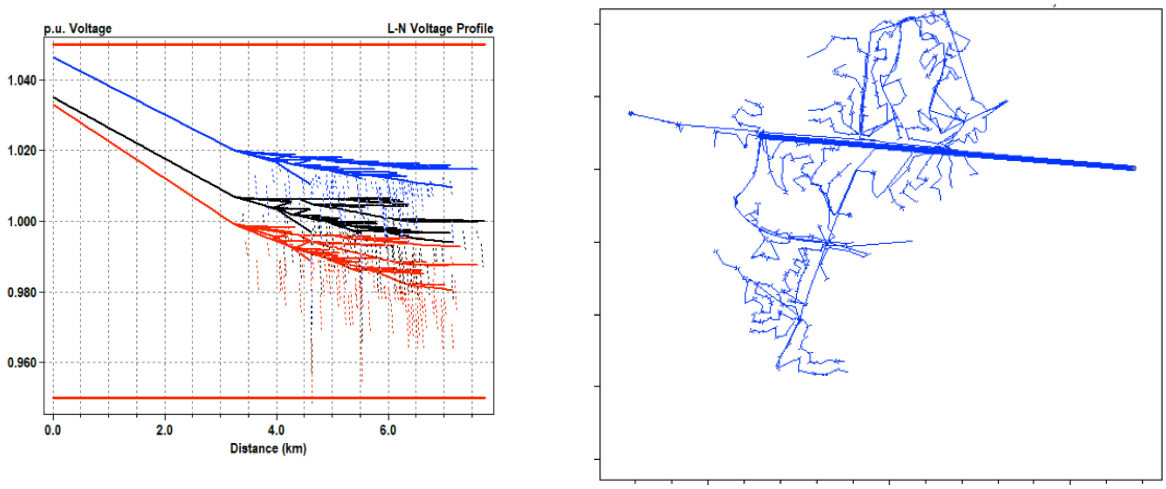

(a) Feeder 1 voltage

(b) Feeder 1 power

Figure 27. Xcel Feeder 1 voltage and power

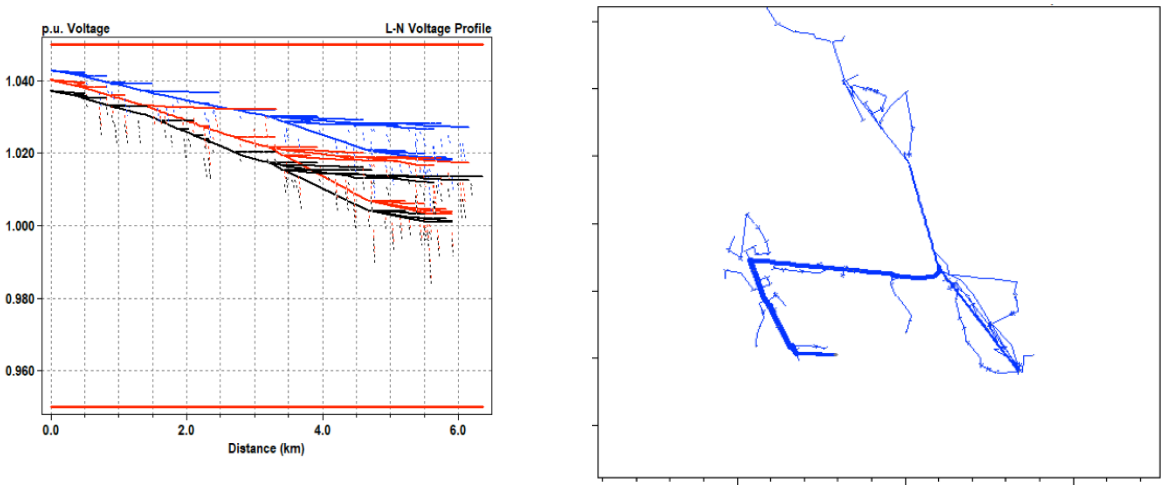

(a) Feeder 2 voltage

(b) Feeder 2 power

Figure 28. Xcel Feeder 2 voltage and power

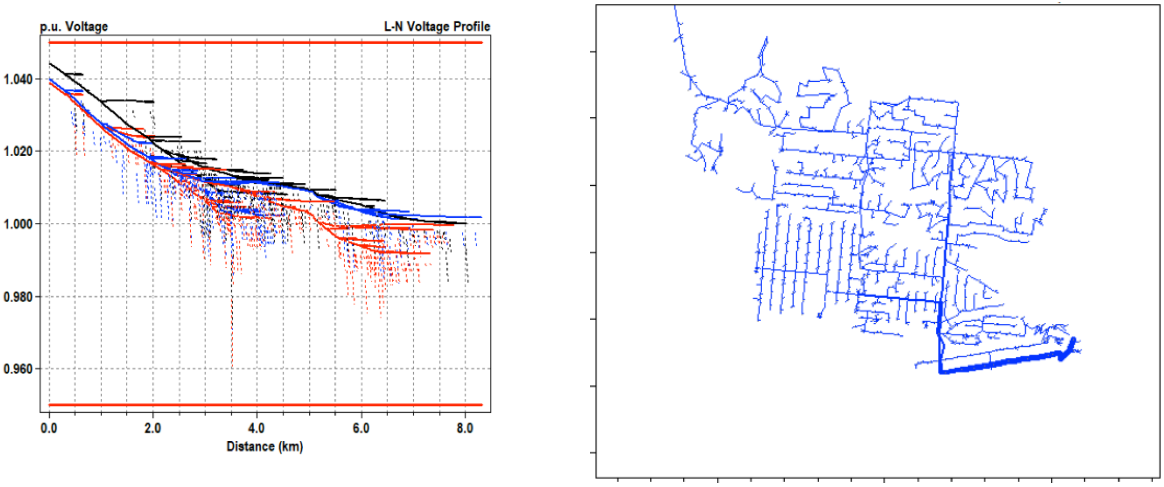

(a) Feeder 3 voltage

(b) Feeder 3 power

Figure 29. Xcel Feeder 3 voltage and power

3.3.1 1547-2003 Response

The aggregate results of all 66 feeder simulations for each pessimistic and optimistic responss are presented in Figure 30, alongside the CMPLDWG model aggregate output for the PSLF simulation for comparison. The results serve to highlight how the CMPLDWG model distributed generation response is at first an aggressive trip, followed by a very optimistic recovery with no persisting distributed generation loss. The pessimistic response shows a full distributed generation loss concurrent with the fault. This is not unexpected because this fault exhibits a relatively weak grid response in which electrically near substations experience very low voltages. These trip the distributed generation immediately in accordance with the pessimistic interpretation. The optimistic response shows that half of the distributed generation is lost and the remaining half stays online for the rest of the simulation. The results are displayed for only the first 5 seconds of the simulation because no further change in distributed generation output is observed beyond that period.

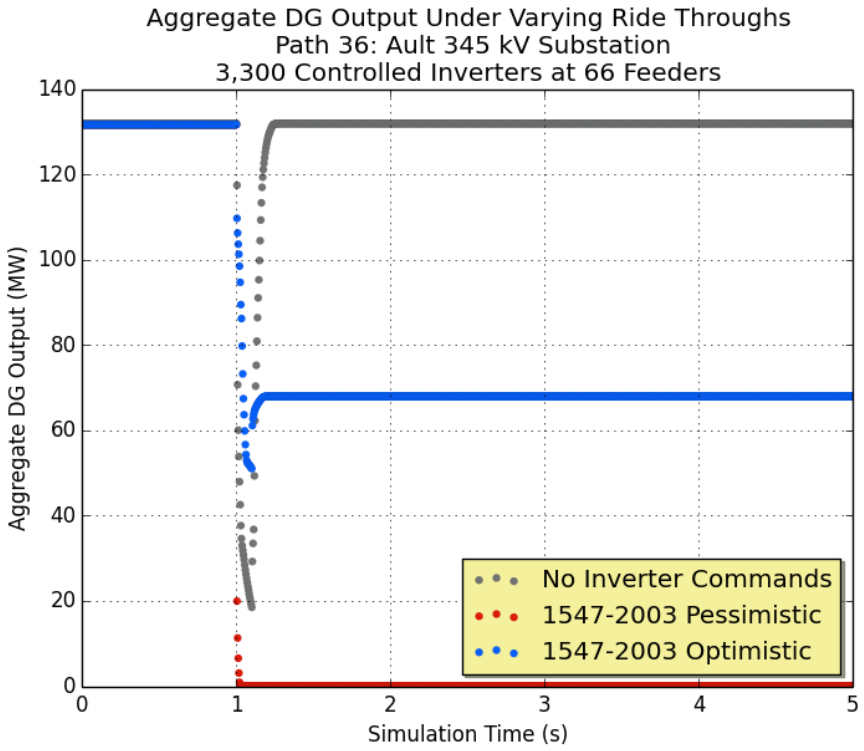

Figure 30. Path 36 aggregate distributed generation output with IEEE 1547-2003 criteria

3.3.2 IEEE 1547-2018 Response

Figure 31 shows the IEEE 1547-2018 criteria output for the Path 36 fault as well as the pessimistic and CMPLDWG (as modeled in PSLF) responses. As shown, for CatI, half of the distributed generation is tripped, and an additional quarter goes into momentary cessation but makes a full recovery within 0.5 second. CatII and CatIII experience momentary cessations, with CatII losing a larger amount of distributed generation initially. They both make a full recovery in accordance with the anticipated response. The comparison shows that the CMPLDWG model exhibits a similar size of distributed generation loss, but the elapsed time in recovery is much more drawn out for the IEEE 1547-2018 criteria. This is mostly representative of the CMPLDWG model exhibiting an instantaneous distributed generation recovery following the voltage recovery, which is a large drawback of this particular model. Again, these results are presented for only the first 5 seconds because no additional change in output is observed.

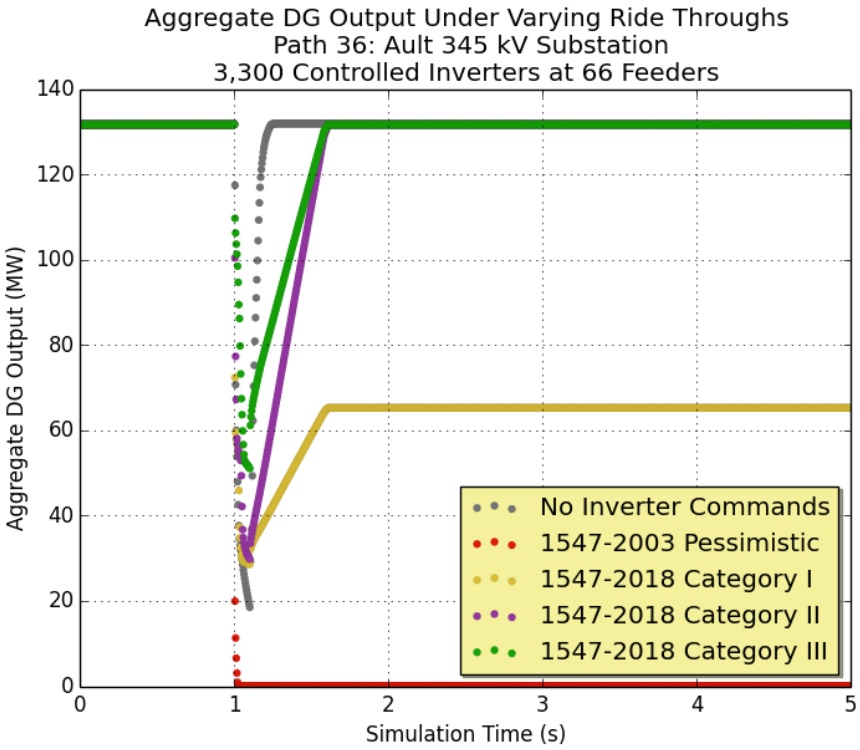

Figure 31. Path 36 aggregate distributed generation output with IEEE 1547-2018 criteria

3.4 Path 61: Southern California Edison

For the Path 61 fault scenario, the majority of influenced CMPLDWG models are in the SCE service territory, making the SCE OpenDSS feeder models most appropriate for the modeling. The three feeders are fit into three classifications: commercial/residential, residential, and industrial. As a result, although they are randomly assigned to the 123 CMPLDWG models that experience significant voltage deviations, the proportions of each type are based on approximate system loading; e.g., Feeder 3 is an industrial feeder, and because approximately 20% of the SCE territory is industrial load, Feeder 3 is assigned to 20% of the load of the 123 feeders. These allocations and basic feeder data are provided in Table 14.

Table 14. Southern California Edison Feeder summary.

Feeder	Native Load (MW)	Type	Load Representation (%)	Allocated CMPLDWGs
1	5.06	Commercial/residential	42	58
2	1.71	Residential	38	40
3	7.82	Industrial	20	25

The feeder voltage and power flow profiles are provided in figures 32, 33, and 34. Feeder 1 is a commercial/residential feeder operating at 12 kV, with a voltage regulator near the sixth kilometer from the feeder head. The voltage regulator maintains the initial tap position throughout the distribution simulations. This feeder is quite long, with a length from feeder head to final customer of more than 20 km. Feeder 2 is a low-voltage residential feeder operating at 4 kV. The drop on the secondaries is substantial but not far enough beyond the 0.95-p.u. threshold to be of concern for this study. Feeder 3 is a short, industrial feeder at a voltage of 16 kV. As a result, the voltage drop across the entire feeder is relatively small, which means that the voltage at any of the inverters will be much closer to the feeder head (CMPLDWG model) voltage. This is in contrast to the rest of the feeders, which have a more significant voltage drop.

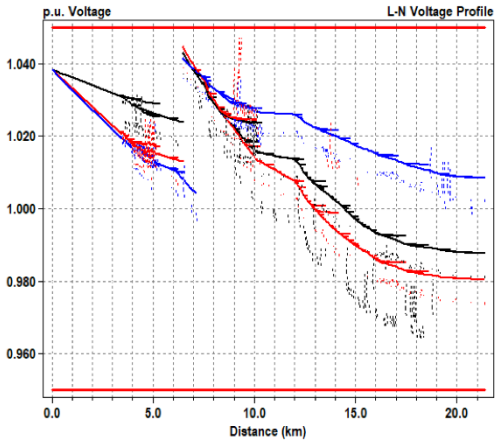

(a) Feeder 1 voltage

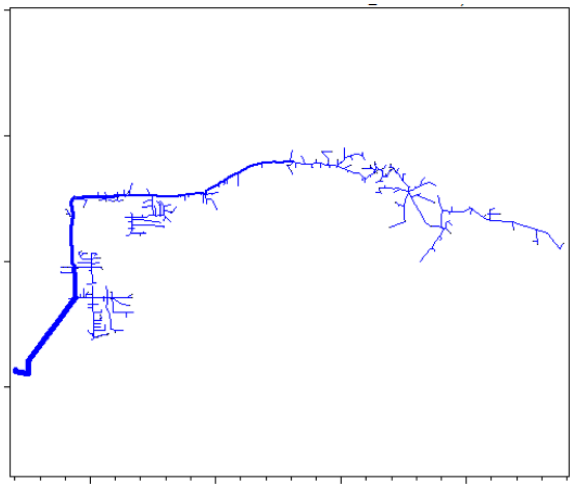

(b) Feeder 1 power

Figure 32. SCE Feeder 1 voltage and power

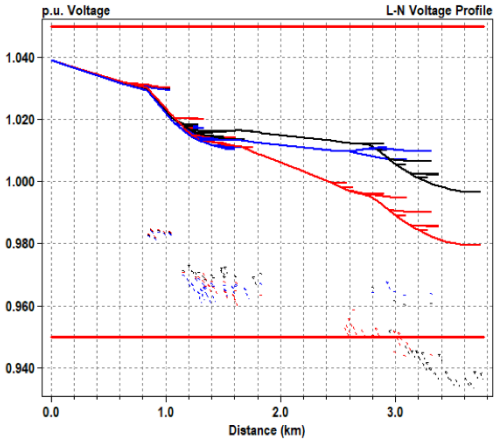

(a) Feeder 2 voltage

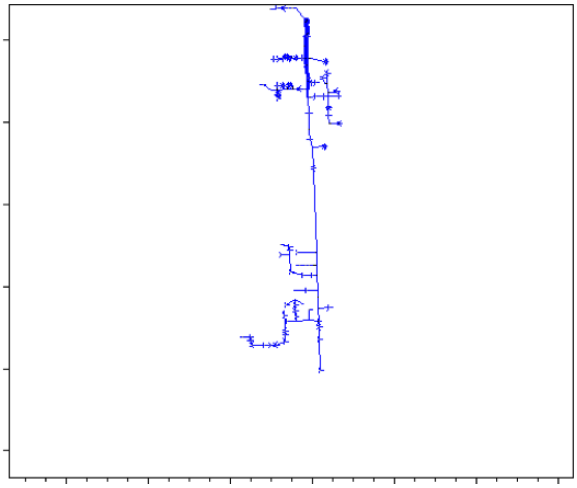

(b) Feeder 2 power

Figure 33. SCE Feeder 2 voltage and power

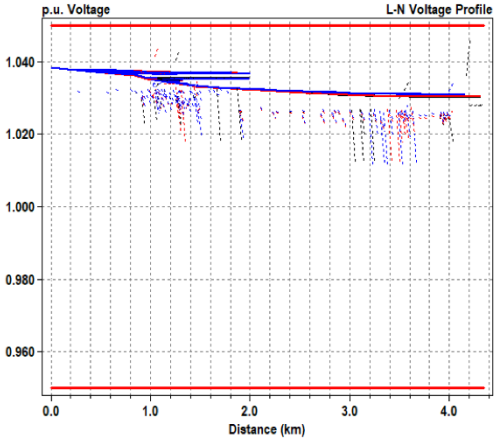

(a) Feeder 3 voltage

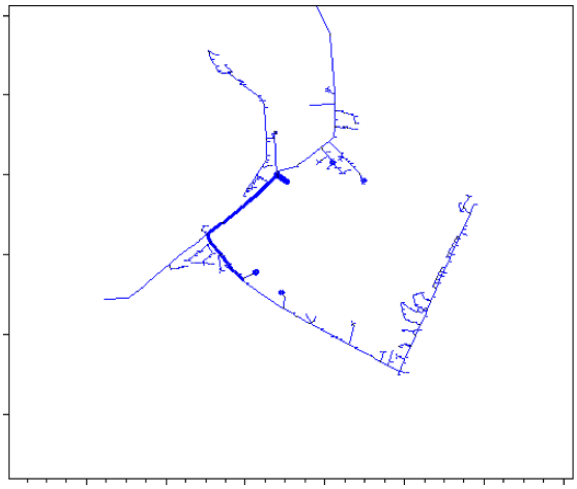

(b) Feeder 3 power

Figure 34. SCE Feeder 3 voltage and power

3.4.1 IEEE 1547-2003 Response

As in the simulations for Path 36, the aggregate response of all 123 feeder simulations (6,150 inverters) is provided for the IEEE 1547-2003 responses, with the normal PSLF CMPLDWG model only operation (i.e., transmission-level simulation only) plotted for comparison. As expected, for the pessimistic operation, a massive loss of distributed generation results concurrently with the fault. This loss of nearly 4 GW is detrimental to system stability, as discussed extensively in Section 4.3. This is expected when the credible worst-case contingency on the Western Interconnection is currently a double Palo Verde loss at 2.7 GW (North American Electric Reliability Corporation 2002). For the optimistic response, the output persists throughout the initial low voltage, essentially as an aggregate constant current source, until the units experiencing these lower voltages trip offline. Approximately half of the distributed generation remains online, showing that even 2 seconds of ride-through is consistent with a substantial portion of distributed generation not tripping during a typical FIDVR event. The contrast with the CMPLDWG model operation is stark; more than 2 GW of distributed generation will trip even with an optimistic view of inverter operation, which is very different from the near full recovery corresponding with voltage profiles shown for the CMPLDWG model.

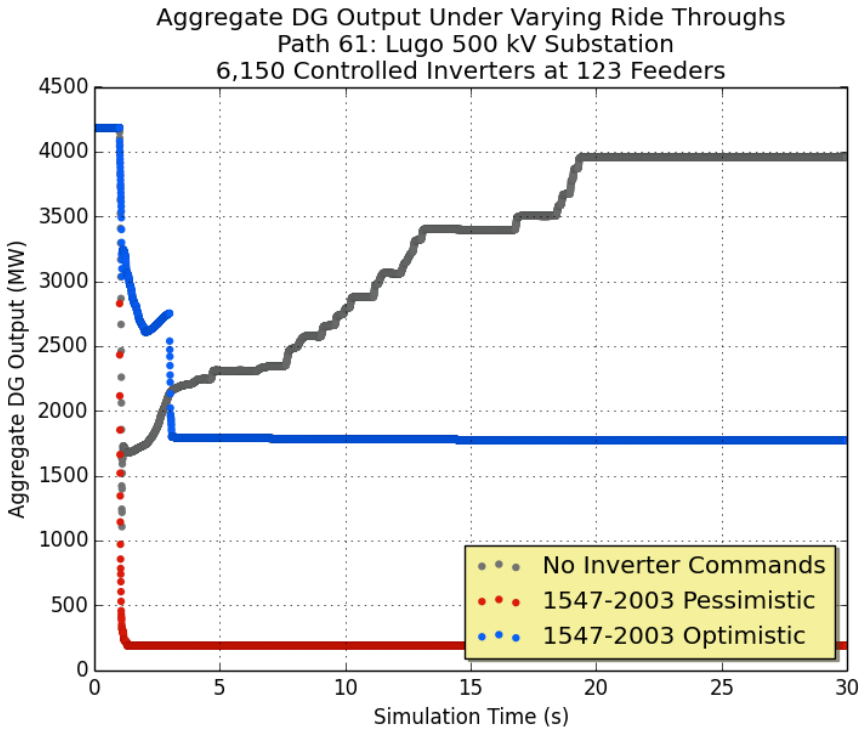

Figure 35. Path 61 aggregate distributed generation output with IEEE 1547-2003 criteria

3.4.2 IEEE 1547-2018 Response

A large diversity in the ensemble inverter response is shown in Figure 36, which charts the IEEE 1547-2018 responses. CatI and CatII responses are similar as anticipated, with CatII yielding a slightly better response. This case shows the full benefit of CatIII compared to the others, because even with inverters tripping 10 and 20 seconds after the fault, nearly 3,000 MW remain online with respect to the other cases. This shows that with an increased ride-through region, a large number of inverters will persist through a normal FIDVR event. Even more interesting is how much more distributed generation remains online with CatIII than in the initial transmission-only model for the first 10 seconds. Appendix 6.3 shows how influential the loss/recovery of distributed generation can be immediately around the time of the fault, which indicates that this ride-through behavior of CatIII—particularly under the FIDVR

conditions, such as that of the Path 61 fault—can be significant to system response. Indeed, this is the case, as is found in Section 4.3.

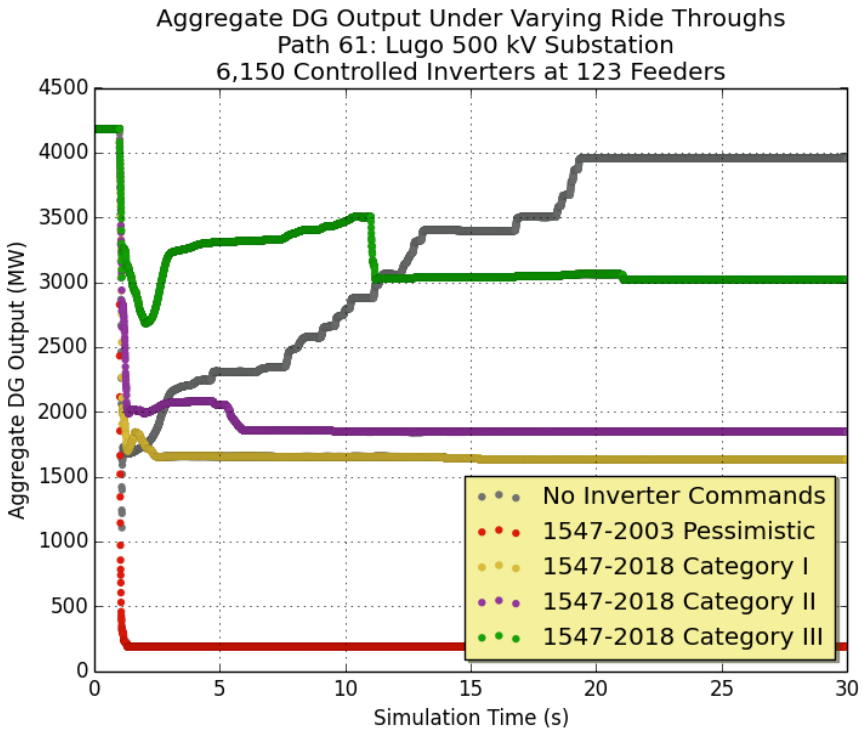

Figure 36. Path 61 aggregate distributed generation output with IEEE 1547-2018 criteria

3.5 Path 54: Arizona Public Service

For the Path 54 simulations of 71 feeders, the same three OpenDSS feeders from the SCE territory were used because region-specific feeder models were not readily available; however, the similarities between the SCE and APS service territory operations/design indicate that this pairing is not unfounded. The feeder summary and load allocation are shown in Table 15. With a more extreme FIDVR event occurring for the Path 54 scenario, we expect more inverters to time out and trip than in the Path 61 scenario.

Table 15. Arizona Public Service Feeder Summary

Feeder	Native Load (MW)	Type	Load Representation (%)	Allocated CMPLDWGs
1	5.06	Commercial/residential	38	27
2	1.71	Residential	47	32
3	7.82	Industrial	15	12

3.5.1 IEEE 1547-2003 Response

Again, in Figure 37, the aggregate response for the IEEE 1547-2003 responses are presented in the same format for the results of the Path 54 scenario. As shown previously, the pessimistic response yields a rapid and significant (1.4 GW, in this case) drop in distributed generation output. The optimistic response yields a 50% maintained distributed

generation output for the first 2 seconds following the fault, until the 2-second timers begin to trip and the majority of the distributed generation goes offline. These are not dissimilar to the CMPLDWG model response, which remains at a significantly reduced output because of the prolonged low voltages in the affected area.

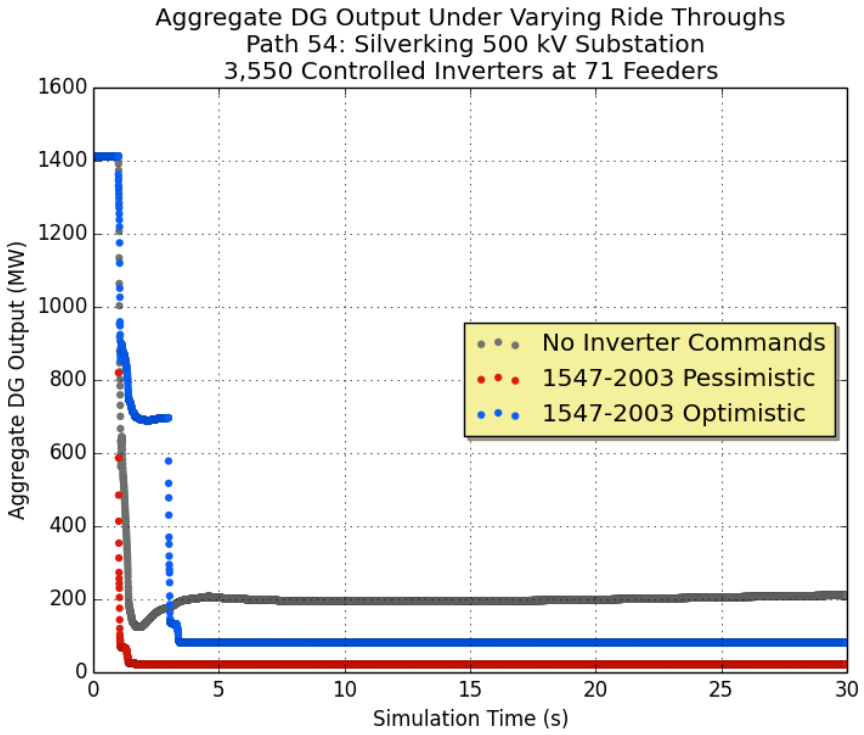

Figure 37. Path 54 aggregate distributed generation output with IEEE 1547-2003 criteria

3.5.2 IEEE 1547-2018 Response

The final chart for these distribution simulations is Figure 38, which shows the IEEE 1547-2018 responses to the Path 54 scenario. CatI and CatII are quite similar, with the exception of a slightly greater output for the first 4 seconds following the fault, during which the outputs converge to the same value for the remainder of the simulation. On great display is the full effect of the 10- and 20-second timers for CatIII-compliant inverters. We see a very significant drop in inverter output only 10 seconds after the fault, followed by a second drop 20 seconds after the fault, after which the output is comparable to CatI and CatII. This indicates that the low voltages on these feeders persist throughout the simulation, but the ride-through criteria very strongly affect the inverter output. The maintenance of this distributed generation output for the CatIII response significantly differs for the CMPLDWG response, which indicates that a different system response is anticipated for a PSLF fault simulation with this distributed generation output.

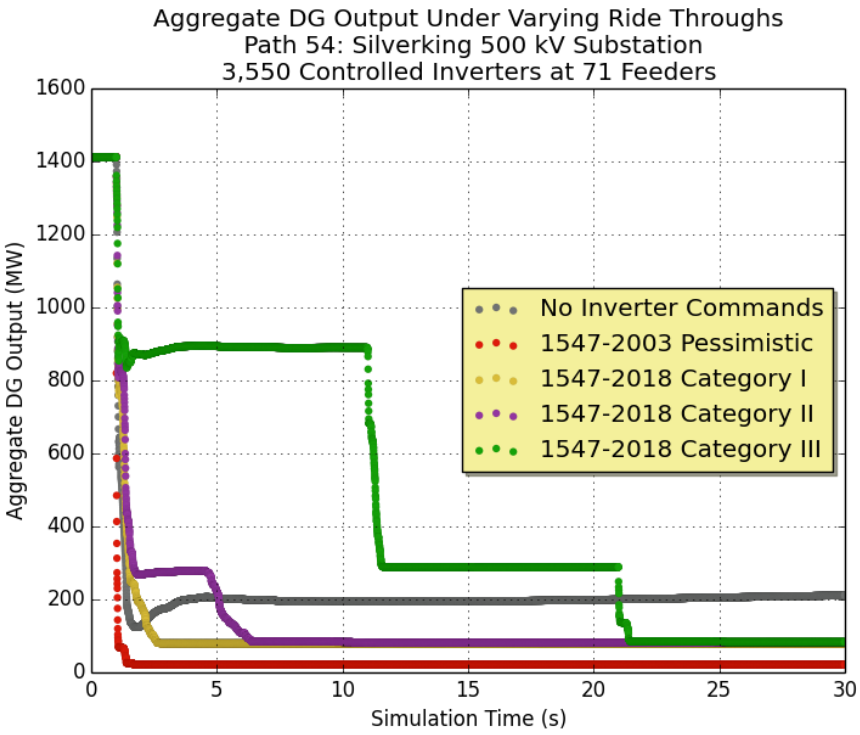

Figure 38. Path 54 aggregate distributed generation output with IEEE 1547-2018 criteria

4 Distribution-Informed Transmission Simulations

With the selected fault scenarios from the PSLF simulations, and the subsequent OpenDSS simulations individually representing the aggregate response of distributed generation considering the voltage diversity present on the distribution systems and the five defined types of IEEE 1547 voltage ride-through functionality, we now turn to the third step of this study: distribution-informed transmission simulations (DITSs). These simulations are essentially reruns of the three regional fault scenarios of interest but with the distributed generation output of the selected CMPLDWG models pertinent to each scenario managed based on the OpenDSS simulation results. The goal of these simulations is to derive any significant change in the system response on account of the commanded distributed generation outputs, which are compliant to the selected type of IEEE 1547 class. As will soon be evident, the response of the system changes significantly for the pessimistic and CatIII ride-through cases, particularly when the aggregate quantity of varying distributed generation is large.

It is helpful to remember that the coloring scheme is consistent throughout this section (and previous sections); i.e., all curves representing the pessimistic result are always red, all curves representing the optimistic result are always blue, etc. Even for the case of multiple solution iterations, as in Category III, the different iteration results are simply different shades of green, the CatIII color. Further, the legend coloring is representative of the data being presented; i.e., lime green is a frequency plot, beige is the faulted bus voltage profile, etc. The full description of the coloring scheme can be found in Section 1.3.1.

4.1 PSLF Simulations with Distributed Generation Commands

The DITSs are performed by resimulating the fault scenarios in the exact manner as in the initial transmission studies (the fault impedance and timing remain the same) but with time-series changes to the Vt1, Vt0, and Imax values of the CMPLDWG models based on the distribution studies, which are informed based on the IEEE 1547 ride-through criteria pertinent to that simulation; i.e., for the Path 36 pessimistic simulation, the parameters at the 66 CMPLDWGs of interest for this fault are changed throughout the simulation to generate the pessimistic distributed generation output response as modeled in the OpenDSS simulations. The following conditions are applicable to these DITSs:

- The minimum time between distributed generation output commands (requiring a pause in the PSLF simulation) is set at two cycles for reasons discussed comprehensively in Appendix 6.4.
- No distributed generation output updates are possible during the fault (from 1–1.1 seconds). Therefore, the Vt0 and Vt1 parameters are tuned to generate the distributed generation output found in the distribution simulations during the faulted condition.
- The distributed generation output is corrected based on the measured voltage at the low-side bus of the CMPLDWG to nullify current limiting because this is already accounted for in the OpenDSS simulations.

4.2 Path 36: Xcel

As is standard, we begin with the results for the Path 36 scenario. For these DITS, the distributed generation output for the five derived types of IEEE 1547 classes at the 66 CMPLDWG models is commanded according to the distribution simulation results. The outputs follow the results for figures 30 and 31. Note that the outputs in those figures are the aggregates for all 66 distribution simulations. For the DITS, these outputs remain separate and are individually commanded at each of the 66 CMPLDWG models.

4.2.1 IEEE 1547-2003 Commanded Response

For the IEEE 1547-2003 classes, the variations from the initial PSLF simulation are minimal, with no indication of the need for iteration. Figure 39 shows the overall system frequency for the initial, pessimistic, and optimistic simulations. The pessimistic response creates a decreased frequency condition, but noting the scale of the y-axis, it is evident that this is on the order of a small-scale load change that is continually managed on the power system (5 mHz). The optimistic response shows the least variation from the nominal frequency. Again, the variation in the other two cases is still quite small.

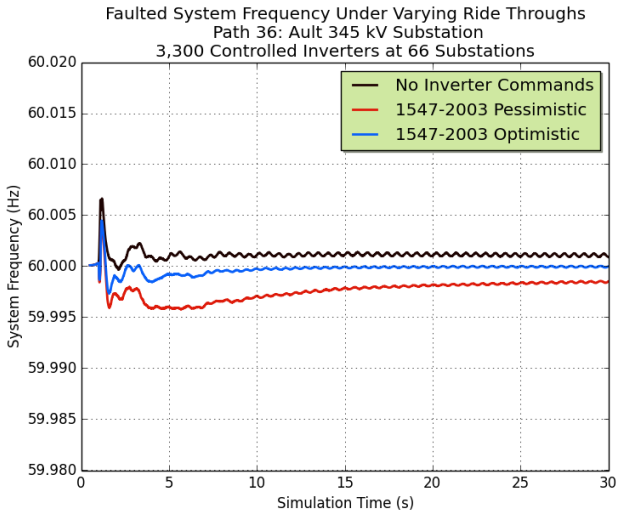

Figure 39. DITS: Path 36 system frequencies for IEEE 1547-2003 commands

Figure 40 gives the faulted substation voltage and the running volt-sec metric for this DITS. The responses of the pessimistic and optimistic simulations are nearly identical, and hence the red curve is seemingly absent in the charts. We see slight voltage oscillations that are not coincident with the initial PSLF simulation, although all three simulations have reached a settling voltage by the third second. This difference is likely on account of the deeper voltage dip in the initial PSLF simulation. The greater depth in this voltage dip at the faulted bus is not immediately understood, although the fault impedance is maintained. The running volt-sec metric shows that all buses have returned to voltages in excess of 0.95 p.u. within 200 ms of the fault clearing.

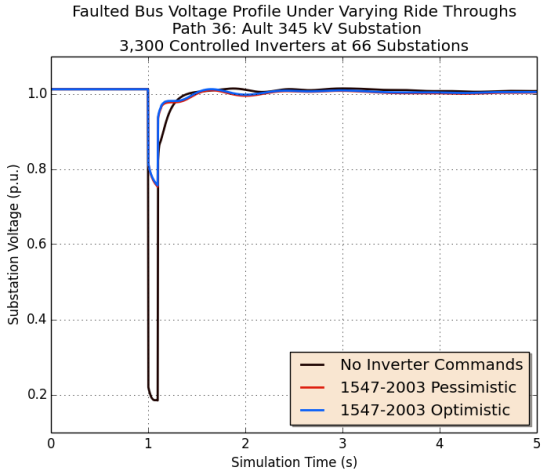

(a) Path 36 Ault 345-kV voltage profiles for IEEE 1547-2003 commands (pessimistic curve covered by optimistic curve)

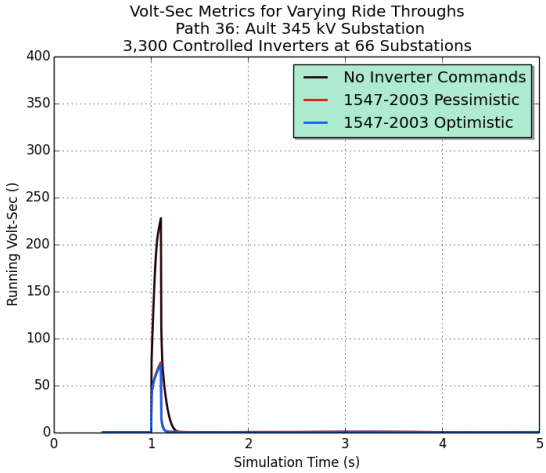

(b) Path 36 running volt-sec metrics for IEEE 1547-2003 commands (pessimistic curve covered by optimistic curve)

Figure 40. DITS: Path 36 Ault 345-kV voltage and running volt-sec metrics for IEEE 1547-2003 commands

4.2.2 IEEE 1547-2018 Commanded Response

As anticipated from the DITS for IEEE 1547-2003 ride-through events, the system responses for the new 1547-2018 ride-through events are not significantly different for the initial simulation. Again, this is likely on account of the small quantity of affected distributed generation (130 MW total), for which a disturbance of that magnitude the system is designed to handle on a regular basis. Figure 41 shows the system frequency chart for these simulations. The CatI, CatII, and CatIII responses are bounded by the initial and pessimistic frequency curves, indicating very minimal changes in the system responses with these distributed generation outputs.

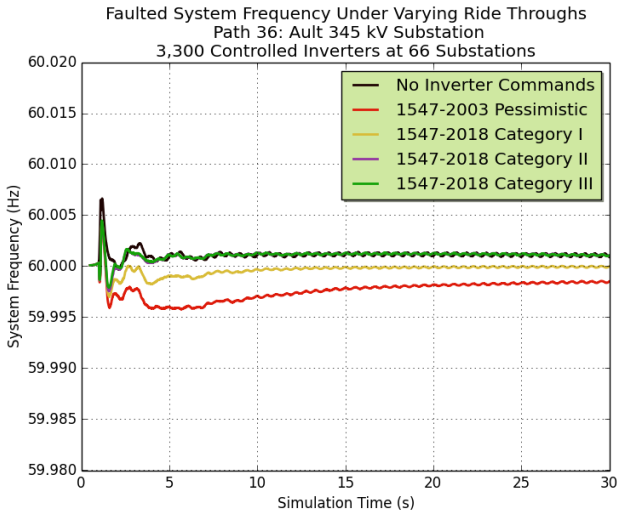

Figure 41. DITS: Path 36 system frequencies for IEEE 1547-2018 commands

The substation voltage profile and running volt-sec metrics are shown in Figure 42. As with the responses for the IEEE 1547-2003 classes, these show that all voltages recover very rapidly, with only slight oscillation at the sub-

station voltages. At the end of the Path 36 scenario DITSs, it seems reasonable to conclude that the various IEEE 1547 ride-through categories have a minimal effect on the overall system response. But, as shown in the following sections, this is not the case for faults impacting a larger area and greater quantities of distributed generation.

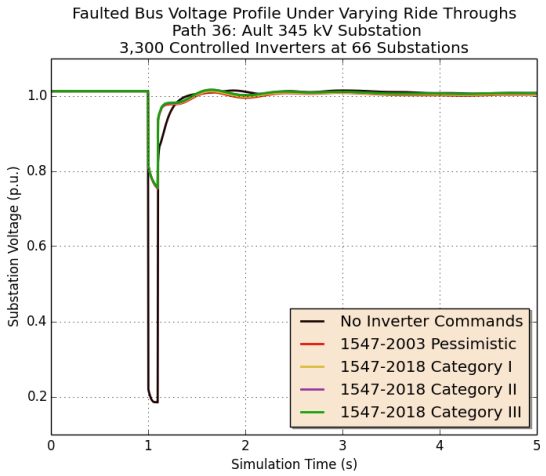

(a) Path 36 Ault 345-kV voltage profiles for IEEE 1547-2018 commands

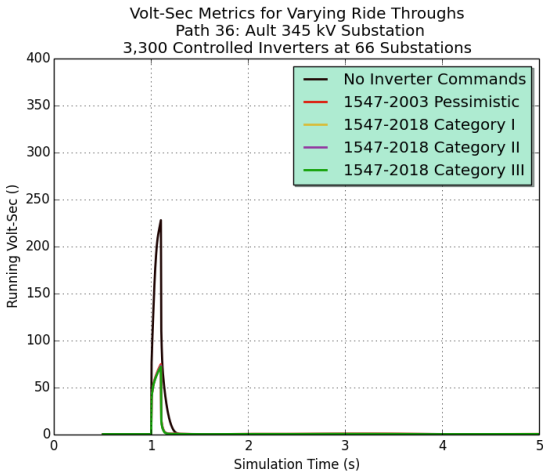

(b) Path 36 running volt-sec metrics for IEEE 1547-2018 commands

Figure 42. DITS: Path 36 Ault 345-kV voltage and running volt-sec metrics for IEEE 1547-2018 commands

4.3 Path 61: Southern California Edison

Because of the magnitude of distributed generation impacted in the Path 61 scenario, with more than 1,000 MW eventually tripping offline in the best-case IEEE 1547 class, we anticipate a larger impact on the system than in the Path 36 case. Additionally, with the FIDVR event and subsequent losses of various distributed generation quantities for many seconds after the fault depending on the IEEE 1547 class, a variety of responses are expected.

4.3.1 IEEE 1547-2003 Commanded Response

The system frequency measurements in Figure 43 show three significantly different responses. First, the immediate drop of nearly 4 GW of distributed generation in the pessimistic case right at the fault is detrimental to system stability, and in fact the simulation fails to render a full solution. The steady increase in system frequency shown as the red curve is indicative of this simulation divergence, and the termination of the pessimistic curve in figures 43 and 44 show the results of the simulation ending. This is marked by the vertical dotted curve and label. As a reminder, this simulation represents the tripping of any distributed generation experiencing voltage less than 0.88 p.u., a not unrealistic anticipated inverter response with IEEE 1547-2003 compliance. For the optimistic scenario, the frequency deviation is rapidly damped, followed by a slight underfrequency period because of the the loss of distributed generation, which is accompanied by normal load consumption because of the FIDVR mitigation. Finally, note that although distributed generation tripping alone would cause the frequency to decrease (the system essentially sees a load increase), in these cases we see frequency increases because the voltage-dependent load reduction is greater than the distributed generation loss (in real power consumption) as a result of the FIDVR event.

The Lugo 500-kV substation (fault location) voltage profiles, shown in Figure 44, show the start of the simulation failing to converge for the pessimistic case. In the optimistic class, the voltage profile shows that although the deeper FIDVR voltage depression does not occur, the voltage decreases by nearly 10% of steady state for the remainder of the simulation. The running volt-sec metrics tell a similar story, with an enormous rise in the pessimistic score before

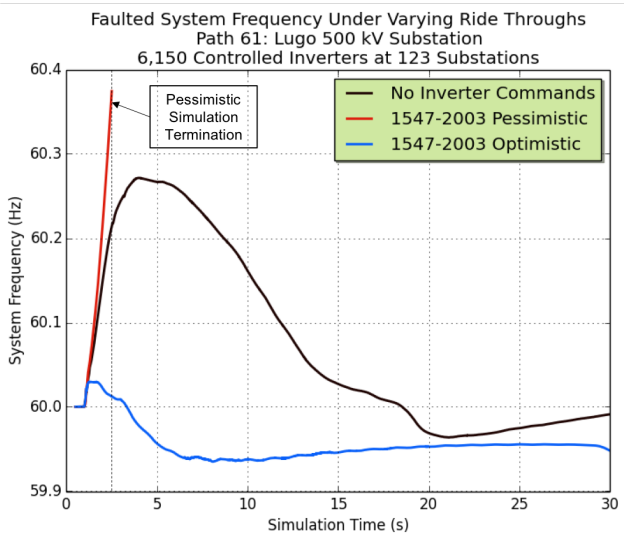

Figure 43. DITS: Path 61 system frequencies for IEEE 1547-2003 commands

the simulation is terminated. The optimistic curve corroborates the FIDVR mitigation claim, or at least the spatial extent of the FIDVR. The persistent score of around 25 indicates that some buses maintain voltages less than 0.95 p.u.

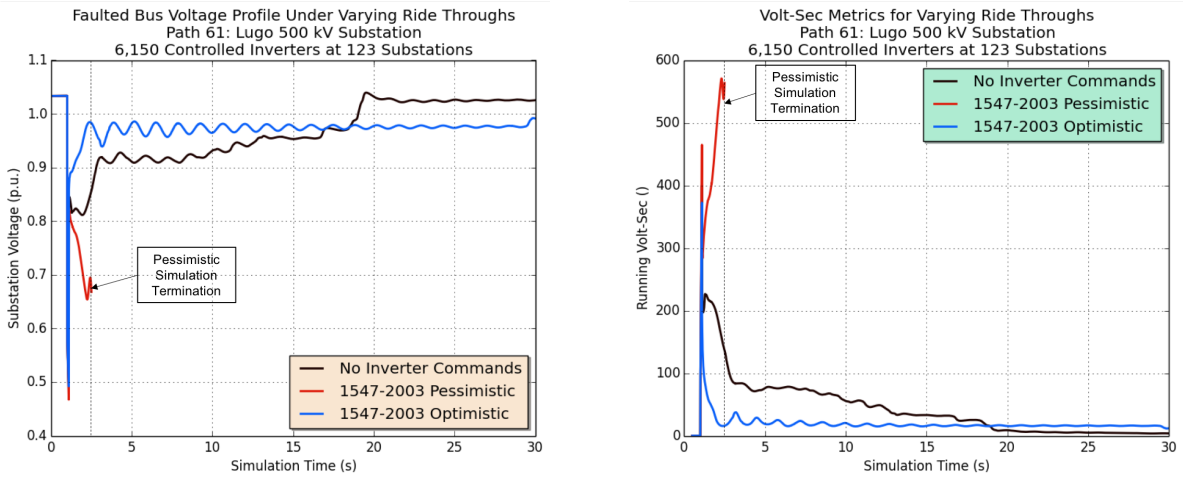

(a) Path 61 Lugo 500-kV voltage profiles for IEEE 1547-2003 commands

(b) Path 61 running volt-sec metrics for IEEE 1547-2003 commands

Figure 44. DITS: Path 61 Lugo 500-kV voltage and running volt-sec metrics for IEEE 1547-2003 commands

4.3.2 IEEE 1547-2018 Commanded Response

The CatI, CatII, and CatIII classes also provide a variety of system responses, with none causing any sort of simulation failure. Figure 45 shows that CatI experiences an overall system frequency similar to the initial transmission-only simulation, although the tail end of the simulation shows a growing difference. CatII results in a decreased peak in the system frequency, but throughout the 30-second simulation this does not cross back to the nominal. With the

CatIII response, we see the largest change from the initial simulation. Although the frequency increases briefly after the fault by about 40 mHz, this increase is arrested, and a return to nominal is achieved before 4 seconds. After this, even with the periodic distributed generation loss because of the 10- and 20-second timers, the frequency remains quite stable.

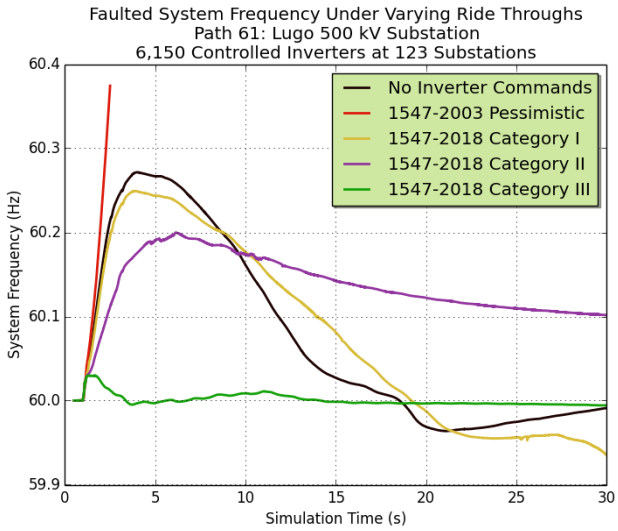

Figure 45. DITS: Path 61 system frequencies for IEEE 1547-2018 commands

The faulted voltage profile and running volt-sec metric in Figure 46 tell a few stories. First, we see that CatI follows the initial simulation profile, but it does not recover in kind with the standard FIDVR event. Toward the end of the simulation, however, this voltage begins to increase. Notice that the shapes of the running volt-sec metrics are often similar to the faulted substation, which is the case here, as shown by the similar response initially, with a slower recovery. For the CatII response, the initial voltage depression is not as deep as that for the initial simulation and CatI, but there is very little movement otherwise throughout the remainder of the simulation.

Again, the significant change in response is with the CatIII class. The faulted substation voltage profile shows a relatively quick recovery to near prefault levels accompanied by minor oscillations. A slight phase jump in these oscillations occurs around 10 seconds, right when around 500 MW of distributed generation trips offline because of the 10-second timer for voltages between 0.5 and 0.7 p.u. The running volt-sec metric shows a very favorable result with a very low metric following the fault clearing.

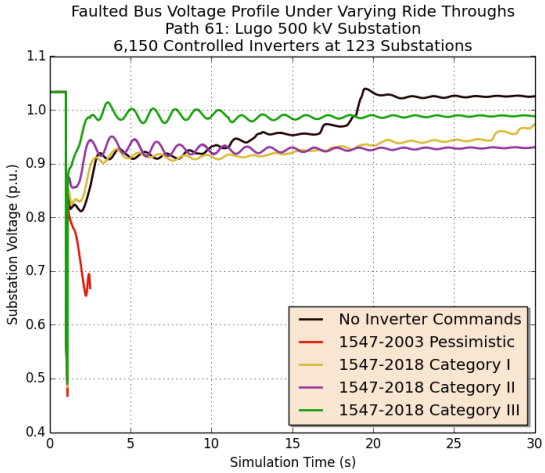

(a) Path 61 Lugo 500-kV voltage profiles for IEEE 1547-2018 commands

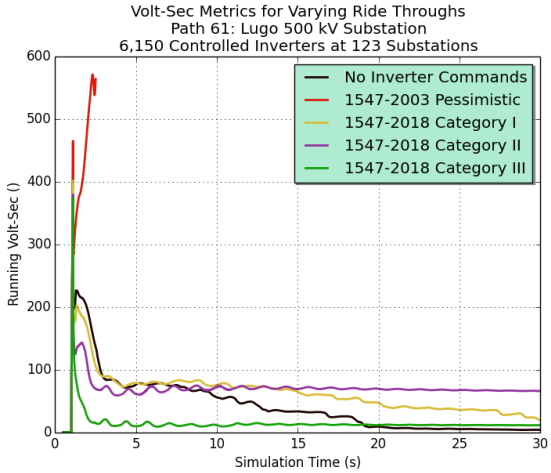

(b) Path 61 running volt-sec metrics for IEEE 1547-2018 commands

Figure 46. DITS: Path 61 Lugo 500-kV voltage and volt-sec metrics for IEEE 1547-2018 commands

4.3.3 Category III Iterations

Because the IEEE 1547 voltage ride-through implementation in this study is entirely guided by the voltage at the inverter terminals, the implications of the running volt-sec metric are that the distributed generation output response might differ substantially if the voltage waveforms from this DITS are used for a second iteration of distribution simulations. The goal of this iterative approach is for the modeled dynamic transmission system in PSLF, the distribution system (modeling voltage diversity among many distributed generators) and the individual distributed generation functionality models to converge in regards to the PSLF voltage profile outputs and the OpenDSS profiles of DER loss (i.e., the data connections between the cosimulated transmission and distribution systems). Ideally, communication between these cosimulated tools would be on a quarter-cycle, or higher, time frame; however, current limitations in the ability to seamlessly and quickly interface the tools together led to the development of this alternate form of "profile" interfacing taking the entire 30-second profiles from each tool and using that as the cosimulation connection. Although not ideal, the general separation of the dynamic voltage experienced at transmission buses and the real power potentially lost due to low voltage on the distribution system helps decouple the interaction between these two tools and thus makes this "very loosely coupled" cosimulation technique possible. We performed the iteratively solved technique for the case of the CatIII class because the system response is much better than for the initial transmission simulation (i.e., there is a relatively large difference in the PSLF CMPLDWG modeled results and the OpenDSS results in terms of distributed generation loss). No other cases are considered because the running volt-sec metrics are either similar, or worse, than the initial simulation, which indicates that the distributed generation output will not significantly change, at least with any sort of benefit. Because the optimistic class is mostly for comparison with the pessimistic, we do not iterate these results either.

In the following simulations, and with the iteration-based study on the CatIII class with the Path 54 scenario, we use shades of green for each data curve. The shade darkens with each progressive iteration. The labelling is such that the "first iteration" represents the first round-trip simulation; i.e., the initial simulation informs the distributed generation output that is used for the first DITS. Thus, the first iteration results are those presented in Section 4.3.2. See Figure 2 for a visualization of this simulation methodology.

Figure 47 provides the aggregate distributed generation output for the simulation iterations, with the first iteration represented as CatIII in Figure 36. Having noted the volt-sec recovery and therefore resimulating, we see that the results of the second iteration have a substantial increase in the overall output of distributed generation throughout the

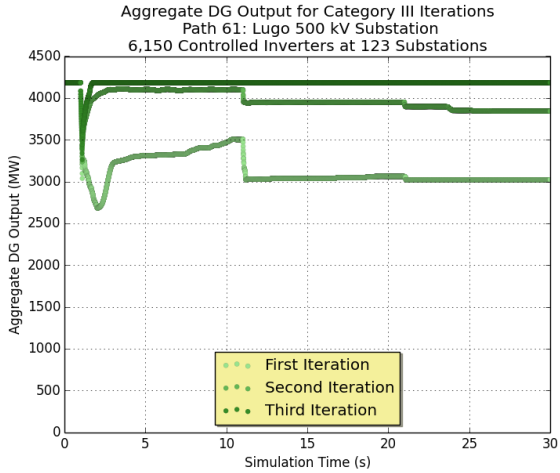

(a) Path 61 aggregate distributed generation output for Category III iterations

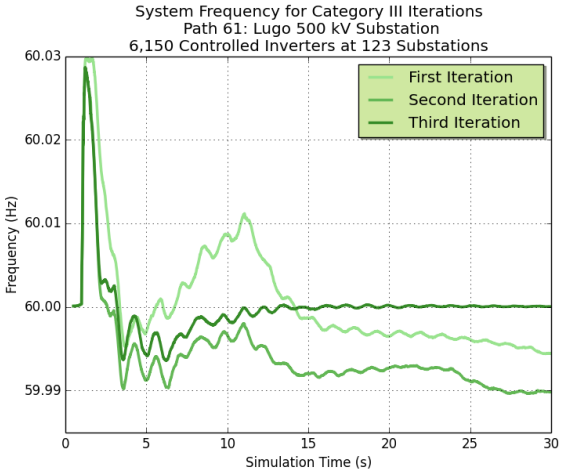

(b) Path 61 system frequency for Category III iterations

Figure 47. DITS: Path 61 aggregate distributed generation output and system frequency for Category III iterations

simulation. Certainly, reductions in distributed generation output occur concurrent with the initial voltage sag caused by the inverter current limiting and subsequent timer expirations at 10 and 20 seconds; however, the magnitudes of the distributed generation reductions are significantly reduced. The frequency response shows an overall reduction in system frequency to nominal with respect to the first iteration. Figure 48 shows that the substation voltage profile and the running volt-sec metric have improved substantially again, with the substation voltage immediately returning to prefault levels and the running volt-sec moving to zero nearly immediately as well. These improvements in the results indicate that a third iteration was a reasonable step.

Figures 47 and 48 show the results of a third iteration on each of the respective charts as the darkest green curve. We see that the distributed generation output has not changed from full output except for the brief period during and immediately after the fault when the inverters are current limited because of the low voltages. In the frequency plot, the change in the final result is slight, with a return to nominal midway through the simulation. Note that the frequency divisions on this plot are 10 mHz, whereas in Figure 45 they are 100 mHz. Finally, there is very little change in either the substation voltage or the running volt-sec, indicating that the responses between the second and third iteration have mostly converged with respect to further distributed generation output changes.

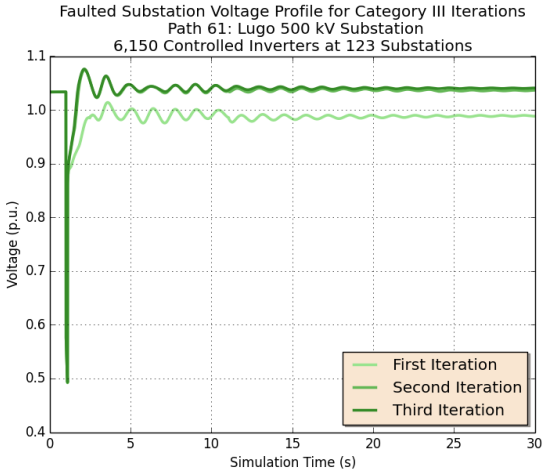

(a) Path 61 Lugo 500-kV voltage profiles for Category III iterations

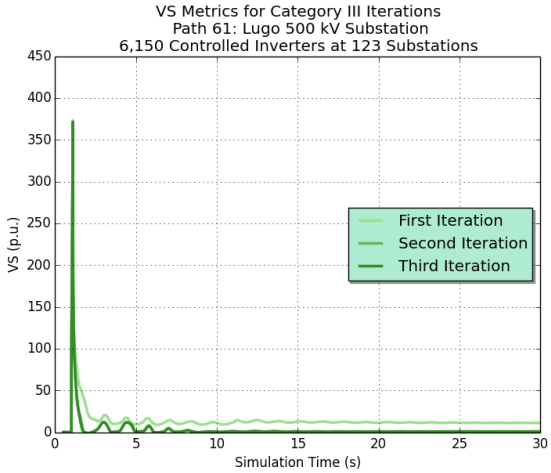

(b) Path 61 running volt-sec metrics for Category III iterations

Figure 48. DITS: Path 61 Lugo 500-kV voltage and running volt-sec metrics for Category III iterations

4.4 Path 54: Arizona Public Service

Rounding out the DITSs, we turn to the Path 54 scenario with the extreme FIDVR event. We find that all of the responses except for CatIII are very similar to the initial simulation. This indicates that iterations on the CatIII response are warranted.

4.4.1 IEEE 1547-2003 Commanded Response

The pessimistic and optimistic overall system frequency and the substation voltage/running volt-sec results are presented in figures 49 and 50. Evidently, the response of the pessimistic case is nearly identical to that of the initial simulation. We observe from Figure 37 that the distributed generation outputs for the initial and pessimistic scenarios are quite similar, so similar system responses are expected. The presence of roughly half the distributed generation output for 2 seconds after the simulation does change the system response. We see that the frequency deviation is arrested very quickly, with a peak deviation of 60 mHz instead of 250 mHz. The faulted substation voltage settles at a level 10% greater than the initial simulation, whereas the running volt-sec metric shows an overall improvement in the system voltages. As with the Path 61 scenario, the optimistic response seems comparable to the CatIII response, at least for the first 2 seconds following the fault. This indicates that iterations will be necessary for the CatIII ride-through case.

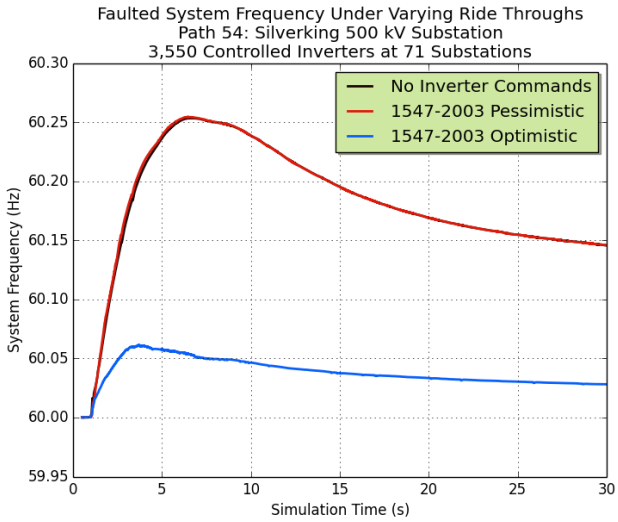

Figure 49. DITS: Path 54 system frequencies for IEEE 1547-2003 commands

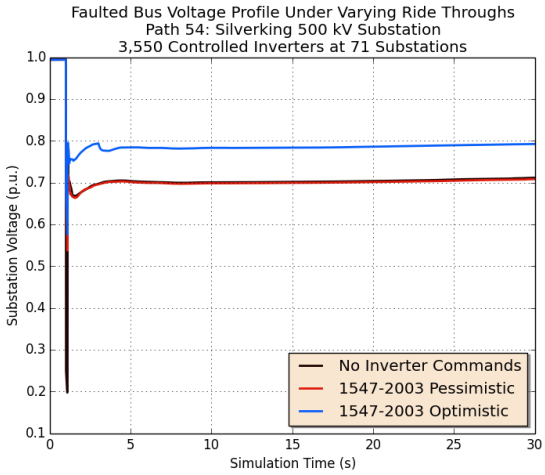

(a) Path 54 Silver King 500-kV voltage profiles for IEEE 1547-2003 commands

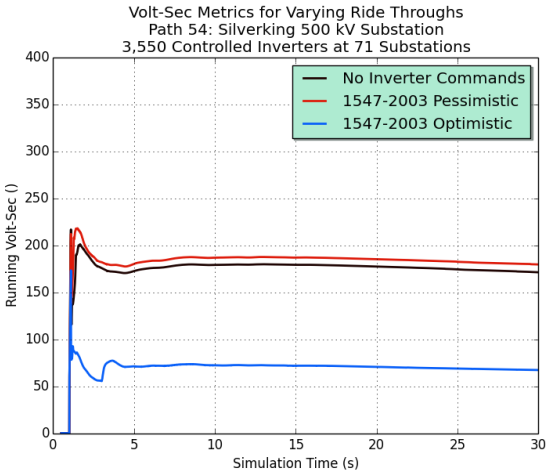

(b) Path 54 running volt-sec metrics for IEEE 1547-2003 commands

Figure 50. DITS: Path 54 Silver King 500-kV voltage and running volt-sec metrics for IEEE 1547-2003 commands

4.4.2 IEEE 1547-2018 Commanded Response

The IEEE 1547-2018 DITS responses are shown in figures 51 and 52. For CatI and CatII, the responses are not significantly different from the initial simulation. Again, these results are expected because of the comparable loss and lack of recovery in distributed generation output. The system frequencies are both within 25 mHz of the initial simulation, with the slight reduction caused by the minimal, immediate ride-through before a near total loss of distributed generation output. With near identical responses, no iterations are performed for these two cases.

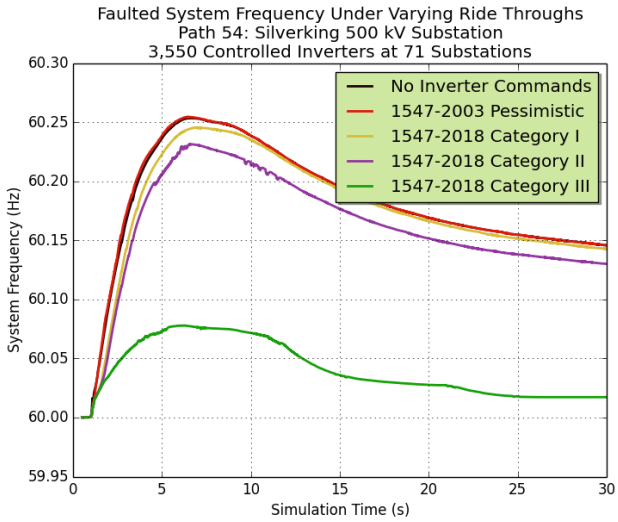

Figure 51. DITS: Path 54 system frequencies for IEEE 1547-2018 commands

CatIII shows a substantial benefit in the system response. The frequency deviation is reduced by 75%, with the recovery within 30 seconds of simulation coming much closer to a nominal frequency level. The substation profile shows a 0.1-p.u. rise in the settling voltage, although the losses in distributed generation because of the timeout of the inverters at 10 and 20 seconds are visible and nontrivial. These perturbations are present in the frequency as well, where slope changes in the recovery are seen at 11 and 21 seconds. Finally, the running volt-sec shows a large improvement in the system-wide voltage profile. These results indicate that iterations will result in substantially different aggregate distributed generation output responses for the CatIII class.

4.4.3 Category III Iterations

For the Path 54 CatIII responses, four iterations were performed, and the results are included in figures 53 and 54. From the aggregate distributed generation output plot, we see an improvement with each iteration, although the presence of output step-downs remains 10 and 20 seconds after the fault. The system frequencies improve from the first iteration, but, interestingly enough, the DITS with the closest frequency to nominal is the third iteration, not the fourth. This might indicate that this iterative procedure results in an overshoot that could temper with further iterations. Regardless, the frequency deviations are substantially less than the initial simulation. Again, note that the frequency divisions are in 20 mHz instead of 100 mHz in Figure 51.

The substation voltage profiles show a convergence to a post-fault value of 0.94 p.u., much greater than the 0.8 p.u. in the first iteration or the 0.7 p.u. in the initial simulation. The running volt-sec confirms the improvement in the system voltages because the metrics show a near-zero score for the second and third iterations. Again, there is a seeming reduction in improvement with the fourth iteration, the cause of which is not entirely known.

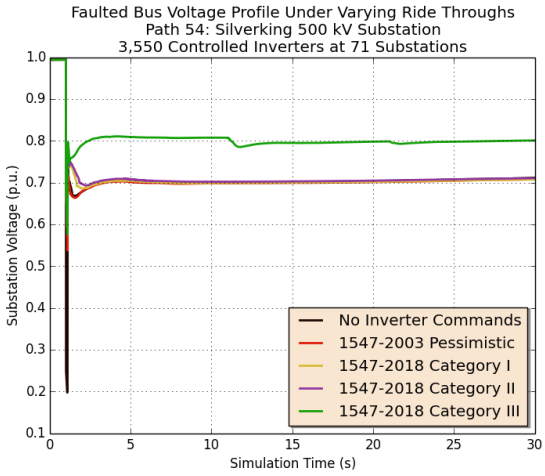

(a) Path 54 Silver King 500-kV voltage profiles for IEEE 1547-2018 commands

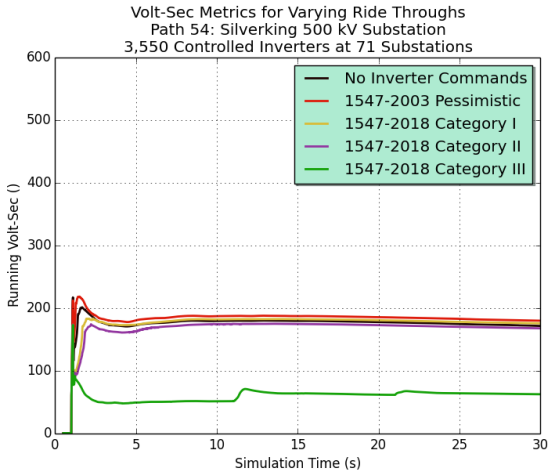

(b) Path 54 running volt-sec metrics for IEEE 1547-2018 commands

Figure 52. DITS: Path 54 Silver King 500-kV voltage and volt-sec metrics for 1547-2018 commands

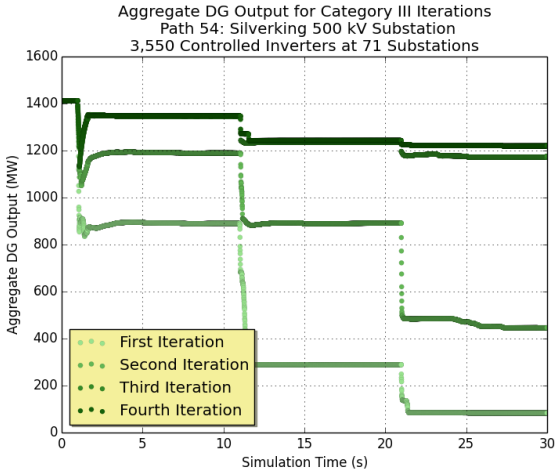

(a) Path 54 aggregate distributed generation output for Category III iterations

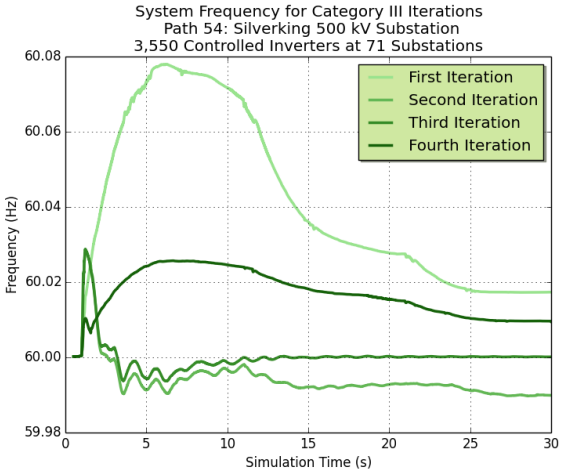

(b) Path 54 system frequency for Category III iterations

Figure 53. DITS: Path 54 aggregate distributed generation output and system frequency for Category III iterations

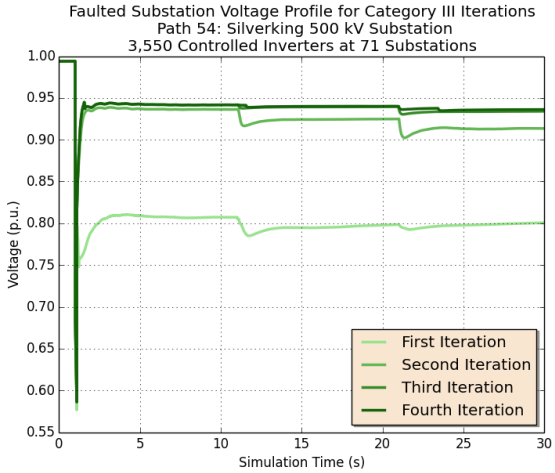

(a) Path 54 Silver King 500-kV voltage profiles for Category III solution iterations

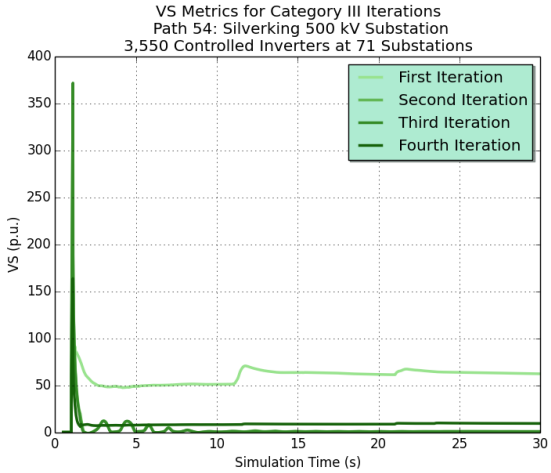

(b) Path 54 running volt-sec metrics for Category III solution iterations

Figure 54. DITS: Path 54 Silver King 500-kV voltage and running volt-sec metrics for Category III iterations

4.5 Summary of Results

The following is a brief table providing the peak quantity of distributed generation lost for the three fault scenarios, and the four different performance categories. The IEEE 1547-2003 optimistic results are omitted.

Table 16. Peak Distributed Energy Resource Real Power Reduction by Performance Criteria

Location: Faulted Path	2003	2018 Category I	2018 Category II	2018 Category III
Xcel: Path 36	130 MW	100 MW	100 MW	80 MW
APS: Path 54	1,390 MW	1,330 MW	1,330 MW	1,330 MW
SCE: Path 61	4,000 MW	2,550 MW	2,340 MW	1,500 MW

5 Conclusion and Future Research

5.1 Conclusion

After performing a large quantity of transmission and distribution simulations for three regions in the Western Interconnection, along with final transmission simulations informed by distribution simulation results, we found that the type of ride-through implemented by DERs is a significant factor to the overall power system response to transmission-level faults. This impact is particularly high for transmission-level faults that depress voltage levels for high numbers of substations (i.e., for cases that experience large regional voltage sags). Because of the programmed nature of the ride-through of IEEE 1547-compliant DERs, the potential for large reductions in real power injection are possible based on IEEE 1547 interpretation and specific implementation. In this study, we made a first attempt to determine the quantity of DERs affected by a variety of transmission-level faults as well as a granular response of distribution-simulated DERs to a few different types of IEEE 1547-2003 interpretations and IEEE 1547-2018 voltage ride-through categories. Finally, through distribution-informed transmission studies, it was shown that the category of IEEE 1547 adherence, particularly with the new 2018 standard, can have a significant impact on the amount of DER-based generation lost following transmission-level fault events. Following is a summary of the study's conclusions:

Key Findings

- Under heavy loading conditions representative of summer peak load in the Western Interconnection, the potential for a widespread influence on voltage profiles following a transmission-level fault is significant. This highlights the potential for large losses of DERs depending on the implemented low-voltage ride-through criteria; however, even with this large influence, the colocation of the fault with high DER penetrations is the primary factor when considering potential generation losses caused by faults (see the magnitude differences between the Colorado Front Range and Southern California cases in Table 16).
- The newly introduced volt-sec and volt-sec-DG metrics provide suitable analysis tools for making relative comparisons of the influence of a variety of transmission-level faults on the overall power system voltage profiles. In particular, the volt-sec-DG metric effectively highlights the relative impact of these faults on potential DER loss.
- The specific performance of DERs during fault conditions can have a large impact on the recovery of the power system. This highlights the importance of understanding the true operation of inverter-based generation during power system transient events and the need for improved models.
- FIDVR events generate persistent low-voltage profiles at distribution-voltage levels, which can in some instances persist beyond the trip times specified in the IEEE-2018 ride-through criteria, leading to the loss of DER generation.
- The IEEE 1547-2003 standard allows for a nearly immediate momentary reduction in the power output of DERs for relatively small voltage deviations from nominal, which can potentially result in a large loss of generation. For instance, the large penetrations of DERs in California lead to a nearly 4 GW loss of generation for specific faults in Southern California. Other interpretations or implementations of IEEE 1547-2003 could allow significant voltage ride-through capability, greatly reducing this potential generation loss.
- Performance categories I and II from IEEE 1547-2018 yield similar aggregate DER real power responses and similar overall system recovery characteristics. Implementation of the Category III ride-through criteria of IEEE 1547-2018 yields respectively smaller total real power output reductions.

5.2 Future Research

This study provides valuable insights into mechanisms necessary for the Western Interconnection to experience a widespread DER tripping event and provides scenario-based analysis showing how the voltage ride-through performance categories of IEEE 1547-2018 and default settings of IEEE 1547-2003 partially mitigate such events; however, a number of improvements in the underlying analysis have been identified that should be considered in future work. These are listed as follows:

- The results from iterated distribution-informed transmission simulations, as presented in Section 4.3.3 and Section 4.4.3, show that a more closely coupled simulation between the transmission simulation and the distribution simulation would provide a more accurate result. The simulation method reported here appears to generally, or potentially, overestimate the amount of DER that would trip for a given transmission-level fault.
- The dynamic response of DERs (i.e., PV inverters) during the faulted conditions in this study is solely modeled using the PVD1 dynamic model in PSLF. The aggregate response of the hundreds or thousands of DERs connected to an entire distribution system that is being represented by the PVD1 model for a single transmission level has not been well characterized. Future work on more accurate dynamic models for individual and aggregate DERs would provide further accuracy to build confidence in studies such as this one.
- One underlying challenge in accurately determining the impact of DERs on the transmission system is uncertainty in the load models used for dynamic analysis. The composite load model (used in this study) is a well-accepted model, but efforts to improve these load models—whose variations in parameterization can significantly change study results—would build the confidence in studies specifically investigating the voltage-related (as opposed to frequency-related) impacts on the transmission system.
- The individual DERs in this study were modeled as if they implemented their corresponding IEEE 1547-2003 or 2018 settings perfectly. DER operation models that include nonidealities such as tracking error in the phase-locked loop of a PV inverter and sampled and filtered voltage and frequency measurement might identify important salient response features relevant to similar studies.
- The DER deployment location and aggregate amount was derived from a previous study completed by NREL nearly 10 years ago. At that time, this amount of DER was a futuristic case. With the rapid growth in DERs, more accurate modeling of the specific location and aggregate amount, as well as an understanding of the programmed IEEE 1547 settings, would likely lead to a better understanding of specific system responses to faults that cause a widespread voltage suppression over a relatively large area. Additionally, any voltage-sensitive protection present on loads or on feeders themselves could also increase the accuracy and usefulness of future study results.

6 Appendix

6.1 Commanding Distributed Generation with Current Limiting

To match the distributed generation output at each composite load model with generation (CMPLDWG) model with the OpenDSS simulations, we make use of the internal PVD1 model, which manages the output of the distributed generation throughout a dynamic simulation. The PVD1 model topology is shown in Figure 55. All distributed generation located at CMPLDWG models inject real power only, which means the control system simplifies significantly with the reactive current branch essentially disabled. Thus, Ipmax is equivalent with Imax, which is a parameter that can be adjusted during pauses throughout a dynamic simulation. The Pref value is a constant (one p.u.), with Pdrp and Pext zero, throughout the simulation. This means the PVD1 output is easily reduced during periods of low voltages. Note that distributed generation exceeding the initialized output is not possible; however, this does not change the approach to these simulations because distributed generation output is only ever reduced from the initial prefault, dispatch.

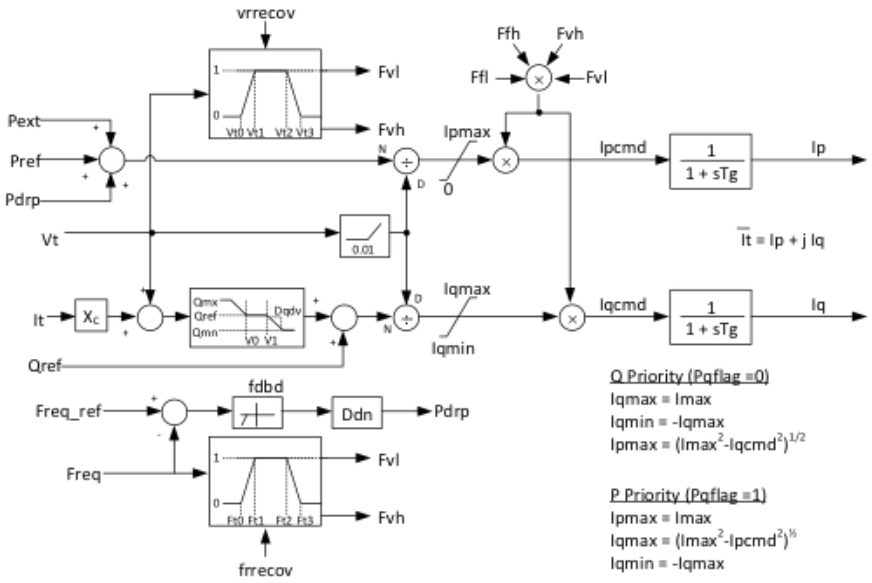

Figure 55. PVD1 control scheme

To control the output during a simulation, a tim -series of the intended per-unitized power output is divided by the current per-unitized voltage at the relevant CMPLDWG model. This serves to nullify any internal voltage correction by the PVD1 model because this is already compensated in the OpenDSS simulation. This value is then set as the Imax value for the CMPLDWG. The result is a distributed generation output equivalent to the OpenDSS simulations at each step in the distribution-informed transmission simulations (DITSs). To prevent a low-voltage ride-through action from the PVD1 model, the Vt0 and Vt1 parameters are set to zero; however, these parameters are not set to zero until after the fault because the simulation cannot be successfully paused while in the faulted condition. This requires internal PVD1 action to reduce the distributed generation output during the fault. Therefore, a basic tuning of the Vt0 and Vt1 parameters for each transmission/distribution simulation was performed, with the set points provided in Section 6.6.

6.2 Measuring System Frequency

A primary metric for assessing the response of the system after a fault and subsequent distributed generation operation is the system-wide frequency. This metric is calculated by using a weighted average approach of all synchronous machines connected and operational during the dynamic simulation. Mathematically, this is accomplished as shown in Eq. 6.1.

$$\omega(t) = \frac{\sum_{i=1}^{n}(MVA_i * \omega(t)_i)}{\sum_{i=1}^{n} MVA_i} \tag{6.1}$$

Where:
$\omega(t)$ is the calculated system frequency at time t.
$\omega_i(t)$ is the frequency of generator i at time t.
MVA_i is the apparent power rating of generator i.

Although this average system frequency approach obscures localized frequency deviations, it is an effective way to measure the overall health of the system following disturbances. Because of the dominance of the swing equation in power system dynamics, the system frequency can be interpreted as an indicator of load-generation balance. Frequencies greater than 60 Hz indicate overgeneration, and frequencies less than 60 Hz indicate undergeneration.

6.3 Distributed Generation Timing Impact: Sensitivity Analysis

Initial simulation work, and a bit of intuition, revealed a very strong link between the timing of distributed generation loss, with respect to the fault initiation and clearing, and subsequent system recovery. This is particularly relevant when the quantity of distributed generation tripping is substantial—for instance, as in the Path 61 pessimistic responses. Therefore, a brief sensitivity analysis was performed to better understand the impact of the distributed generation loss timing. The subsequent sections provide an overview of this timing analysis as well as a brief look at the impact of distributed generation recovery. These simulations were performed for the Path 61 scenario, with a fault on the Lugo 500-kV substation.

6.3.1 Distributed Generation Step-Loss Analysis

For the distributed generation loss analysis, 2,400 MW of distributed generation at 54 CMPLDWG models were commanded as a single-step function; i.e., all distributed generation at all 54 substations was tripped offline at the same simulation time step. The amount of 2,400 MW was chosen instead of the total influenced distributed generation for the Path 61, measuring a total of 4,000 MW, because the simulation simply fails to converge when 4,000 MW is tripped off; thus, there is no sensitivity to observe. At 2,400 MW, this quantity is on par with the credible double contingency of two Palo Verde units. Figure 56 shows three different moments when all of these 2,400 MW of distributed generation were stepped: 1 second, the moment the fault is initiated; 1.1 seconds, the moment the fault is cleared; and 1.2 seconds, six cycles after the fault is cleared. Three different simulations were preformed for these three timings. All 2,400 MW at these 54 CMPLDWG models were stepped off for each of these three simulations, and they were kept at zero output for the remainder of the simulation. The curve coloring is consistent for each simulation.

Figure 57 shows the voltage at the Lugo substation for each of these three simulations as well as the running volt-sec metric for each simulation. When the distributed generation is tripped off at the fault initiation, a low voltage persists for the majority of the simulation; however, this simulation fails to converge around 28 seconds, and hence the curve terminates. When the distributed generation is tripped at the moment of fault clearing, a low-voltage condition exists, but recovery is prolonged, with the voltage still around 0.9 p.u. at the end of the simulation. Interestingly, when the distributed generation is tripped six cycles after the fault clears, no extended low-voltage event is recorded. The

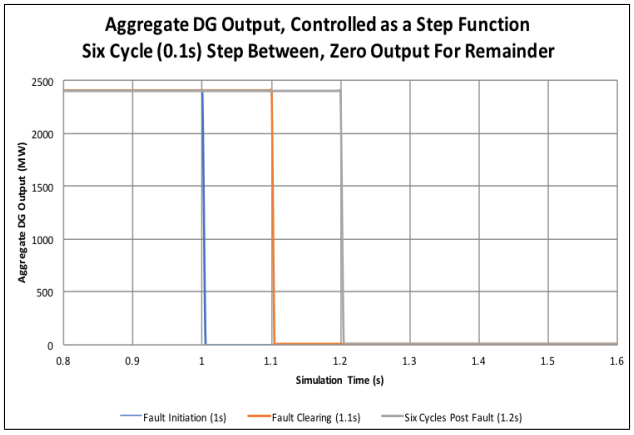

Figure 56. Aggregate distributed generation step-loss timing

running volt-sec metric shows that overall system voltage response is worse with the distributed generation tripping at the fault initiation, but a recovery is clearly underway before the simulation has convergence issues. When the distributed generation trip occurs at the fault clearing, a large volt-sec metric occurs again, although not as significant as the previous case. Finally, when the distributed generation is tripped six cycles after the fault, the overall voltage response shows a minimal voltage deviation.

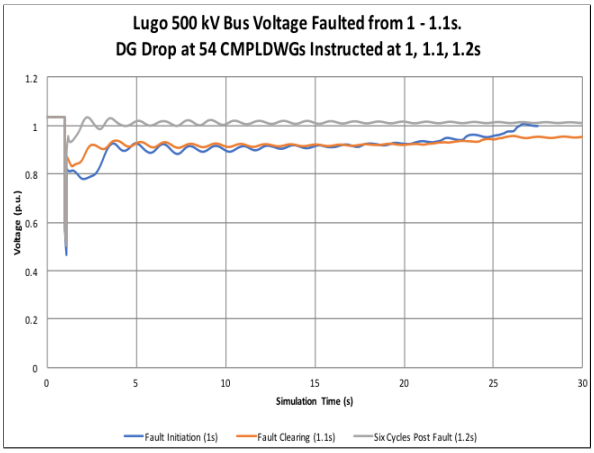

(a) Lugo 500-kV voltage response to varied distributed generation step losses

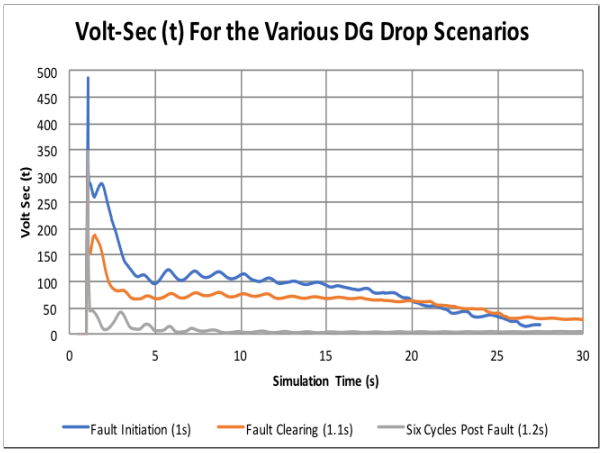

(b) Running volt-sec comparison for varied distributed generation step losses

Figure 57. Lugo 500-kV voltage and running volt-sec response to varied distributed generation step losses

6.3.2 Distributed Generation Step-Recovery Analysis

Taking the distributed generation step-off at the fault initiation, which is evidently the worse-case simulation based on the running volt-sec, we now experiment with different timings on the recovery of this distributed generation. This consideration is important to understand the impact of aggregated inverter-based distributed generation's transient response to the grid fault. Although such transients can clearly not be modeled in the dynamic time frame, it is still important to understand the assumptions and their sensitivities. Inverter operation during a voltage sag will depend on many things, such as the waveform shape of the voltage during the fault (i.e., harmonics), the phase-locked

loop performance of the inverter, and other control loops and the general control methods employed within the inverter systems. As before, all 2,400 MW are stepped off, but five different recovery scenarios occur with a step to full output at 0, 6, 12, 30, and 60 cycles after the fault clearing. Figure 58 shows the five different recovery scenarios as well as the aggregate distributed generation output of these 54 CMPLDWG models for the standard Path 61 simulation; i.e., there are no commands otherwise. We see that the standard simulation results in a significantly reduced distributed generation output with respect to these undergoing step recoveries.

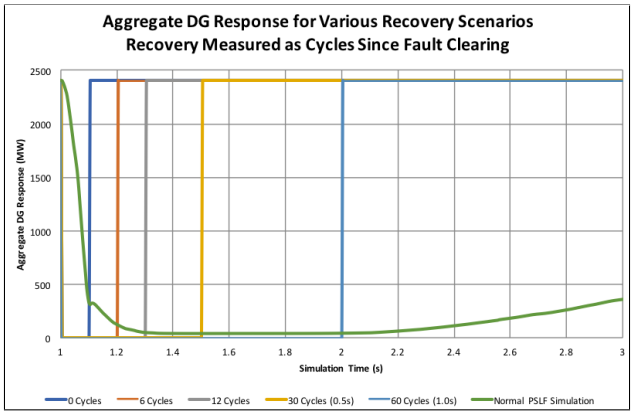

Figure 58. Aggregate distributed generation recovery steps

Figure 59 shows the Lugo substation voltage profiles for these five step-recovery simulations as well as the standard simulation. It is evident that the rapid recovery of the distributed generation—i.e., within 12 cycles of the fault clearing—yields a rapid recovery from what would otherwise remain a FIDVR event. As shown in Figure 60, however, the simulation with distributed generation recovery at the fault clearing results in severe oscillations (this explains the truncation of the trace).

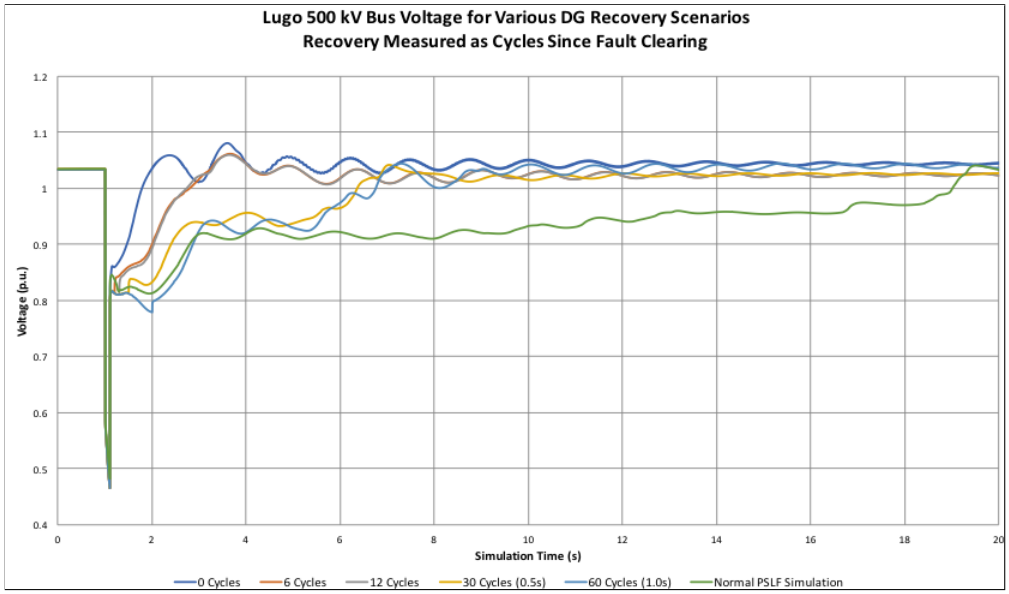

Figure 59. Lugo 500-kV response to varied step distributed generation recoveries

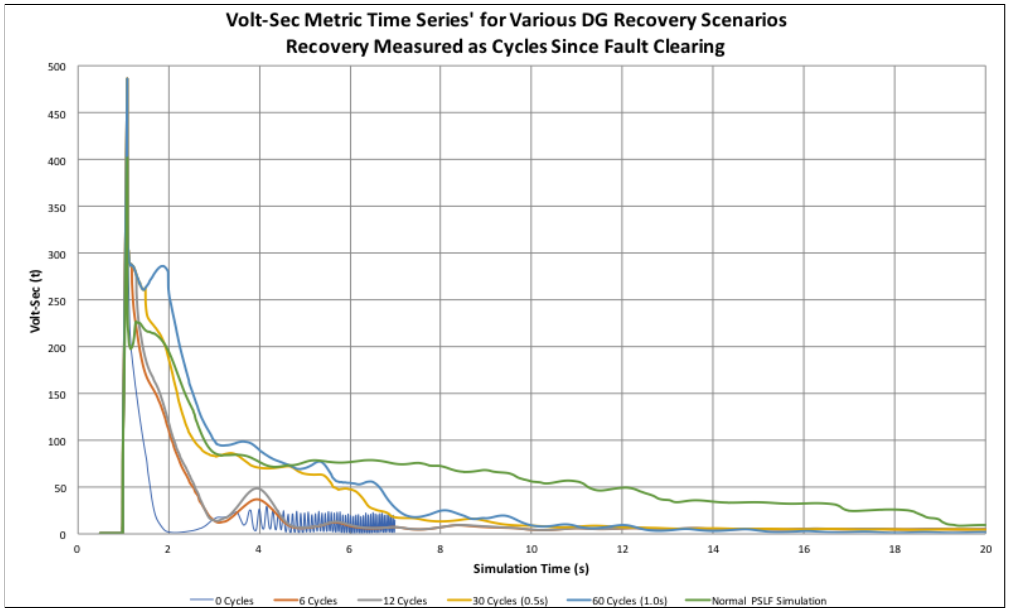

Figure 60. Running volt-sec metric comparison for varied-step distributed generation recoveries

6.4 PSLF Simulation: Too Many Simulation Pauses

A quirk in the Positive Sequence Load Flow (PSLF) simulations—recognized only when minute changes in distributed generation output were attempted, resulting in simulations pauses nearly every quarter cycle—is that the dynamic simulation advances two time steps for every instance of pause, even though the output channels print a single time step. This results in a distorted system response, both in time dilation and actual system states. As an example, an identical simulation (fault at 1 second, clears after six cycles) was performed five times with equal interval pausing for five different interval lengths. The system frequency for each simulation is presented in Figure 61, where a substantial difference in system frequency is present, with the overall difference from the simulation with only two pauses (fault initiation and fault clearing) increasing as the interval between pauses is reduced. Note that the curves for pausing every 4 and 16 cycles are very similar to the normal (i.e., non-paused and free-running) simulation. Because no obvious PSLF remedy was available to mitigate this issue, the authors elected to define a minimum amount of time between the simulation of pauses to be two cycles, or 1/30 of a second. This was considered suitable for distributed generation output updates while minimizing the impact of pausing on the simulation results.

6.5 IEEE 1547-2018 Ride Through Overlays

The graphical representations of the voltage ride-through capabilities for the Institute of Electrical and Electronics Engineers (IEEE) 1547-2018 Category I and Category II are presented in figures 62 & 63, respectively.

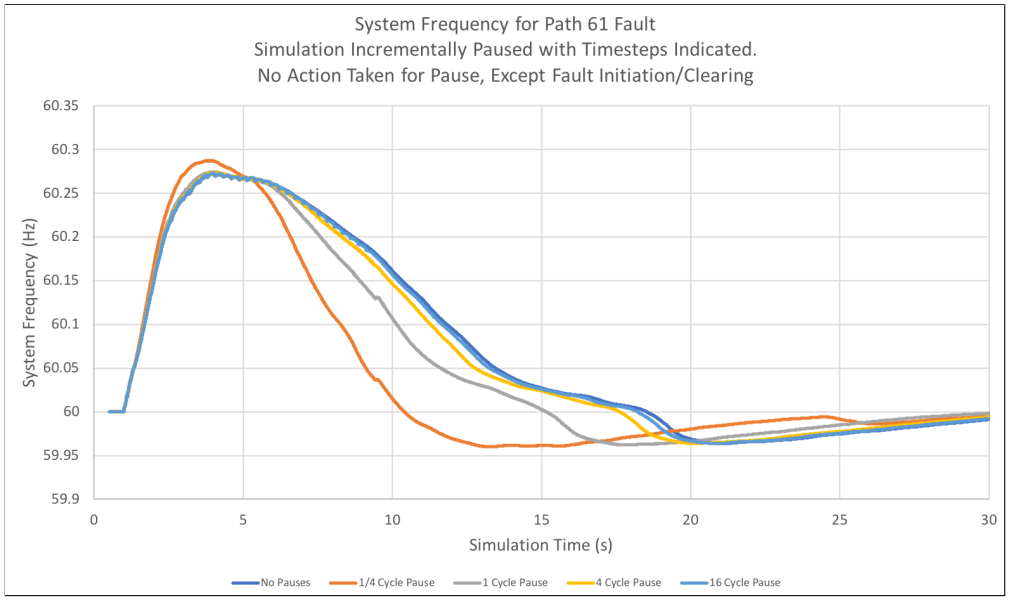

Figure 61. System frequency for varying pause time steps

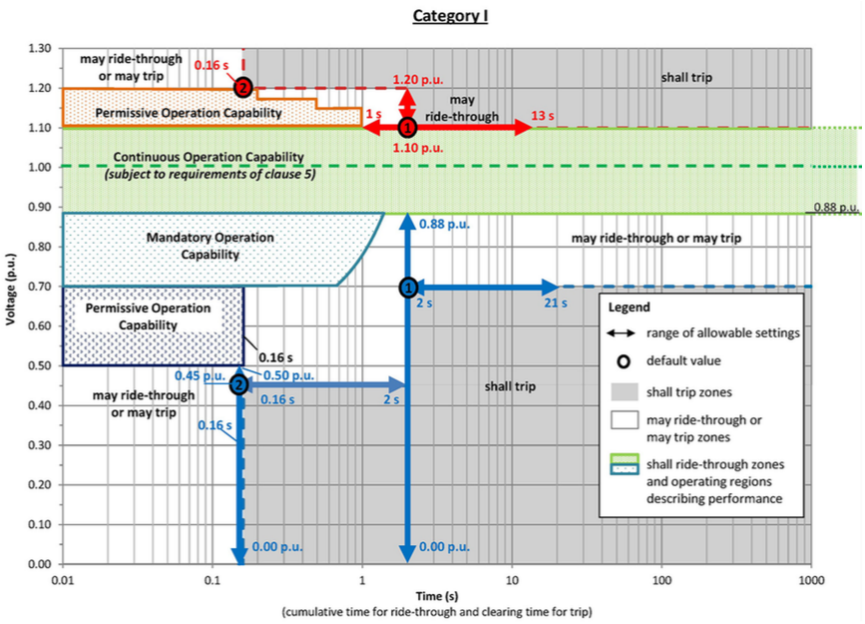

Figure 62. IEEE 1547-2018 Category I abnormal voltage ride-through (used with permission)

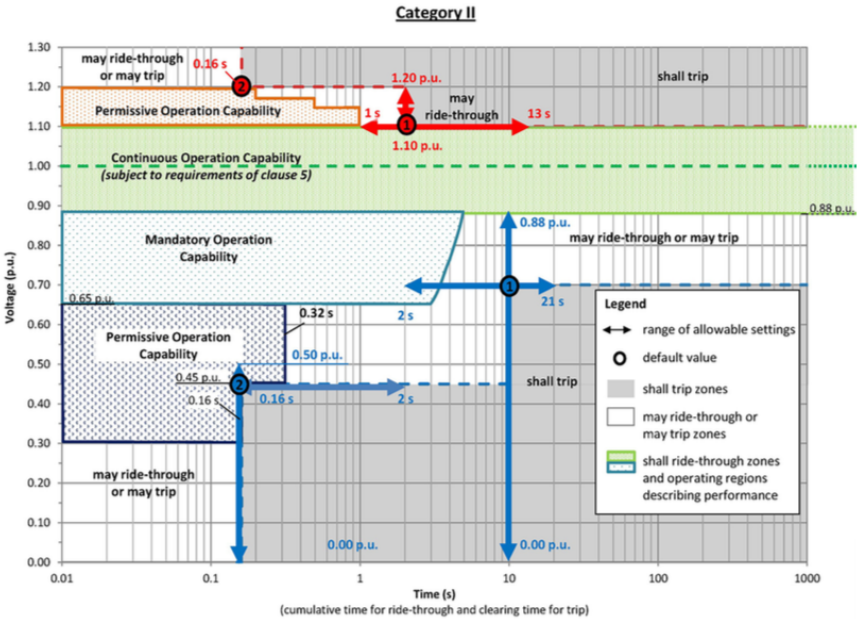

Figure 63. IEEE 1547-2018 Category II abnormal voltage ride-through (used with permission)

6.6 Table of Vt0 and Vt1 Parameters

For each DITSs, the Vt0 and Vt1 PVD1 parameters contained in the CMPLDWG model were tuned to achieve the aggregate distributed generation output during the presence of a faulted condition (i.e., before a line was tripped clearing the modeled fault). This process is necessary because the simulation pauses during the fault were not possible with the simulation setup. Only the parameters at the CMPLDWGs being commanded were changed; i.e., for the 66 CMPLDWG models in the Path 36 scenario, only these 66 models had their Vt0 and Vt1 parameters adjusted. After the fault clears, both Vt0 and Vt1 were set to zero to allow the Imax adjustments full control over the distributed generation output. The Vt0 and Vt1 parameters for the first DITSs are shown in Figure 64. The parameters for the two sets of iterations of the CatIII responses, of both the Path 61 and Path 54 scenarios, are shown in Figure 65.

Path Scenario	Pessimistic (Vt0, Vt1)	Optimistic (Vt0, Vt1)	Category I (Vt0, Vt1)	Category II (Vt0, Vt1)	Category III (Vt0, Vt1)
36	0.9, 0.95	0.7, 0.95	0.8, 0.95	0.8, 0.95	0.7, 0.95
61	0.8, 0.95	0.0, 0.7	0.2, 0.95	0.1, 0.8	0.0, 0.7
54	0.8, 0.95	0.2, 0.95	0.25, 0.95	0.25, 0.95	0.2, 0.95

Figure 64. DITS Vt0 and Vt1 parameters

Path Scenario	Iteration	Vt0	Vt1
61	1	0.0	0.7
61	2	0.0	0.4
61	3	0.0	0.4
54	1	0.2	0.95
54	2	0.1	0.75
54	3	0.1	0.75
54	4	0.1	0.75

Figure 65. DITS Category III Iteration Vt0 and Vt1 parameters

References

Abed, N., and A. Salazar. 2014. “Simulations and evaluation of FIDVR using PMU data”. In *2014 IEEE PES General Meeting*. doi:10.1109/PESGM.2014.6939939.

Bravo, R. J., and D. P. Chassin. 2016. “Fault Induced Delayed Voltage Recovery (FIDVR) Model Validation”. In *Proceedings of the 2016 IEEE/PES Transmission and Distribution Conference and Exposition (T&D)*. doi:10.1109/TDC.2016.7520045.

Bravo, R. J., et al. 2015. “Distributed Energy Resources Challenges for Utilities”. In *Proceedings of the 2015 IEEE 42nd Photovoltaic Specialist Conference (PVSC)*. doi:10.1109/PVSC.2015.7356262.

California Independent System Operator. n.d. *"Today's Outlook"*. Visited on 09/06/2018. http://www.caiso.com/Pages/default.aspx.

Distributed Energy Resources Task Force. 2017. *Distributed Energy Resources: Connection Modeling and Reliability Considerations*. Atlanta, GA: North American Electric Reliability Corporation. https://www.nerc.com.

Electric Power Research Institute. 2016. *Analysis of Voltage and Frequency Performance of the Bulk System with High Levels of Variable Generation and Distributed Energy Resources: Case Studies and Lessons Learned*. Palo Alto, CA.

Federal Energy Regulatory Commission. 2018. *Distributed Energy Resources: Technical Considerations for the Bulk Power System* (AD18-10-000). Washington, D.C.

GE Energy Consulting. n.d. *PSLF*. https://www.geenergyconsulting.com/.

Heine, Pirjo, and Matti Lehtonen. 2003. “Voltage Sag Distributions Caused by Power System Faults”. *IEEE Transactions on Power Systems* 18 (4): 1367–1373.

IEEE 1547-2003. 2003. *IEEE Standard for Interconnecting Distributed Resources with Electric Power Systems*.

IEEE 1547-2014a. 2014. *IEEE Standard for Interconnecting Distributed Resources with Electric Power Systems Amendment 1*.

IEEE 1547-2018. 2018. *IEEE Standard for Interconnection and Interoperability of Distributed Energy Resources with Associated Electric Power Systems Interfaces*.

Kaestle, G, and T.K. Varna. 2011. “Improved Requirements for the Connection to the Low Voltage Grid”. In *21st International Conference on Electrical Distribution*.

Kenyon, R. W., and B. Mather. 2018. “Quantifying Transmission Fault Voltage Influence and Its Potential Impact on Distributed Energy Resources”. In *2018 IEEE Electronic Power Grid (eGrid)*, 1–6. doi:10.1109/eGRID.2018.8598661.

Miller, N.W., et al. 2014. *Western Wind and Solar Integration Phase 3- Frequency Response and Transient Stability*. (SR-5D00-62906). Golden, CO: NREL.

Mohammadi, Younes, Mohammad H. Moradi, and Roberto Chouhy Leborgne. 2017. “Locating the source of voltage sags: Full review, introduction of generalized methods and numerical simulations”. *Renewable and Sustainable Energy Reviews* 77:821 –844. ISSN: 1364-0321. doi:https://doi.org/10.1016/j.rser.2017.04.017. http://www.sciencedirect.com/science/article/pii/S1364032117305208.

North American Electric Reliability Corporation. 2002. *1996 System Disturbances*. Report. Atlanta, GA.

– . 2017. *1,200 MW Fault Induced Solar Photovoltaic Resource Interruption Disturbance Report*. Report. Atlanta, GA.

– . 2018a. *900 MW Fault Induced Solar Photovoltaic Resource Interruption Disturbance Report*. Report. Atlanta, GA.

– . 2018b. *Loss of Solar Resources during Transmission Disturbances due to Power Inverter Settings - II*. Atlanta, GA. https://www.nerc.com/pa/rrm/bpsa/Alerts20DL/NERC_Alert_Loss_of_Solar_Resources_during_Transmission_Disturbance-II_2018.pdf.

Plet, Cornelis A., and Timothy C. Green. 2014. "Fault Response of Inverter Interfaced Distributed Generators in Grid-Connected Applications". *Electric Power Systems Research*. Visited on 08/30/2018. doi:10.1016/j.epsr.2013.07.013. http://linkinghub.elsevier.com/retrieve/pii/S0378779613001946.

Romero-L, M., and L. Gallego. 2017. "Analysis of Voltage Sags Propagation in Distribution Grids Using a SI Epidemic Model". In *2017 IEEE Workshop on Power Electronics and Power Quality Applications (PEPQA)*. doi:10.1109/PEPQA.2017.7981685.

UL 1741. 2010. *Standard for Inverters, Converters, Controllers and Interconnection System Equipment for Use With Distributed Energy Resources*.

Western Electricity Coordinating Council. 2016. *2016 State of the Interconnection*. Salt Lake City, UT.

Xu, Guangyue, and Vijay Vittal. 2010. "Slow Coherency Based Cutset Determination Algorithm for Large Power Systems". *IEEE Transactions on Power Systems* 25 (2): 877–884.

Zhu, S., et al. 2018. "Modeling Inverter-Based Resources in Stability Studies". In *2018 IEEE Power Energy Society General Meeting (PESGM)*. doi:10.1109/PESGM.2018.8586157.